ROCKETDYNE
A DIVISION OF NORTH AMERICAN AVIATION, INC.
6633 CANOGA AVENUE, CANOGA PARK, CALIFORNIA

R-6929

ENGINE SYSTEM TRANSFER FUNCTIONS FOR SUPPORT OF S-V VEHICLE LONGITUDINAL STABILITY (POGO) ANALYSIS PROGRAM

(NASA-CR-144163) ENGINE SYSTEM TRANSFER FUNCTIONS FOR SUPPORT OF S-V VEHICLE LONGITUDINAL STABILITY (POGO) ANALYSIS PROGRAM (Rocketdyne) 109 p

N76-71541

Unclas
00/98 13407

Contract NASw-16
Para. III General to Mod.71
and NASA Letter Dated
26 April 1965 (07448RC)

PREPARED BY

Rocketdyne Engineering
Canoga Park, California

APPROVED BY

D.E Aldrich
D. E. Aldrich
F-1 Program Manager

NO. OF PAGES 102 & x

REVISIONS

DATE 8 March 1967

DATE	REV. BY	PAGES AFFECTED	REMARKS

FORM R18-G REV. 4-64

UNCLASSIFIED
Security Classification

DOCUMENT CONTROL DATA - R&D

(Security classification of title, body of abstract and indexing annotation must be entered when the overall report is classified)

1. ORIGINATING ACTIVITY (Corporate author) Rocketdyne, a Division of North American Aviation, Inc., 6633 Canoga Avenue, Canoga Park, California	2a. REPORT SECURITY CLASSIFICATION Unclassified
	2b. GROUP

3. REPORT TITLE
ENGINE SYSTEM TRANSFER FUNCTIONS FOR SUPPORT OF S-V VEHICLE LONGITUDINAL STABILITY (POGO) ANALYSIS PROGRAM

4. DESCRIPTIVE NOTES (Type of report and inclusive dates)

5. AUTHOR(S) (Last name, first name, initial)
Rocketdyne Engineering

6. REPORT DATE 8 March 1967	7a. TOTAL NO. OF PAGES 112	7b. NO. OF REFS 6
8a. CONTRACT OR GRANT NO. NASw-16	9a. ORIGINATOR'S REPORT NUMBER(S) R-6929	
b. PROJECT NO.		
c.	9b. OTHER REPORT NO(S) (Any other numbers that may be assigned this report)	
d.		

10. AVAILABILITY/LIMITATION NOTICES

11. SUPPLEMENTARY NOTES	12. SPONSORING MILITARY ACTIVITY

13. ABSTRACT

F-1 engine system transfer functions are presented. These transfer functions are required to perform a vehicle longitudinal stability (POGO) investigation. The transfer functions were obtained as a result of a combined analytical evaluation and component test program. Pump dynamics were determined empirically using data supplied by the George C. Marshall Space Flight Center. Overall engine system response was then obtained analytically.

I

DD FORM 1 JAN 64 1473

UNCLASSIFIED
Security Classification

UNCLASSIFIED
Security Classification

14. KEY WORDS	LINK A ROLE	LINK A WT	LINK B ROLE	LINK B WT	LINK C ROLE	LINK C WT
Vehicle Longitudinal Stability						
Transfer Functions						
Pump Dynamics						
Linear Engine Model						
Analysis Program						
Pump Cavitation Dynamics						

INSTRUCTIONS

1. ORIGINATING ACTIVITY: Enter the name and address of the contractor, subcontractor, grantee, Department of Defense activity or other organization *(corporate author)* issuing the report.

2a. REPORT SECURITY CLASSIFICATION: Enter the overall security classification of the report. Indicate whether "Restricted Data" is included. Marking is to be in accordance with appropriate security regulations.

2b. GROUP: Automatic downgrading is specified in DoD Directive 5200.10 and Armed Forces Industrial Manual. Enter the group number. Also, when applicable, show that optional markings have been used for Group 3 and Group 4 as authorized.

3. REPORT TITLE: Enter the complete report title in all capital letters. Titles in all cases should be unclassified. If a meaningful title cannot be selected without classification, show title classification in all capitals in parenthesis immediately following the title.

4. DESCRIPTIVE NOTES: If appropriate, enter the type of report, e.g., interim, progress, summary, annual, or final. Give the inclusive dates when a specific reporting period is covered.

5. AUTHOR(S): Enter the name(s) of author(s) as shown on or in the report. Enter last name, first name, middle initial. If military, show rank and branch of service. The name of the principal author is an absolute minimum requirement.

6. REPORT DATE: Enter the date of the report as day, month, year; or month, year. If more than one date appears on the report, use date of publication.

7a. TOTAL NUMBER OF PAGES: The total page count should follow normal pagination procedures, i.e., enter the number of pages containing information.

7b. NUMBER OF REFERENCES: Enter the total number of references cited in the report.

8a. CONTRACT OR GRANT NUMBER: If appropriate, enter the applicable number of the contract or grant under which the report was written.

8b, 8c, & 8d. PROJECT NUMBER: Enter the appropriate military department identification, such as project number, subproject number, system numbers, task number, etc.

9a. ORIGINATOR'S REPORT NUMBER(S): Enter the official report number by which the document will be identified and controlled by the originating activity. This number must be unique to this report.

9b. OTHER REPORT NUMBER(S): If the report has been assigned any other report numbers *(either by the originator or by the sponsor)*, also enter this number(s).

10. AVAILABILITY/LIMITATION NOTICES: Enter any limitations on further dissemination of the report, other than those imposed by security classification, using standard statements such as:

(1) "Qualified requesters may obtain copies of this report from DDC."

(2) "Foreign announcement and dissemination of this report by DDC is not authorized."

(3) "U. S. Government agencies may obtain copies of this report directly from DDC. Other qualified DDC users shall request through
____."

(4) "U. S. military agencies may obtain copies of this report directly from DDC. Other qualified users shall request through
____."

(5) "All distribution of this report is controlled. Qualified DDC users shall request through
____."

If the report has been furnished to the Office of Technical Services, Department of Commerce, for sale to the public, indicate this fact and enter the price, if known.

11. SUPPLEMENTARY NOTES: Use for additional explanatory notes.

12. SPONSORING MILITARY ACTIVITY: Enter the name of the departmental project office or laboratory sponsoring *(paying for)* the research and development. Include address.

13. ABSTRACT: Enter an abstract giving a brief and factual summary of the document indicative of the report, even though it may also appear elsewhere in the body of the technical report. If additional space is required, a continuation sheet shall be attached.

It is highly desirable that the abstract of classified reports be unclassified. Each paragraph of the abstract shall end with an indication of the military security classification of the information in the paragraph, represented as *(TS)*, *(S)*, *(C)*, or *(U)*.

There is no limitation on the length of the abstract. However, the suggested length is from 150 to 225 words.

14. KEY WORDS: Key words are technically meaningful terms or short phrases that characterize a report and may be used as index entries for cataloging the report. Key words must be selected so that no security classification is required. Identifiers, such as equipment model designation, trade name, military project code name, geographic location, may be used as key words but will be followed by an indication of technical context. The assignment of links, rules, and weights is optional.

UNCLASSIFIED
Security Classification

ATTENTION

AS NOTED IN THE NTIS ANNOUNCEMENT, PORTIONS OF THIS REPORT ARE NOT LEGIBLE. HOWEVER, IT IS THE BEST REPRODUCTION AVAILABLE FROM THE COPY SENT TO NTIS.

FOREWORD

This report was prepared in compliance with Contract NASw-16 under G.O. 8533.

ABSTRACT

F-1 engine system transfer functions are presented. These transfer functions are required to perform a vehicle longitudinal stability (POGO) investigation. The transfer functions were obtained as a result of a combined analytical evaluation and component test program. Pump dynamics were determined empirically using data supplied by the George C. Marshall Space Flight Center. Overall engine system response was then obtained analytically.

CONTENTS

ILLUSTRATIONS

iii

TABLES

V

INTRODUCTION

Vehicle longitudinal oscillations are known to have occurred in Thor/Agena and Titan II flights. Such oscillations can be detrimental to critical payload instrumentation. In manned spaceflight, knowledge of vehicle longitudinal stability is essential to ensure crew safety. This report presents a dynamic description of the F-1 engine system developed by Rocketdyne engineering. A prediction of vehicle longitudinal stability can be made by incorporating this engine system description with representations of vehicle structural dynamics and suction feed line dynamics.

The vehicle oscillations are typically in the range of 1 to 30 cps. The term "POGO" has come to be used to characterize these oscillations. This term is derived from the resemblance of the vehicle oscillations to the simple motion of two masses connected by a spring. It is to be emphasized that the POGO phenomenn is a system closed loop interaction between vehicle structural dynamics and engine system dynamics. No single engine or vehicle component is, in itself, responsible for POGO oscillations. A brief description of the basic loop can begin with the consideration of suction pressure oscillations at the engine turbopump inlets. Such pressure oscillations can result in perturbations in the engine thrust. Engine thrust perturbations, in turn, may excite structural resonances and cause tank pressure oscillations or flow disturbances in the propellant suction lines. These oscillations as well as structural resonances can combine to produce turbopump suction pressure oscillations, thus closing the loop. Stability of this interaction is determined by the total phase shift and gain around the loop.

The capability for predicting POGO oscillations depends therefore on the knowledge of vehicle component dynamics. Engine system dynamics, which are presented in this report, have been determined by a combined analytical and empirical approach. Excluding pump cavitation dynamics, experience has shown that the rest of the engine fluid process can be described analytically for the frequency range of interest. However, analytic analysis of pump cavitation dynamics is extremely difficult because of the physical complexity of the two-phase conditions existing at pump inlets. Some compliance is always present at a pump inducer even though a pump may not be operating in deep cavitation. Component testing is required for the empirical determination of the dynamics associated with the cavitation compliance.

F-1 turbopump POGO testing was performed by MSFC to obtain dynamic data which could be used to identify the cavitation compliance associated with the LOX and fuel pumps and to verify dynamic descriptions of these pumps. The data supplied by MSFC were analyzed and the preparation of optimized pump models was developed through the application of a continuous parameter identification method.

Descriptions of pump cavitation dynamics determined experimentally were incorporated with a linearized engine description prepared analytically. The fluid dynamic transfer functions thus obtained are supplemented by a structural dynamic description of the engine for incorporation into an overall vehicle structural model. The results of the F-1 engine system analysis are presented in this report as sets of transfer functions for the following models:

1. Linear engine model excluding pump cavitation dynamics (interface at pump inlet flanges)

2. Linear engine model including pump cavitation dynamics (interface at pump inlet flanges)

3. Structural dynamic engine description

SUMMARY

Effort has been completed on the preparation of F-1 engine system transfer functions in support of the Saturn V POGO Analysis.

The F-1 engine system transfer functions were prepared from engine analytical descriptions. Pump representations were prepared empirically through the analysis of component test data supplied by the Marshall Space Flight Center. Three sets of engine system transfer functions are presented:

1. Engine system excluding cavitation dynamics
2. Engine system including cavitation dynamics
3. Engine system structural dynamics.

TECHNOLOGICAL ADVANCEMENT RESULTING FROM THE F-1 POGO ANALYSIS PROGRAM

A technique of automatic, continuous identification of optimized model parameter values was used to prepare the descriptions of pump dynamics. The basis for the methods employed are developed in Ref. 1, 2, and 3. Certain modifications were developed so that the approach could be used in the analysis of turbopump cavitation dynamics. This analysis, which was conducted concurrently with the study presented in Ref. 3, is apparently the first time that continuous parameter identification has been used for such a purpose. Significant cost and time savings resulted from the use of this technique, and it is recommended for future pump dynamics analysis.

ANALYTICAL MODEL DEVELOPMENT

The F-1 engine system transfer functions for support of Saturn V vehicle POGO studies are as follows:

1. Linear engine model (interface at the pump flanges)
2. Pump cavitation dynamics
3. F-1 engine structural models

A block diagram of their interrelation with the vehicle is shown in Fig. 1. Models (1) and (3) are developed in this section. Model (2), which is essentially a description of the pump dynamics, is developed in the section entitled "LOX and Fuel Pump Testing and Evaluation."

A nomenclature list for the system variables is shown in Appendix A.

LINEAR ENGINE MODEL

Nonlinear equations describing the engine processes were written. Typical equations for the significant components are as follows:

Propellant Feed System

Flow Ducts. All propellant ducts are simulated by the following fluid flow lumped parameter expression

$$p_a - p_b = R\dot{w}^2 + L\ddot{w} \tag{1}$$

Preceding page blank

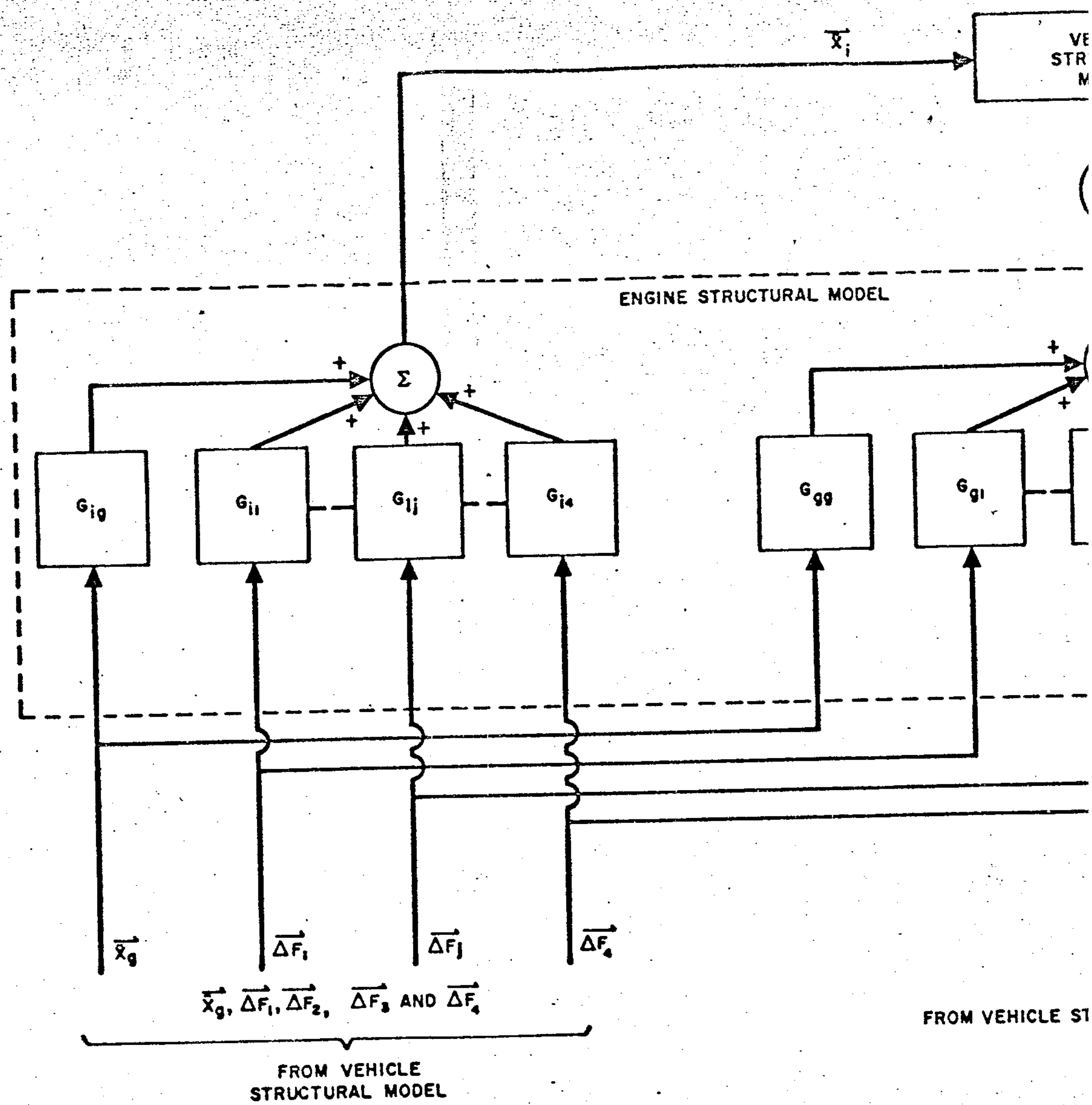

$\vec{X}_i$
VE
STR
M
ENGINE STRUCTURAL MODEL
G_{ig}
G_{i1}
G_{ij}
G_{i4}
G_{gg}
G_{g1}
$\vec{X}_g$
$\overrightarrow{\Delta F_1}$
$\overrightarrow{\Delta F_j}$
$\overrightarrow{\Delta F_4}$
$\vec{X}_g$, $\overrightarrow{\Delta F_1}$, $\overrightarrow{\Delta F_2}$, $\overrightarrow{\Delta F_3}$ AND $\overrightarrow{\Delta F_4}$
FROM VEHICLE STRUCTURAL MODEL
FROM VEHICLE ST

8-A

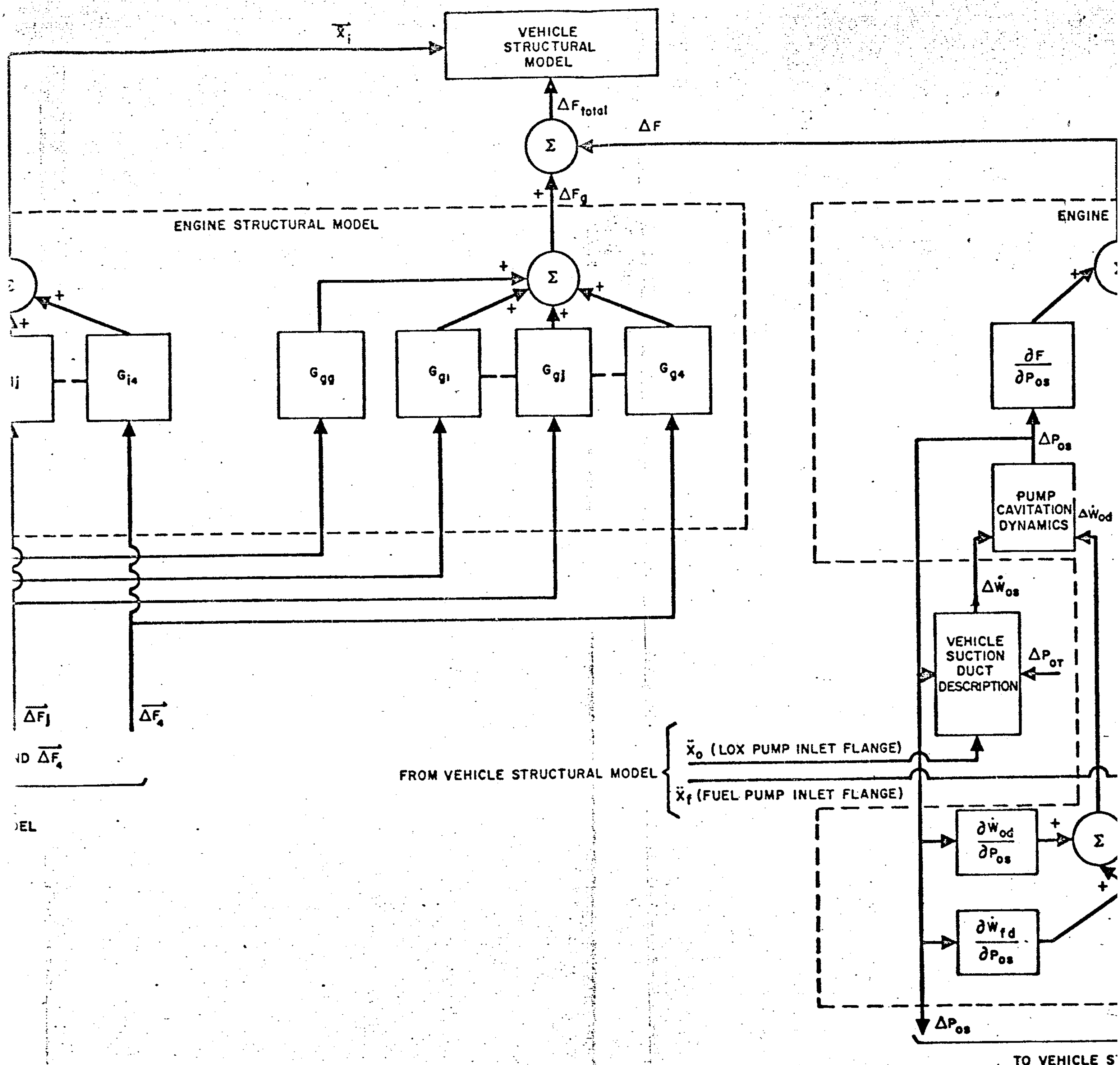

$\overrightarrow{X}_i$
VEHICLE STRUCTURAL MODEL
ΔF_{total}
ΔF
Σ
+
ΔF_g
ENGINE STRUCTURAL MODEL
G_{i4}
G_{gg}
G_{g1}
G_{gj}
G_{g4}
$\overrightarrow{\Delta F_j}$
$\overrightarrow{\Delta F_4}$
ND $\overrightarrow{\Delta F_4}$
EL
ENGINE
$\frac{\partial F}{\partial P_{os}}$
ΔP_{os}
PUMP CAVITATION DYNAMICS
$\Delta \dot{W}_{od}$
$\Delta \dot{W}_{os}$
VEHICLE SUCTION DUCT DESCRIPTION
ΔP_{oT}
FROM VEHICLE STRUCTURAL MODEL
$\ddot{X}_o$ (LOX PUMP INLET FLANGE)
$\ddot{X}_f$ (FUEL PUMP INLET FLANGE)
$\frac{\partial \dot{W}_{od}}{\partial P_{os}}$
$\frac{\partial \dot{W}_{fd}}{\partial P_{os}}$
TO VEHICLE S

8-A

8-B

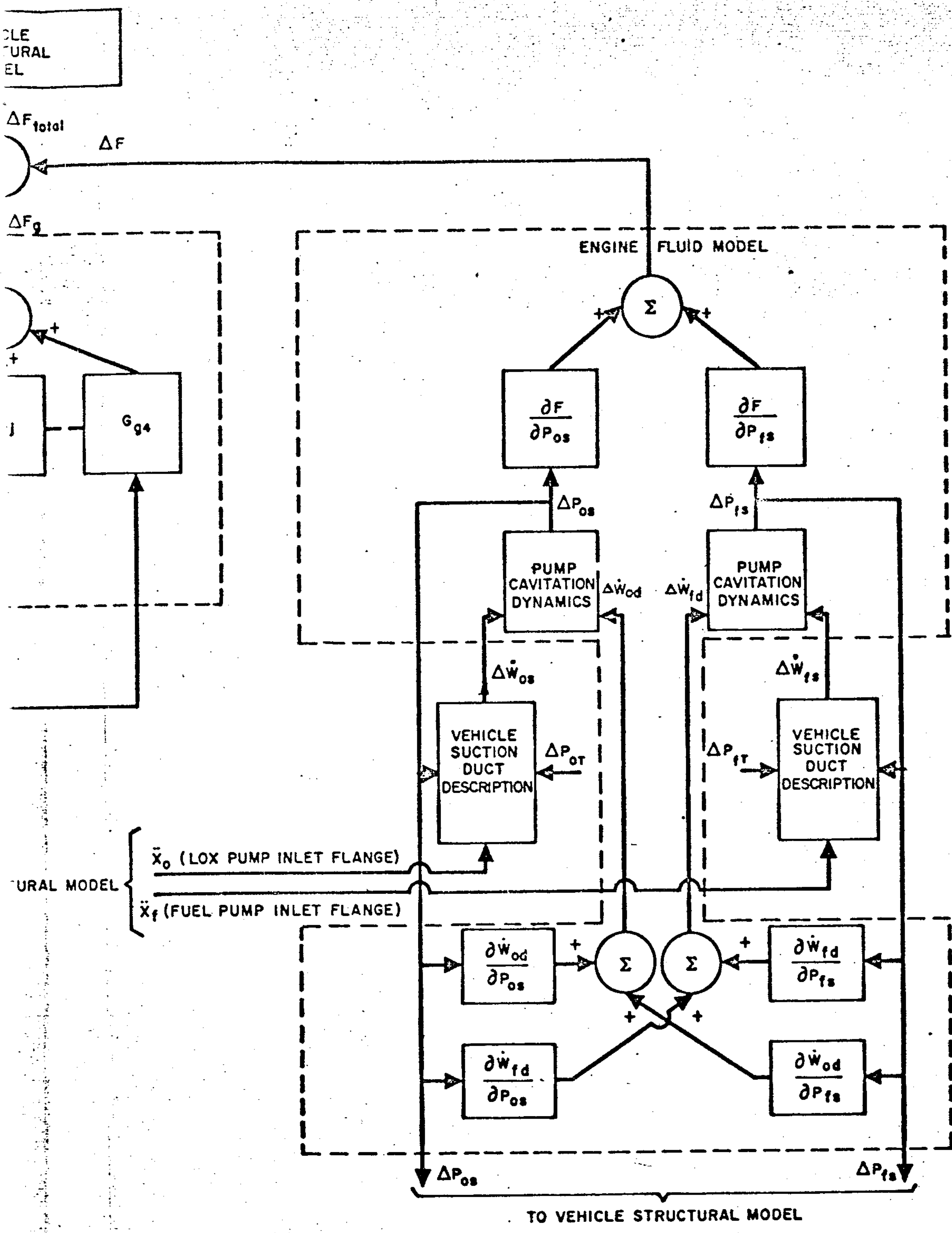

Figure 1. Block Diagram of Engine Structural and Fluid Models

8 - B

Turbopump.

$$P_d - P_s = K\psi N_p^2 \tag{2}$$

$$\varphi = K \frac{\dot{w}_p}{N_p} \tag{3}$$

$$M_p = K \chi N_p^2 \tag{4}$$

$$N_p = \frac{1}{I_{gt}} \int (M_{tn} - M_p)\, dt \tag{5}$$

$$\psi = f_1 (\varphi) \tag{6}$$

$$\chi = f_2 (\psi, \varphi, \eta) \tag{7}$$

The functional relationships of the above dimensionless parameter were obtained from pump tests.

Turbine.

$$M_{tn} = \frac{\dot{w}_{gx} (\Delta H_{tn}) \eta_{tn}}{N_p} \tag{8}$$

$$\dot{w}_{gx} = f(p_{gx}, c^*_g) \tag{9}$$

$$\Delta H_t = f(C_{pg}, P_r, T_{gg}) \tag{10}$$

The generated torque was obtained using the conventional efficiency vs tip speed to isentropic spouting velocity ratio relationship.

Thrust Chamber. (The processes described below are similar for the gas generator.)

$$P_c = \frac{R_u}{V_c} \frac{T_c}{MW_c} (w_{oc} + w_{fc}) \tag{11}$$

$$w_{oc} = \int \left[\dot{w}_{oI} - (LF_c)\, \dot{w}_{cx} \right] dt \tag{12}$$

$$w_{fc} = \int \left[\dot{w}_{fI} - (1 - LF_c)\, \dot{w}_{cx} \right] dt \tag{13}$$

$$LF_c = \frac{w_{oc}}{w_{oc} + w_{fc}} \tag{14}$$

$$\dot{w}_{cx} = f\,(A_t, P_c, c^*_c) \tag{15}$$

$$\frac{T_c}{MW_c} = f\,(LF_c) \tag{16}$$

$$c^*_c = f\,(LF_c) \tag{17}$$

The nonlinear system equations are in lumped parameter form. Furthermore, the assumption is made that the gas in the gas generator and thrust chamber is ideal and the fluids in the feed system are incompressible. A schematic representation of the engine system showing the direction of flow is shown in Fig. 2.

The nonlinear system equations were linearized by small perturbation analysis. The mainstage operating condition was the reference solution about which the linearization was made. Each variable was normalized with respect to its mainstage value.

The set of normalized linear engine equations is shown in Table 1. Included in this model is a description of fuel and LOX pump cavitation

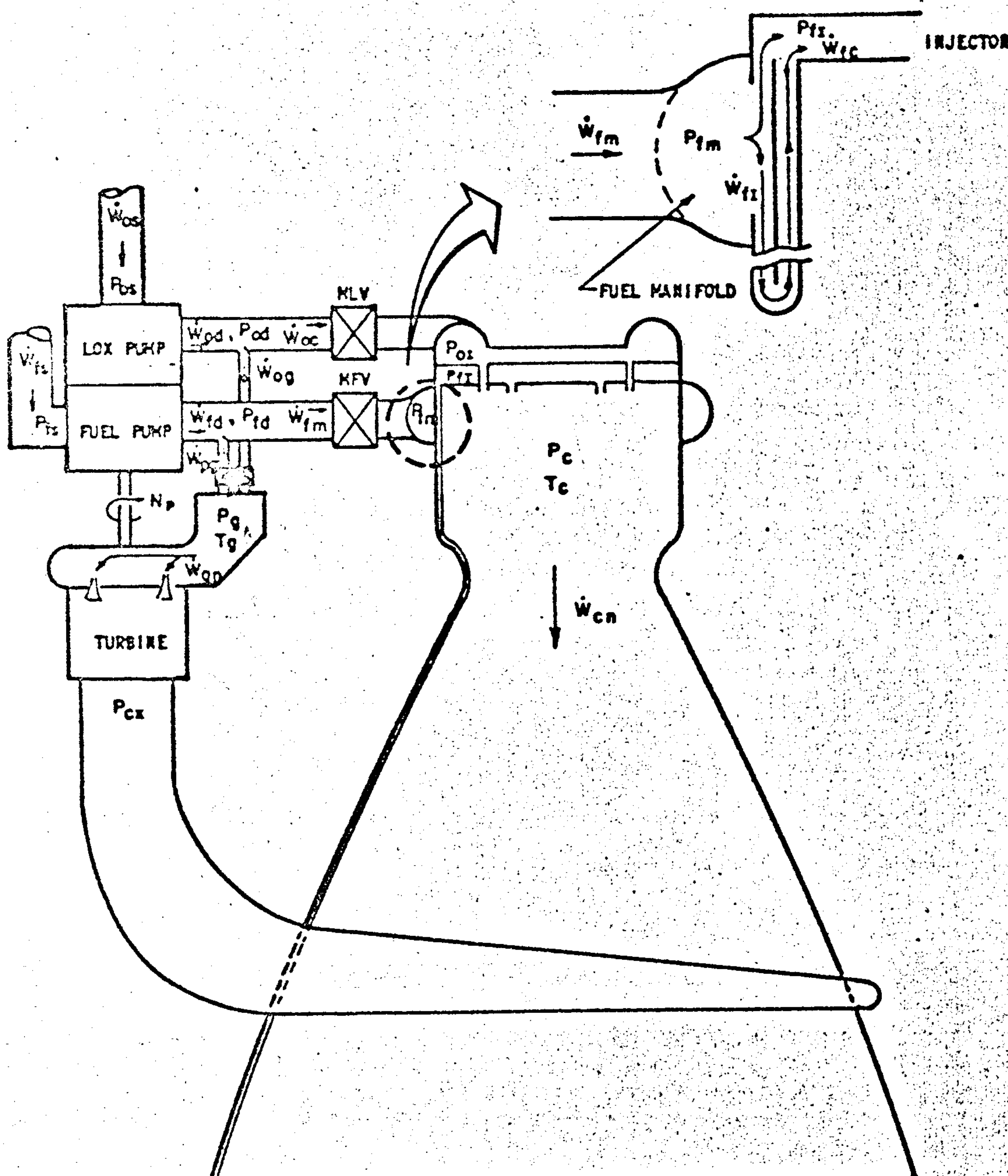

Figure 2. Engine System Schematic Diagram

TABLE 1

F-1 ENGINE LINEARIZED MODEL EQUATIONS*

1. $\tilde{P}_{od} + 0.6372\, \tilde{\dot{w}}_{od} - 2.5665\, N_p = 0.03536(1+J_o)\, \tilde{P}_{os}$

2. $\tilde{\dot{w}}_{od} - 0.9864\, \tilde{\dot{w}}_{oc} - 0.01351\, \tilde{\dot{w}}_{og} = 0$

3. $\dfrac{d\, \tilde{\dot{w}}_{oc}}{dt} + 103.3\, \tilde{P}_c + 131.52\, \tilde{\dot{w}}_{oc} - \tilde{P}_{od}\, (169.04) = 0$

4. $\dfrac{d\, \tilde{\dot{w}}_{og}}{dt} + 234.61\, \tilde{P}_g + 268.89\, \tilde{\dot{w}}_{og} - 369.06\, \tilde{P}_{od} = 0$

5. $\tilde{P}_{fd} + 0.4075\, \tilde{\dot{w}}_{fd} - 2.359\, \tilde{N}_p = 0.02392\, (1+J_f)\, \tilde{P}_{fs}$

6. $\tilde{\dot{w}}_{fd} - 0.9286\, \tilde{\dot{w}}_{fm} - 0.0713\, \tilde{\dot{w}}_{fg} = 0$

7. $\dfrac{d\, \tilde{\dot{w}}_{fm}}{dt} + 198.67\, \tilde{P}_{fm} + 74.28\, \tilde{\dot{w}}_{fm} - 235.8\, \tilde{P}_{fd} = 0$

8. $\dfrac{d\, \tilde{P}_{fm}}{dt} - 1756.0\, \tilde{\dot{w}}_{fm} + 1088.0\, \tilde{\dot{w}}_{f1} + 669.0\, \tilde{\dot{w}}_{f2} = 0$

9. $\dfrac{d\, \tilde{\dot{w}}_{f1}}{dt} - 131.7\, \tilde{P}_{fm} + 107.1\, \tilde{P}_{fI} + 49.16\, \tilde{\dot{w}}_{f1} = 0$

10. $\tilde{\dot{w}}_{f2} - 2.679\, \tilde{P}_{fm} + 2.179\, \tilde{P}_{fI} = 0$

11. $\tilde{\dot{w}}_{fc} - 0.6200\, \tilde{\dot{w}}_{f1} - 0.3800\, \tilde{\dot{w}}_{f2} = 0$

12. $\tilde{P}_{fI} - 0.8712\, \tilde{P}_c - 0.2575\, \tilde{\dot{w}}_{fc} = 0$

13. $\dfrac{d\, \tilde{\dot{w}}_{fg}}{dt} + 256.6\, \tilde{P}_g + 313.0\, \tilde{\dot{w}}_{fg} - 413.2\, \tilde{P}_{fd} = 0$

*NOTE: Nomenclature is shown in Appendix A

TABLE 1
(Continued)

14. $\tilde{M}_o - 0.3656\,\tilde{w}_{od} - 1.634\,\tilde{N}_p = 0.0366\ \ J_o\,\tilde{P}_{os}$

15. $\tilde{M}_f - 0.4236\,\tilde{w}_{fd} - 1.576\,\tilde{N}_p = 0.0245\ \ J_f\,\tilde{P}_{fs}$

16. $\frac{d\tilde{N}_p}{dt} - 4.505\,\tilde{M}_{tn} + 2.685\,\tilde{M}_o + 1.821\,\tilde{M}_F = 0$

17. $\tilde{p}_g - \tilde{T}_g - 1.435\,\tilde{LF}_g - 0.3007\,\tilde{w}_{og} - 0.6992\,\tilde{w}_{fg} = 0$

18. $\frac{d\tilde{w}_{og}}{dt} - 46.59\,\tilde{w}_{og} + 46.59\,\tilde{w}_{gn} + 46.59\,\tilde{LF}_g = 0$

19. $\frac{d\tilde{w}_{fg}}{dt} - 46.59\,\tilde{w}_{fg} + 46.59\,\tilde{w}_{gn} - 20.03\,\tilde{LF}_g = 0$

20. $\tilde{LF}_g - 0.6992\,\tilde{w}_{og} + 0.6992\,\tilde{w}_{fg} = 0$

21. $\tilde{w}_{gn} - p_g + 0.9973\,\tilde{LF}_g = 0$

22. $$\frac{d\tilde{T}_g}{dt} - 48.41\,\tilde{w}_{og} - 4.729\,\tilde{w}_{fg} + 53.14\,\tilde{T}_g + 53.14\,\tilde{w}_{gn} + 0.3007\,\frac{d\tilde{w}_{og}}{dt} + 0.6992\,\frac{d\tilde{w}_{fg}}{dt} - 0.1292\,\frac{d\tilde{LF}_g}{dt} = 0$$

23. $\tilde{M}_{tn} - \tilde{w}_{gn} + 1.076\,\tilde{LF}_g + 0.5475\,\tilde{N}_p - 0.7737\,\tilde{T}_g = 0$

TABLE 1

(Concluded)

24. $\tilde{p}_c - 0.4504\,\tilde{w}_{oc} - 0.5496\,\tilde{w}_{fc} = 0$

25. $\dfrac{d\,\tilde{w}_{oc}}{dt} - 559.1\,\tilde{w}_{oc} + 559.1\,\tilde{w}_{cn} + 163.9\,\tilde{w}_{oc} - 163.9\,\tilde{w}_{fc} = 0$

26. $\dfrac{d\,\tilde{w}_{fc}}{dt} - 559.1\,\tilde{w}_{fc} + 559.1\,\tilde{w}_{cn} - 395.2\,\tilde{w}_{oc} + 395.2\,\tilde{w}_{fc} = 0$

27. $\tilde{w}_{cn} - \tilde{p}_c - 0.07811\,\tilde{w}_{oc} + 0.07811\,\tilde{w}_{fc} = 0$

28. $\tilde{F}_c - 1.1508\,\tilde{p}_c - 0.07358\,(\tilde{w}_{oc} - \tilde{w}_{fc}) = 0$

gains J_f and J_o. These gains were used to describe the effects of small slope changes in the NPSH-head curves, and were hypothesized to be due to small perturbations in LOX and fuel density. The values of the cavitation gain are found and discussed in the section entitled "LOX and Fuel Pump Testing and Evaluation."

STRUCTURAL DYNAMIC DESCRIPTION OF F-1 ENGINE

Structural dynamic mathematical models were developed for the F-1 engines of the Saturn-V vehicle. These models of the flexible line engine (2011-2016) configuration and the hard line (2017-2028) configuration were used to determine structural transfer functions relating the output accelerations or forces to input accelerations or forces at the engine-to-vehicle interfaces. The transfer functions express engine axial responses for specified axial excitations within a frequency range of 0 to 100 cps.

The primary weight components of the engine considered in the development of the engine structural models were the thrust chamber, the turbopump, and the heat exchanger. The thrust chamber was considered as being effectively rigid since the analysis showed that there was no elastic bending or axial modes of the thrust chamber in the 0- to 100-cps frequency range.

The approach used to develop a mathematical description of the system included the formulation of the stiffness matrix for the structure. The structure is considered as an assemblage of parts, and each part is assigned a stiffness matrix relating forces and displacements at its terminals. The stiffness matrix for the complete structure is obtained by combining the component stiffness matrices. The inertia matrix formed by including the masses and inertias at the nodal points completes the array necessary for an eigenvalue analysis. The eigenvalues and eigenvectors obtained are used to determine the structural transfer functions.

DATA ANALYSIS TECHNIQUES

TECHNIQUES UTILIZED

Analysis of the F-1 turbopump dynamic test data was accomplished by utilizing a continuous parameter identification method which was mechanized on a high-capacity, general-purpose, analog computer. Scalings, flowrate reconstruction, and optimization were performed on line as data on magnetic tape were played back.

The method of line domain parameter optimization used in the analysis of F-1 POGO test data is identical in every significant respect to the method which was developed and successfully employed in the H-1 POGO analysis program. The theoretical basis of this method is presented in Appendix C, which is extracted from Ref. 3.

LOX AND FUEL PUMP TESTING AND EVALUATION

POGO TESTING OF F-1 (MARK 10) TURBOPUMPS

F-1 turbopump test data were supplied by the George C. Marxhall Space Flight Center. A Block I pump was modified to Block II specifications. Testing was conducted at the "Bobtail" facility schematically shown in Fig. 3. The pump was operated at nominal (φ–ψ) conditions, and a range of NPSH levels on both LOX and fuel pumps was surveyed.

Pulsing

The purpose of the POGO testing was to generate data that would enable dynamic descriptions of the LOX and fuel pumps to be empirically constructed and verified. Such data must indicate the manner in which flowrate and pressure oscillations are transmitted through the individual turbopumps.

The data used in this study were obtained through the use of the discharge bypass pulsing systems shown in Fig. 4. The operation of the discharge pulsers produced a flowrate disturbance at the pump discharge flange. This perturbation contained both the fundamental and higher harmonics of the programmed pulsing frequency. The frequency of pulsing was increased in steps throughout a bandwidth designed to excite resonances of the pump inlet ducts associated with cavitation-line inertance dynamics.

Instrumentation (Measurement Program)

The arrangement whereby testing was accomplished at MSFC and the analysis at Rocketdyne made it imperative that measured test information be specified and well verified. Adequate instrumentation, carefully located and properly installed, was prerequisite to obtaining meaningful data. The initial step

Preceding page blank

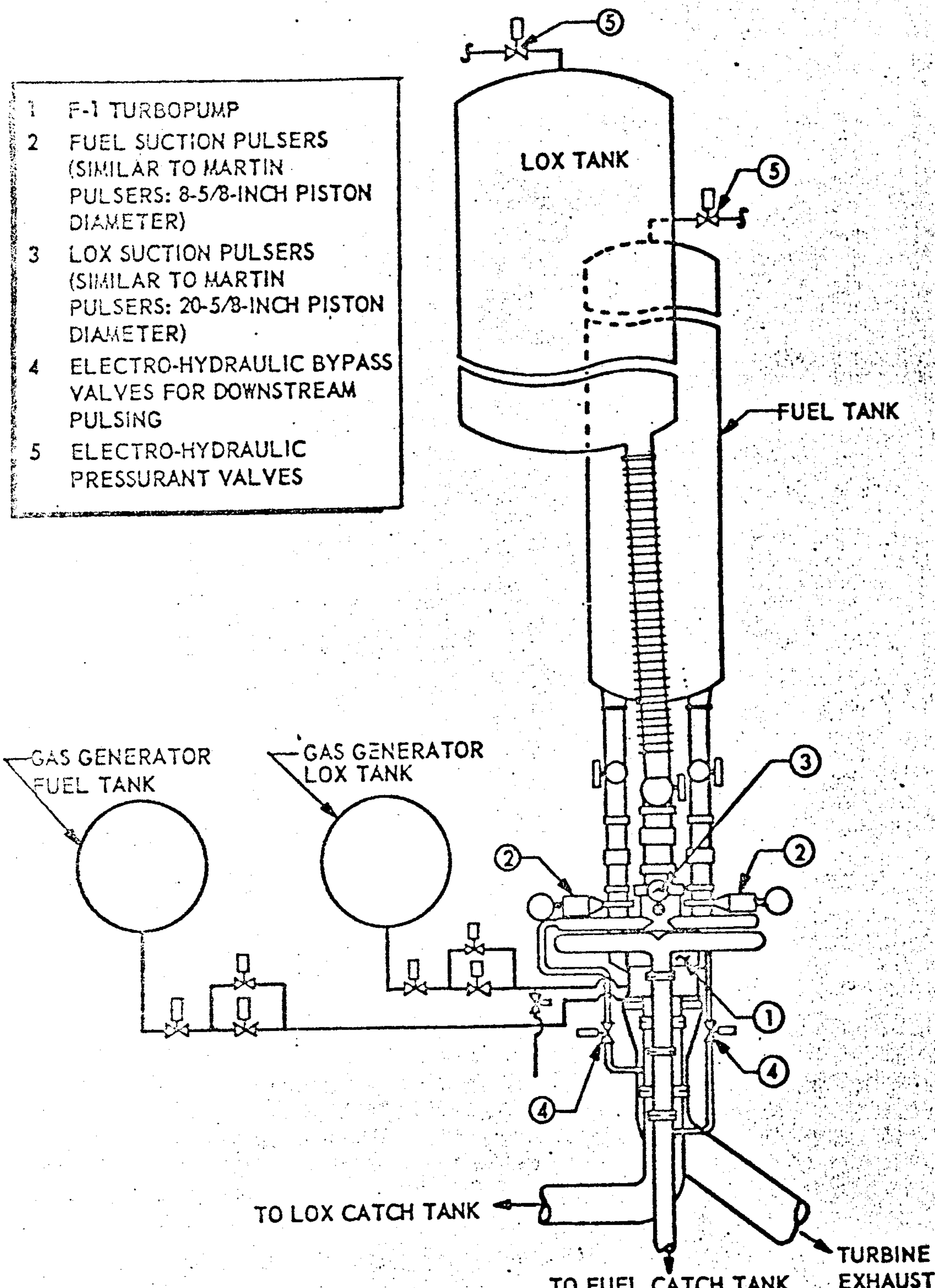

Figure 3. F-1 POGO Test Stand

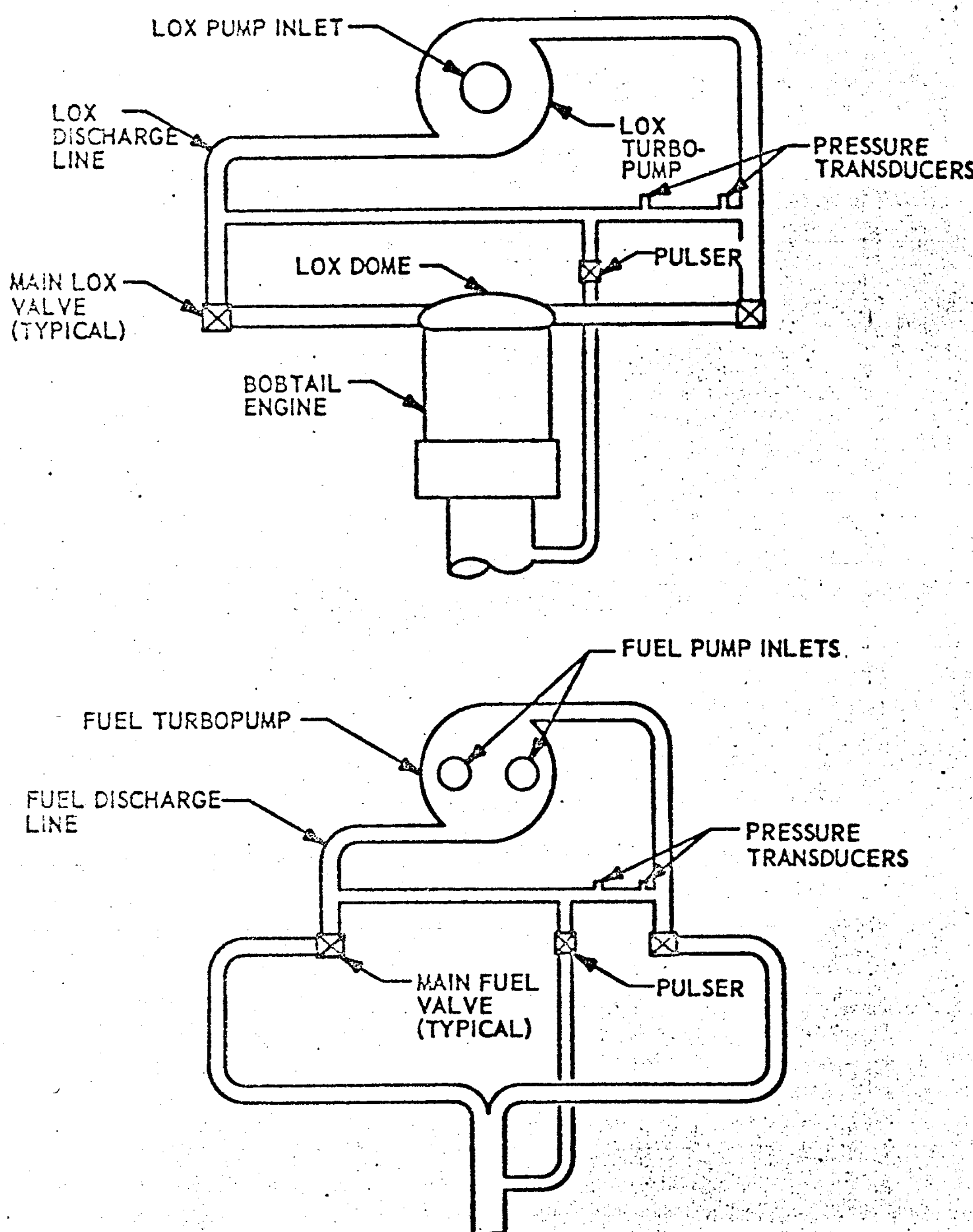

Figure 4. Schematic of F-1 Discharge Pulser Systems at MSFC Bobtail Engine Facility

taken to minimize instrumentation problems was a coordinated selection of the necessary instrumentation by Rocketdyne and MSFC. The high-frequency response instrumentation was of special interest because a POGO analysis requires that the content of the data be dynamical. Only through such data could the results of the analytical effort be confirmed.

Diametrically opposed pump inlet and discharge pressure transducers were recommended to ensure the recording of these important parameters should one of the transducers fail. At the same time they would be useful in detecting the influence of duct vibrations on the dynamic pressure at these locations. In addition, accelerometers were located at the fuel and LOX pump inlets to monitor vibrations directly in the event that a correlation between the pressures and accelerations was significant. Because dynamic flowmeters were not available, fuel and LOX pulser positions and pulsing line pressures were recorded so that the dynamic flowrate inputs to the system could be generated by means of facility transfer functions.

Three orifices in series in each of the pump discharge lines were employed in an attempt to isolate the downstream fluid dynamics from the rest of the system. The orifices were intended to facilitate the use of simplified transfer functions to describe the discharge system fluid dynamics and precluded the need for more high-frequency response instrumentation in this area. Three tape recorders were required to record the desired parameters. Pump speed and the time code were suggested as common parameters on the recorders. One channel on each recorder was reserved for voice communication. Raw signal recording (i.e., no d-c blocking filters) of the dynamic parameters was requested by Rocketdyne. Following the agreement on the dynamic instrumentation requirements, installation and checkout of the transducers at the MSFC F-1 Bobtail facility was completed.

Static and Dynamic Instrumentation Lists. The dynamic instrumentation employed during the test program is listed in Table 2. The pressure measurements at diametrically opposed locations on the inlet and discharge ducting were important only until it was verified that the influence of vibratory duct motion on the pump inlet and discharge dynamic pressures was insignificant and that a vibration of the pressure sensing mechanism in the transducers was not contaminating the pressure signals. The accelerometer measurement at the pump inlet flange also received less attention later in the program when it was assured that little correlation existed between the pump inlet pressure and the pump inlet flange vibration in the direction of suction flow. This vibration was sensed parallel to the suction duct.

Static measurements were included in the measurement program; however, most of these were not directly related to the POGO analysis. The measurements used are listed in Table 3.

POGO Pump Test Data

A summary of the F-1 POGO tests received by Rocketdyne is given in Table 4. Figure 5 shows the φ-ψ points for the pulsing tests used in the analysis compared to nominal Mark 10 (Block II) turbopump performance curves. The nominal Block II φ-ψ points are:

$$\bar{\varphi}_o = 0.1069$$
$$\bar{\psi}_o = 0.4615$$
$$\bar{\varphi}_f = 0.08222$$
$$\bar{\psi}_f = 0.5540$$

TABLE 2

DYNAMIC MEASUREMENTS

NASA Measurement Number	Description	Transducer	Range
D-118	Pressure, Fuel Pump Inlet No. 1, psi	Photocon	0 to 200
D-120	Pressure, Fuel Pump Inlet No. 2, psi	Photocon	0 to 200
D-124	Pressure, Fuel Pump Discharge No. 1, psi	Photocon	0 to 2500
D-126	Pressure, Fuel Pump Discharge No. 2, psi	Photocon	0 to 2650
D-128	Pressure, LOX Pump Discharge No. 2, psi	Dynisco	0 to 2000
D-130	Pressure, LOX Pump Discharge No. 2, psi	Dynisco	0 to 2000
D-180	Pressure, LOX Pump Inlet, psi	Statham	0 to 250
D-181	Pressure, LOX Pump Inlet, Diametrically Opposite, psi	Statham	0 to 250
D-277	Pressure, LOX Pump Inlet 90-inch Point, psi	Statham	0 to 250
D-354	Pressure, Fuel Pump Inlet No. 1, Diametrically Opposite, psi	Photocon	0 to 160
D-355	Pressure, Fuel Pump Inlet No. 2, Diametrically Opposite, psi	Photocon	0 to 300
D-356	Pressure, LOX Pump Discharge No. 1, Diametrically Opposite, psi	Dynisco	0 to 2000
D-357	Pressure, LOX Pump Discharge No. 2, Diametrically Opposite, psi	Dynisco	0 to 2000
D-358	Pressure, Fuel Pump Discharge No. 1, Diametrically Opposite, psi	Photocon	0 to 2300
D-359	Pressure, Fuel Pump Discharge No. 2, Diametrically Opposite, psi	Photocon	0 to 2400
D-371	Pressure, Main Fuel Valve Inlet No. 1, psi	Photocon	0 to 2500

TABLE 2

(Concluded)

NASA Measurement Number	Description	Transducer	Range
D-372	Pressure, LOX Suction Line Transition, psi	Dynisco	0 to 250
D-381	Pressure, LOX Pulsing Line Upstream, psi	Dynisco	0 to 2000
D-382	Pressure, LOX Pulsing Line Downstream, psi	Dynisco	0 to 2000
D-383	Pressure, Fuel Pulsing Line Upstream, psi	Dynisco	0 to 2000
D-384	Pressure, Fuel Pulsing Line Downstream, psi	Dynisco	0 to 2000
D-392	Pressure, Fuel PVC Inlet No. 1, psi	Photocon	0 to 240
E-075	Vibration, LOX Pump Inlet Flange, g (Sensitive in the Direction of Suction Flow)	Statham	±1
E-082	Vibration, Fuel Pump Inlet Flange, g (Sensitive in the Direction of Suction Flow)	Statham	±1
G-029	Fuel Pulser Position, percent		0 to 100
G-030	LOX Pulser Position, percent		0 to 100

NOTE: This table applies specifically to test C-006-45. Except for certain changes in transducer ranges, it is typical of the instrumentation used in the F-1 POGO test series.

TABLE 3

STATIC MEASUREMENTS

NASA Measurement Number	Description	Transducer	Range
D-121	Pressure, LOX Pump Inlet, psi	Wiancko	0 to 200
D-127	Pressure, LOX Pump Discharge No. 1, psi	Wiancko	0 to 2000
D-117	Pressure, Fuel Pump Inlet No. 1, psi	Wiancko	0 to 50
D-123	Pressure, Fuel Pump Discharge No. 1, psi	Wiancko	0 to 2500
C-265	Temperature, LOX Pump Inlet (90-inch Point), F	RB	-350 to -250
C-285	Temperature, Main Fuel Tank Bulk No. 1, F	TC-CC	-84.5 to 150
F-026	Flow, Main LOX, gpm	Potter	0 to 25,000
F-027	Flow, Main Fuel No. 1, gpm	Potter	0 to 7000
T-001	Speed, F-1 Turbopump, rpm		0 to 7000

TABLE 4

F-1 POGO TESTS

Test	Primary Objective	Scheduled LOX Inlet Pressure, psia	Scheduled Fuel Inlet Pressure, psia	LOX Pulsing Range, cps	Fuel Pulsing Range, cps	Remarks
C-006-40	Pulsing Test of LOX and Fuel Pumps	100	50	4 to 10	6 to 14	Crosstalk noted between LOX and fuel pulser position data. No significant dynamic content in acquired fuel pump discharge pressure data was observed.
C-006-41	Pulsing Test of LOX and Fuel Pumps	125	60	4 to 10	8 to 16	LOX pump inlet pressure drifted during test
C-006-42	Pulsing Test of LOX and Fuel Pumps	150	40	4 to 10	6 to 14	Test aborted
C-006-43	Pulsing Test of LOX and Fuel Pumps	150	40	4 to 10	6 to 14	LOX pump inlet pressure drifted during test
C-006-44	Pulsing Test of LOX and Fuel Pumps	80	30	3 to 9	6 to 14	LOX pump inlet pressure drifted during test
C-006-45	Pulsing Test of LOX and Fuel Pumps	60	60	2 to 8	8 to 16	
C-006-48	Pulsing Test of LOX Pump	80		3 to 9		Repeat LOX pump conditions of test C-006-44
C-006-49	Pulsing Test of LOX Pump	125		4 to 10		Repeat LOX pump conditions of test C-006-41
C-006-50	Pulsing Test of LOX Pump	150		4 to 10		Repeat LOX pump conditions of test C-006-43

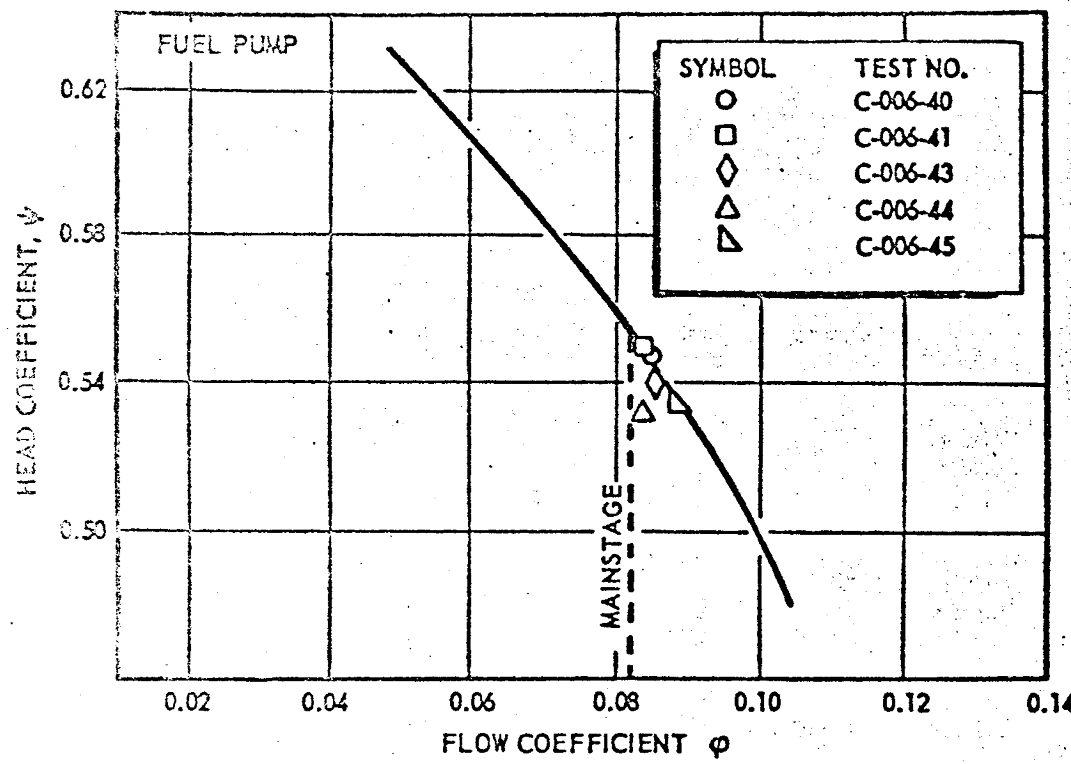

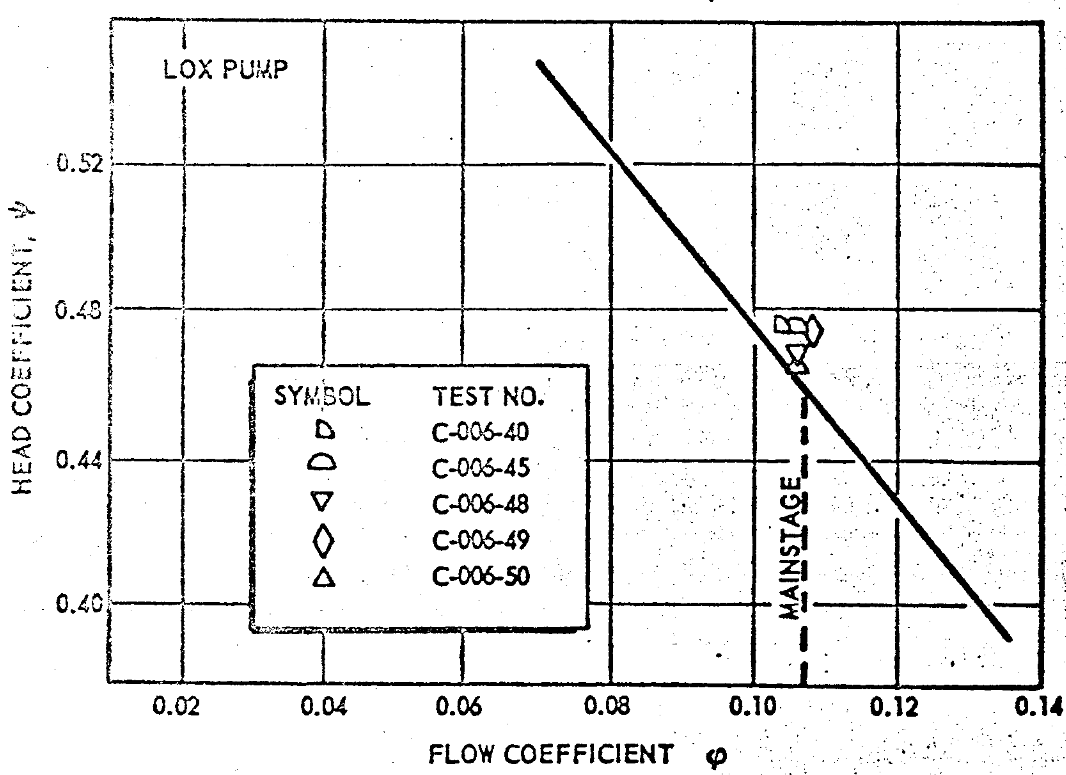

Figure 5. $\varphi - \psi$ Operating Points of Bobtail Facility Tests

The average operating points of the POGO test series are sufficiently close to the points $(\bar{\varphi}_o, \bar{\psi}_o)$ and $(\bar{\varphi}_f, \bar{\psi}_f)$ that the pump dynamic descriptions developed from these data can be said to apply at nominal Block II φ-ψ conditions. The pump descriptions prepared have a functional dependence on $NPSH_o$ and $NPSH_f$ over the ranges tested.

Flowrate Reconstruction

The use of flowmeters to measure dynamic flowrates was precluded for a variety of reasons. Dynamic flowrate data were reconstructed by the use of pressure data and analytic facility representations supplied by MSFC. Equations describing the facility were sent to Rocketdyne, and in the form below were mechanized for analog computation of flowrate data.

Fuel Suction Flowrate Computation.

$$\Delta p_{fs}(t) \longrightarrow \boxed{-\frac{\left[\left(\frac{D}{340.1}\right)^2 + 2\left(\frac{0.002}{340.1}\right) D + 1\right]}{0.002082\, D\left[\left(\frac{D}{668.2}\right)^2 + 2\left(\frac{0.002}{668.2}\right) D + 1\right]}} \longrightarrow \Delta \dot{w}_{fs}(t)$$

Note: The term 0.002082 was replaced by $(0.002082D + 0.001)$ in the actual analog circuit used to ensure low-frequency stability. The effect is equivalent to the addition of a very small resistance in the fuel feed system.

Fuel Discharge Flowrate Computation.

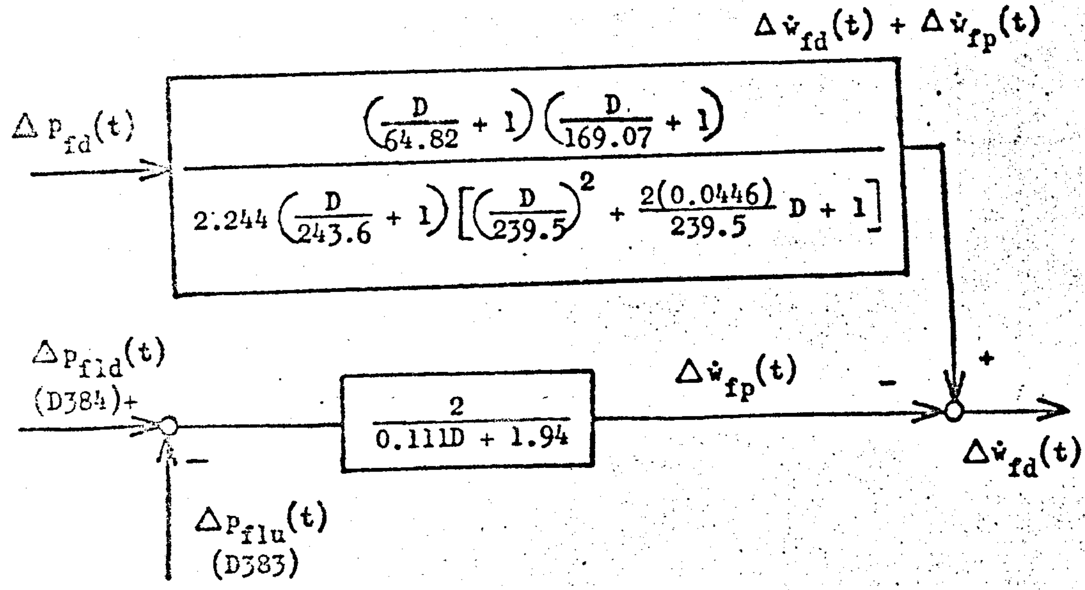

Δp_{fld} = Downstream pressure tap on fuel bypass pulser line (NASA measurement No. D384)

Δp_{flu} = Upstream pressure tap on fuel bypass pulser line (NASA measurement No. D383)

LOX Suction Flowrate Computation.

$$\Delta p_{os}(t) \longrightarrow \boxed{-\frac{\left[\left(\frac{D}{56.88}\right)^2 + \frac{2(0.010)}{56.88}D+1\right]\left[\left(\frac{D}{151.3}\right)^2 + \frac{2(0.0038)}{151.3}D+1\right]\left[\left(\frac{D}{187.12}\right)^2 + \frac{2(0.0031)}{187.12}D+1\right]}{7.5\times10^{-3}\left(\frac{D}{1.154}+1\right)\left[\left(\frac{D}{96.76}\right)^2 + \frac{2(0.006)}{96.76}D+1\right]\left[\left(\frac{D}{168.3}\right)^2 + \frac{2(0.0034)}{168.3}D+1\right]\left[\left(\frac{D}{259.4}\right)^2 + \frac{2(0.002)}{259.4}D+1\right]}} \longrightarrow \Delta\dot{w}_{os}(t)$$

LOX Discharge Flowrate Computation.

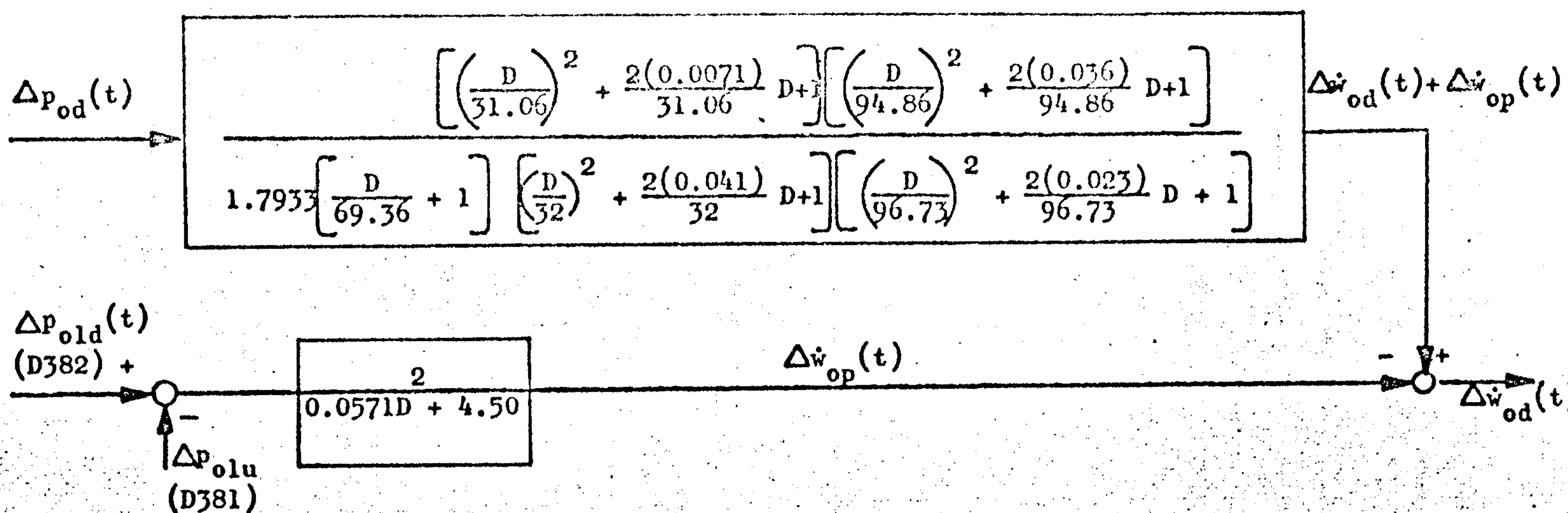

Δp_{old} = downstream pressure tap on LOX bypass pulser line (NASA measurement No. D382)

Δp_{olu} = upstream pressure tap on LOX bypass pulser line (NASA measurement No. D381)

In the above reconstructions, the time records of pressure data shown as inputs were available on magnetic tape.

POGO PUMP TEST DATA EVALUATION

The most obvious features of the dynamic data obtained at the Bobtail facility were the resonances in inlet pressure oscillations that were excited by pulsing. For the LOX pump, these resonances were in the range of 4 to 6 cps; for the fuel pump, the range was 6 to 8 cps. Specific resonant frequencies were dependent on the values of $NPSH_o$ and $NPSH_f$. For each pump, only a single cavitation compliance—line inertance resonance was noted in the pulsing frequency range.

Fuel Pump Self-Driven Oscillations

Significant pressure oscillations not associated with inlet line resonances were noted on fuel pump tests C-006-43 and -44. These pressure oscillations are most apparent in the fuel pump inlet pressure data. They are self-excited and are observed before the pulsing program begins.

For test C-006-43, the frequency of the self-driven oscillations at the pump inlet was 14.5 cps with an amplitude in the range of 5 psi peak-to-peak. The self-driven pump inlet oscillations for test C-006-44 were in the range of 11 to 13 cps with an approximate peak-to-peak amplitude of 12 psi. These tests were conducted at the two lowest $NPSH_f$ levels in the test series. No significant self-driven oscillations were noted at higher $NPSH_f$ values. Rocketdyne experience indicates that such pump self-driven oscillations are nonlinear phenomena. It was noted in test C-006-43 that pulsing at 14 cps resulted in a definite amplification of the 14.5-cps self-driven oscillation. In addition, much of the 7-cps pulsing input power was contributed to reinforcement of the 14.5-cps self-driven oscillation with an attendant loss of power in the linear response to a 7-cps input.

The significance of fuel pump self-driven oscillations for the POGO analysis is twofold:

1. The presence of the self-driven oscillations acted as a strong external noise input and interfered with the determination of fuel pump cavitation compliance at lower $NPSH_f$ levels.
2. Self-driven oscillations should be considered as possible input disturbances when evaluating the overall dynamics of the engine-vehicle system.

Pump Model Selected

The following equations describe the general form of pump description which was used for both the LOX and fuel pump:

$$\Delta p_s = \left(A + \frac{B}{D}\right) \left(\Delta \dot{w}_s - \Delta \dot{w}_d\right) \tag{18}$$

$$\Delta p_d = (1 + J)\, \Delta p_s - R_p\, \Delta \dot{w}_d \tag{19}$$

It is assumed in Eq. 19 that pump speed is held constant. A single integrating element is used to describe cavitation compliance, Eq 18. Only one such term was needed since a single resonance was observed at a given pump inlet for the pulsing frequency range.

The model parameters in Eq. 18 and 19 are treated as unknowns. R_p, the linearized pump resistance, is taken as the absolute value of the slope of ψ vs φ curve for the particular pump (converted into appropriate dimensional form).

The model parameter J is defined as the cavitation gain which is the partial derivative of developed head with respect to suction head, holding pump speed and discharge flowrate constant.

Model parameter B is called the cavitation compliance, which is proportional to an effective spring rate associated with the cavitation bubbles. The term A, which could be called a cavitation resistance, has no strong physical justification. This parameter was incorporated into Eq. 18 primarily to provide an additional degree of freedom into the model, which described bubble compliance. A significant value of A would indicate a dynamic effect other than simple flowrate accumulation.

Computation of Pump Model Parameters

Values of A, B, and J were computed for the LOX and fuel pumps using the POGO pump test data supplied by MSFC. The continuous method of parameter identification developed in Appendix C outlines the theoretical basis of the method. Schematically, the intended application of this technique to a general turbopump is shown in Fig. 6. The terms Y_s and Y_d are the facility suction and discharge admittance functions supplied by MSFC. The steepest descent minimum error optimization loops were designed to adjust the pump model parameters A, B, and J so that the assumed model would correspond with the test data. However, problems associated with the facility discharge admittance functions forced the procedure described above to be modified.

Fuel Pump Cavitation Gain. The presence of two lead terms in the fuel discharge admittance function (page 30) introduced a large amount of noise into the fuel discharge flowrate reconstruction. Even though fourth order Butterworth bandpass filters were used, the presence of this noise resulted in signal-to-noise ratios considerably less than unity. Reasonably accurate determination of J_f using the dynamic data was not possible.

J_f is in theory (Ref. 5) equal to the slope of a developed head vs NPSH curve for constant pump speed and discharge flow. Therefore component test data generated under nominal operating conditions at Rocketdyne's Bravo 2-A facility were fitted with a hyperbola (Fig. 7).

By taking the derivative of the hyperbolic fit with respect to $NPSH_f$, the slope (J_f) as a function of $NPSH_f$ was obtained:

$$J_f = \frac{896.2}{(NPSH_f - 44.7)^2} \tag{20}$$

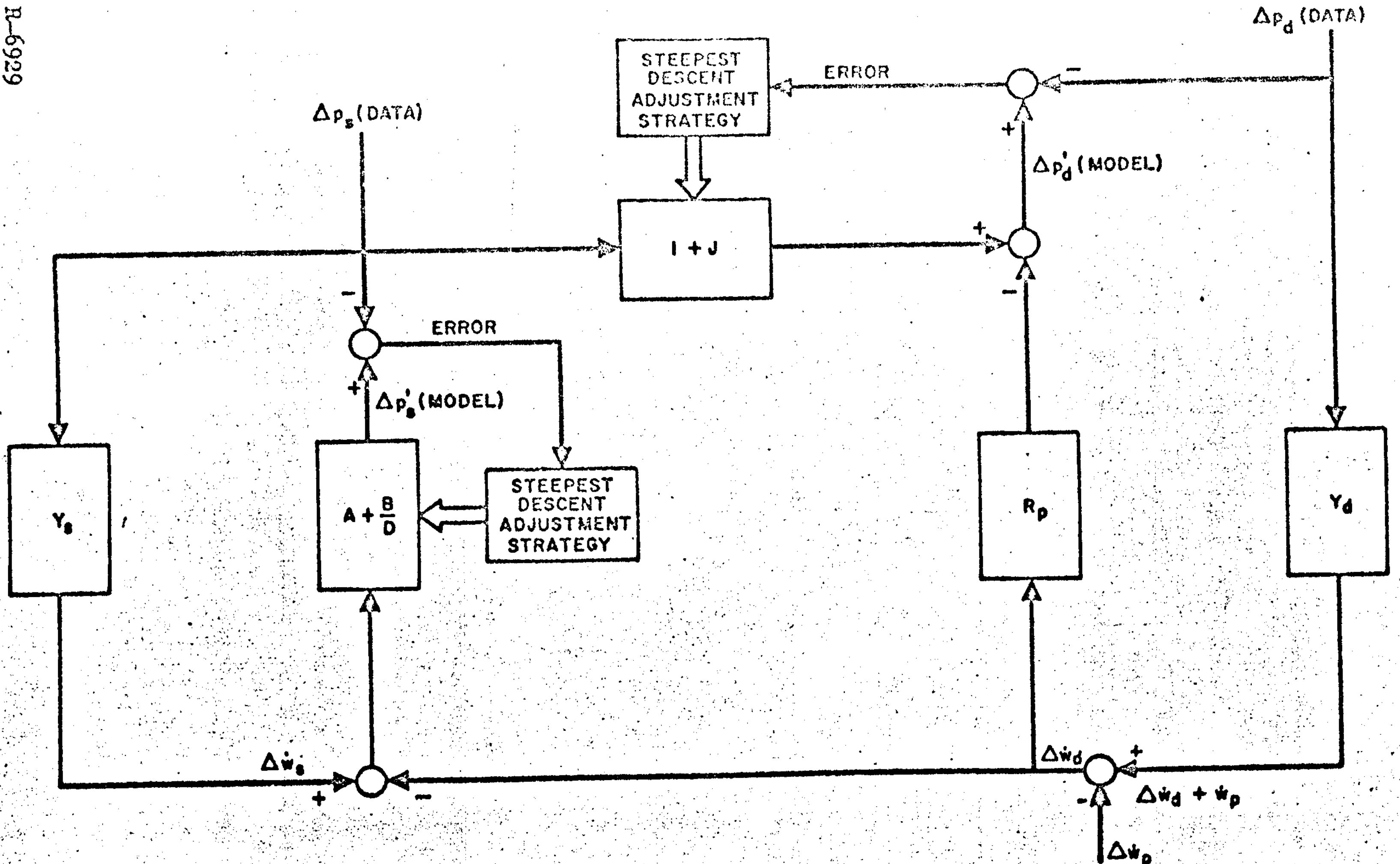

Figure 6. Block Diagram of POGO Pump Test Data Analysis

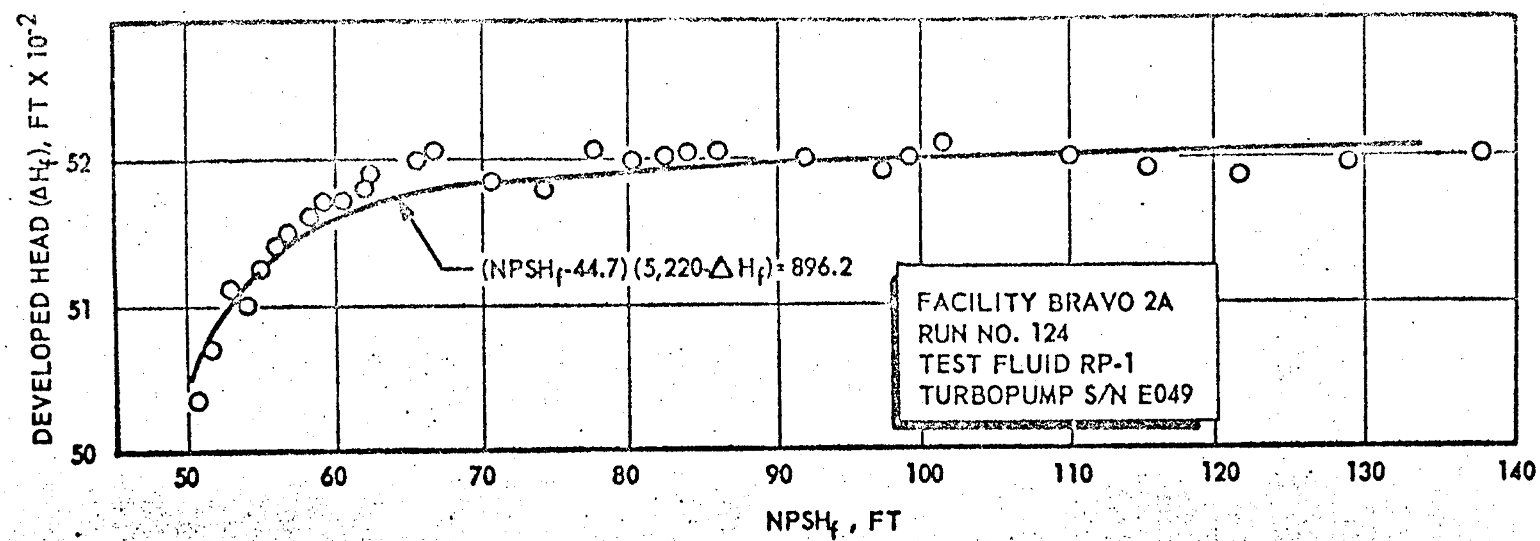

Figure 7. Mark 10 Fuel Pump Developed Head vs NPSH$_f$

Values of J_f for the F-1 POGO tests were computed using the above equation. B_f and A_f were determined by steepest descent optimization as shown in Fig. 6.

LOX Pump Discharge Flowrate Reconstruction. A series of problems were encountered in reconstructing LOX discharge flowrate perturbations. Measurement No. D381 (Δp_{olu}) was found to be defective for tests C-006-41, -45, -48, and -49. It became necessary to construct a correlation between pulser line flowrate ($\Delta \dot{w}_{op}$) and LOX pulser valve position for tests C-006-43, -44, and -50 in order to use valve position data as a means of computing $\Delta \dot{w}_{op}$ for the tests with defective D381 data.

Spectral analysis methods were used to develop the required correlation and excellent results for a reconstructed $\Delta \dot{w}_{op}$ were obtained. Having completed this correlation, reconstruction of pump discharge flowrate ($\Delta \dot{w}_{od}$) was attempted. It became apparent that some discrepancy existed in the facility discharge admittance Y_{od}. The reconstructed $\Delta \dot{w}_{od}$ oscillations were not 180 degrees out of phase with developed head oscillations. The slope of a developed head vs discharge flowrate curve for the Mark 10 turbopump is negative. As developed head increases, discharge flowrate must decrease. The reconstructed $\Delta \dot{w}_{od}$ was found, however, to be almost in phase with the developed head oscillations. This result was obtained using either pulser line flowrate based on the valve position correlation or based on the differential pressure between measurements D381 and D382. After carefully checking computer circuits it was concluded that the method of computing $\Delta \dot{w}_{od}$ shown on page 32 was invalid.

To circumvent the problems discussed above, the following procedure was used to compute discharge flowrate oscillations. Equation 19 may be rewritten as:

$$\Delta \dot{w}_{od} = \frac{-(\Delta p_{od} - [1 + J_o] \Delta p_{os})}{R_{po}} \qquad (21)$$

Equation 21 can be used to compute $\Delta\dot{w}_{od}$ using Δp_{od} and Δp_{os} data if J_o and R_{op} are known. R_{op}, the LOX pump resistance, as previously indicated was found using the slope of the Mark 10 ψ_o vs φ_o curve. J_o was computed in analogous manner to the procedure used in evaluating J_f. $\Delta\dot{w}_{od}$ was then computed using Eq. 21. The results were satisfactory.

Modified Computation of LOX Pump Model Parameters. Suction flowrate perturbations were computed in the normal manner using Y_{os}, the facility admittance function on page 31. Equation 21 was used to evaluate $\Delta\dot{w}_{od}$. With this modification, A_o and B_o then could be determined by steepest descent optimization.

Bravo 2-A data for a Mark 10 LOX pump tested at nominal conditions were fitted with a hyperbola as shown in Fig. 8. Differentiation of the equation for this hyperbola with respect to $NPSH_o$ produces an expression for J_o,

$$J_o = \frac{626.6}{(NPSH_o - 49.15)^2} \tag{22}$$

Values of J_o for the F-1 POGO tests were computed using Eq. 22. These values were used in Eq. 21 to reconstruct discharge flowrate oscillations.

Results of Pump Model Parameter Computations

Table 5 presents the values of A_o, A_f, J_o, and J_f that were determined for the series of F-1 POGO tests. In this table and throughout this report NPSH is defined by:

$$\text{NPSH (feet)} = \frac{[\text{Suction Pressure (psia)} - \text{Vapor Pressure (psia)}] \times 144}{\text{Propellant Density (lb/cu. ft)}} \tag{23}$$

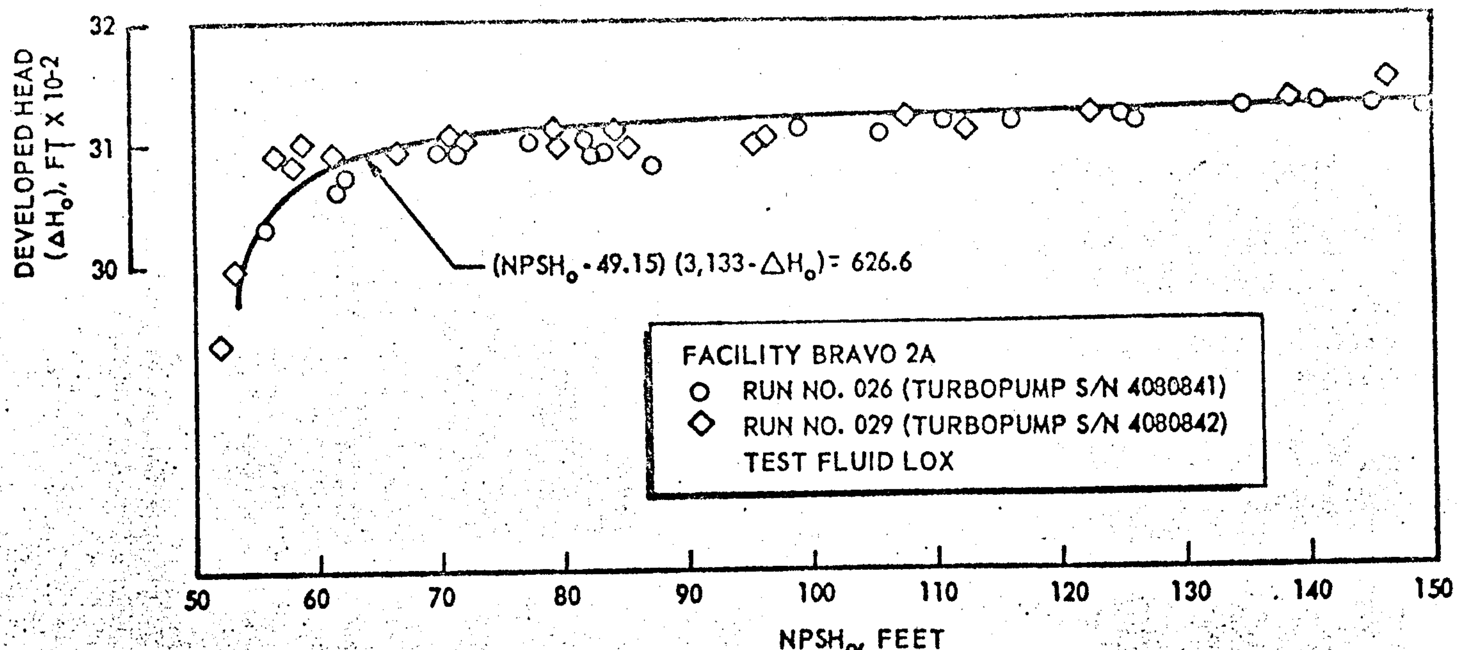

Figure 8. Mark 10 LOX Pump Developed Head vs $NPSH_o$

TABLE 5

VALUES OF A_o, A_f, J_o, and J_f for F-1
POGO TEST SERIES

Test No.	A_o, sec/sq in.	A_f, sec/sq in.	J_o	J_f	$NPSH_o$, feet	$NPSH_f$, feet
C-006-40	0.060	0.022	0.0440	0.105	168.5	137.2
C-006-41	—	0.025	—	0.0596	—	167.3
C-006-43	—	0.019	—	0.189	—	113.6
C-006-44	—	0.025	—	0.644	—	82.0
C-006-45	0.050	0.018	0.313	0.0616	92.6	165.3
C-006-48	0.015	—	0.1214	—	121.0	—
C-006-49	0.025	—	0.0268	—	202.0	—
C-006-50	0.025	—	0.01513	—	252.6	—

The most important parameters that were determined empirically for the pump model are the compliances, B_o and B_f. Figure 9 gives the compliance values B_f vs $NPSH_f$ for the fuel pump tests. Similarly, Fig. 10 presents the results for the LOX pump compliance, B_o.

Nominal Fuel Pump Parameters. The presence of pump self-driven oscillations produced considerable uncertainty in the compliance values found at lower $NPSH_f$ values. In additions, there was a lack of dynamic content in discharge pressure data for test C-006-40 which necessitated driving the fuel admittance function Y_{fd} with a modeled $\Delta p'_{fd}$ (Fig. 6). However, the values of B_f obtained for tests C-006-40, -43, and -44 are relatively consistent. The average value of B_f for these three tests was selected as the nominal compliance value. A nominal value of A_f was obtained by taking the average value over the entire series of fuel pump POGO tests. Nominal J_f was computed using Eq. 20 for a $NPSH_f$ of 128.4 feet.

The nominal fuel pump parameters thus obtained are

$$B_f = 3.37 \text{ l/sq in.}$$

$$A_f = 0.022 \text{ sec/sq in.}$$

$$J_f = 0.128$$

Nominal LOX Pump Parameters. It is apparent from Fig. 10 that no systematic dependence exists between B_o and $NPSH_o$ for the series of LOX pump POGO tests. The reason for this result is the inconsistency found in the LOX pump POGO data. Tests C-006-40 through C-006-45 are characterized by inlet pressure oscillations which are approximately one-half the peak-to-peak value of pressure oscillations observed at corresponding frequencies for the series of tests C-006-48 to C-006-50. The problem appears to be associated with the instrumentation. No change of programmed pulser stroke was made between these series of tests.

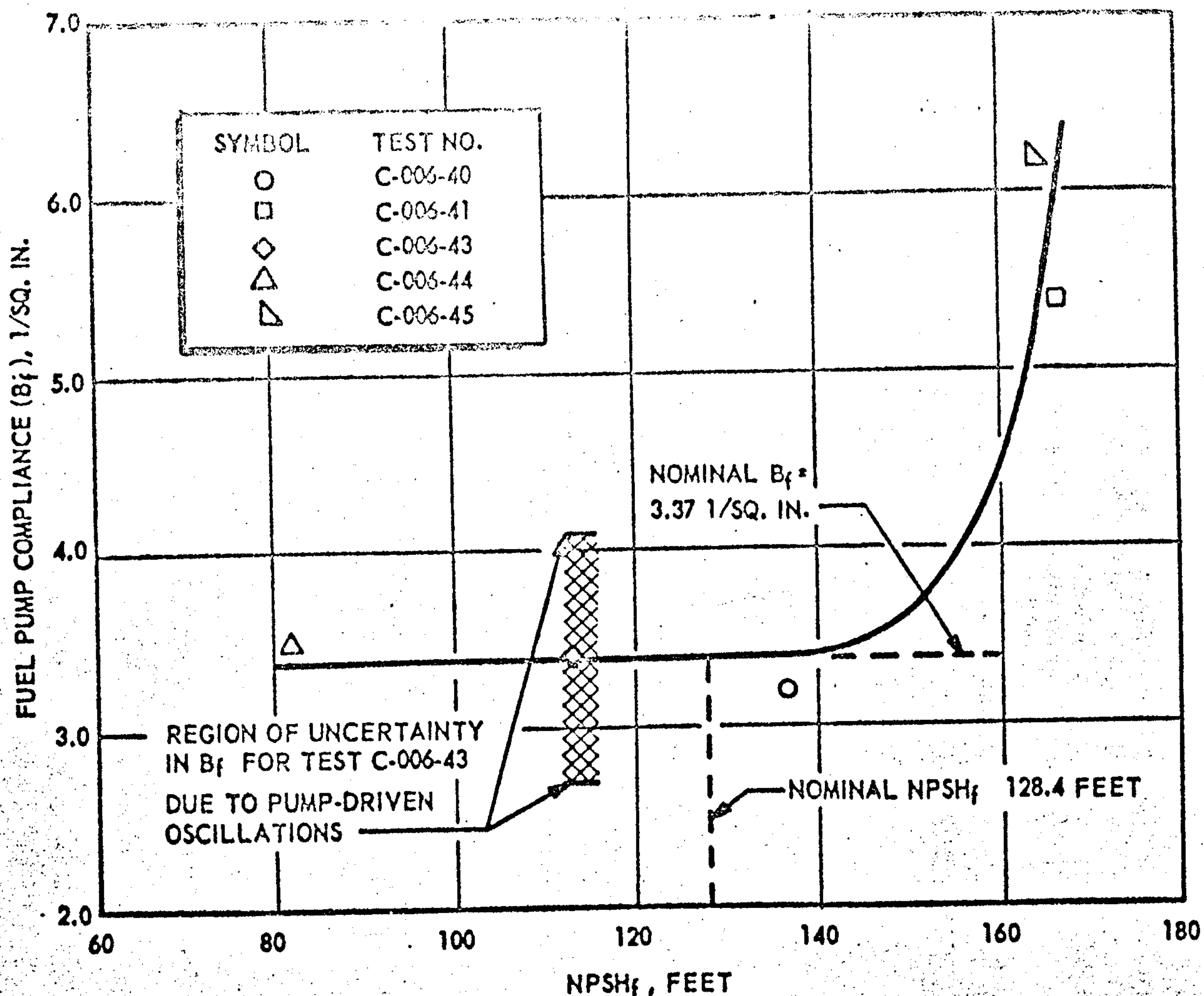

Figure 9. Fuel Pump (Mark 10) Cavitation Compliance vs $NPSH_f$

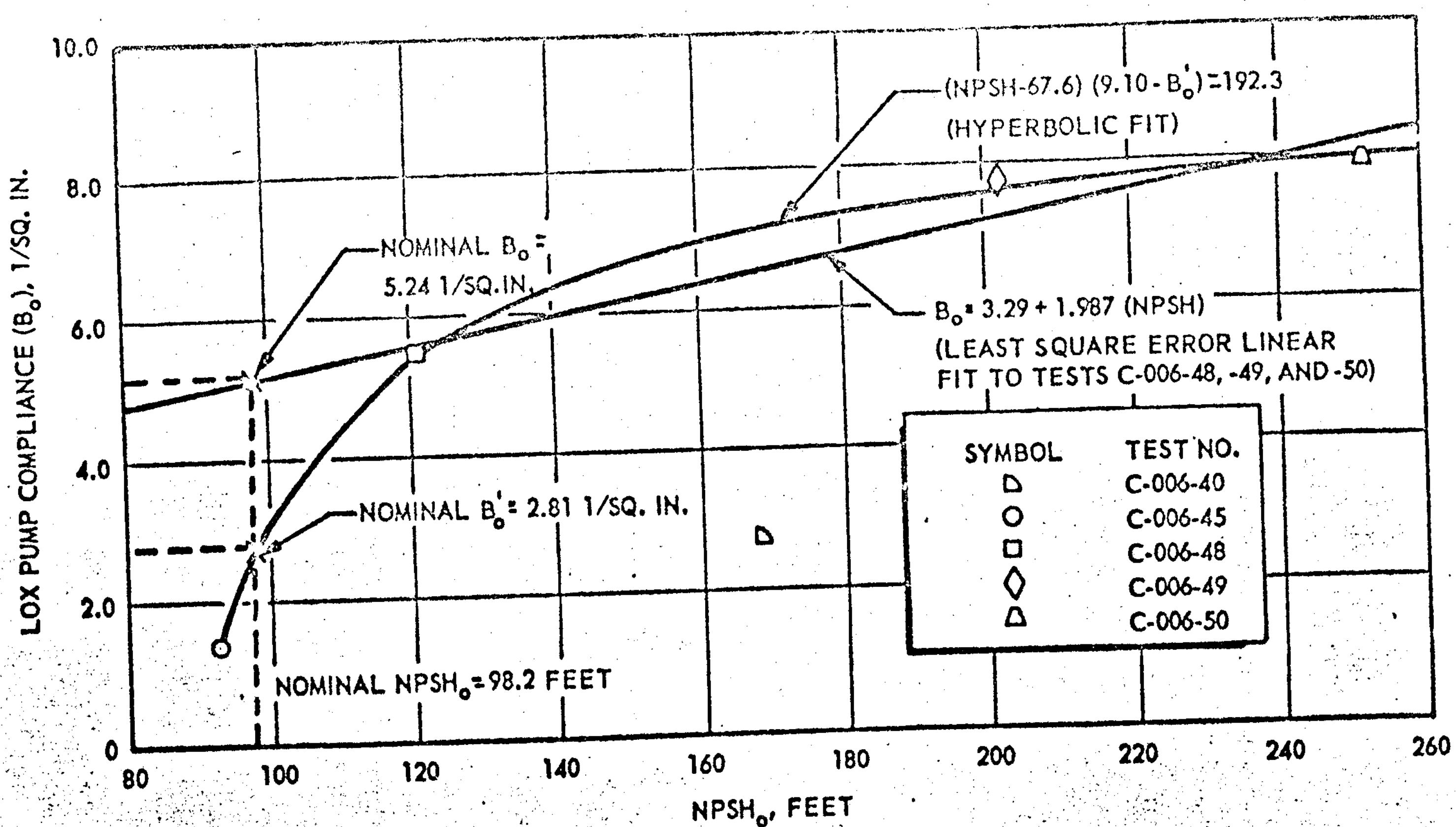

Figure 10. LOX Pump (Mark 10) Cavitation Compliance vs NPSH$_o$

Initially an interpretation of the B_o results was made by assuming that the value for test C-006-40 was invalid. The remaining data were fitted by a hyperbolic curve as indicated in Fig. 10. The resulting nominal value of LOX pump compliance was 2.81 l/sq in. (Bo'). It was concluded that this approach was not realistic. A relatively large value of A_o was found for test C-006-45 (the closest test to nominal $NPSH_o$), which indicated inlet dynamics of a type other than simple mass accumulation.

It was decided, therefore, to place emphasis on the compliance values computed for tests C-006-48, 49, and -50. The residual error between the test data and the pump model was small for these three tests; the corresponding error signals for tests C-006-40 and -45 were large in comparison.

Accordingly, a linear fit was made to the compliance values for tests C-006-48, -49, and -50, which allows the nominal value of B_o to be found by extrapolation. This process results in a nominal value of 5.24 l/sq in. for B_o. It was noted that test C-006-45 indicated that the inlet resonance was between 4 and 4.5 cps, which is assumed to be the range of resonance at a nominal $NPSH_o$ level of 98.2 feet.

The two values of B_o which could be associated with nominal $NPSH_o$ were successively used to terminate the inlet admittance function Y_{os}. This description of the inlet dynamics was driven by a discharge flowrate perturbation and the frequency response which then can be computed is shown in Fig. 11 for the two values of B_o considered.

Using B_o = 5.24 l/sq in. results in an inlet pressure resonance at 4.15 cps, which is in agreement with data from test C-006-45. It is concluded that the best available estimate for nominal LOX compliance, B_o, is given by the linear extrapolation.

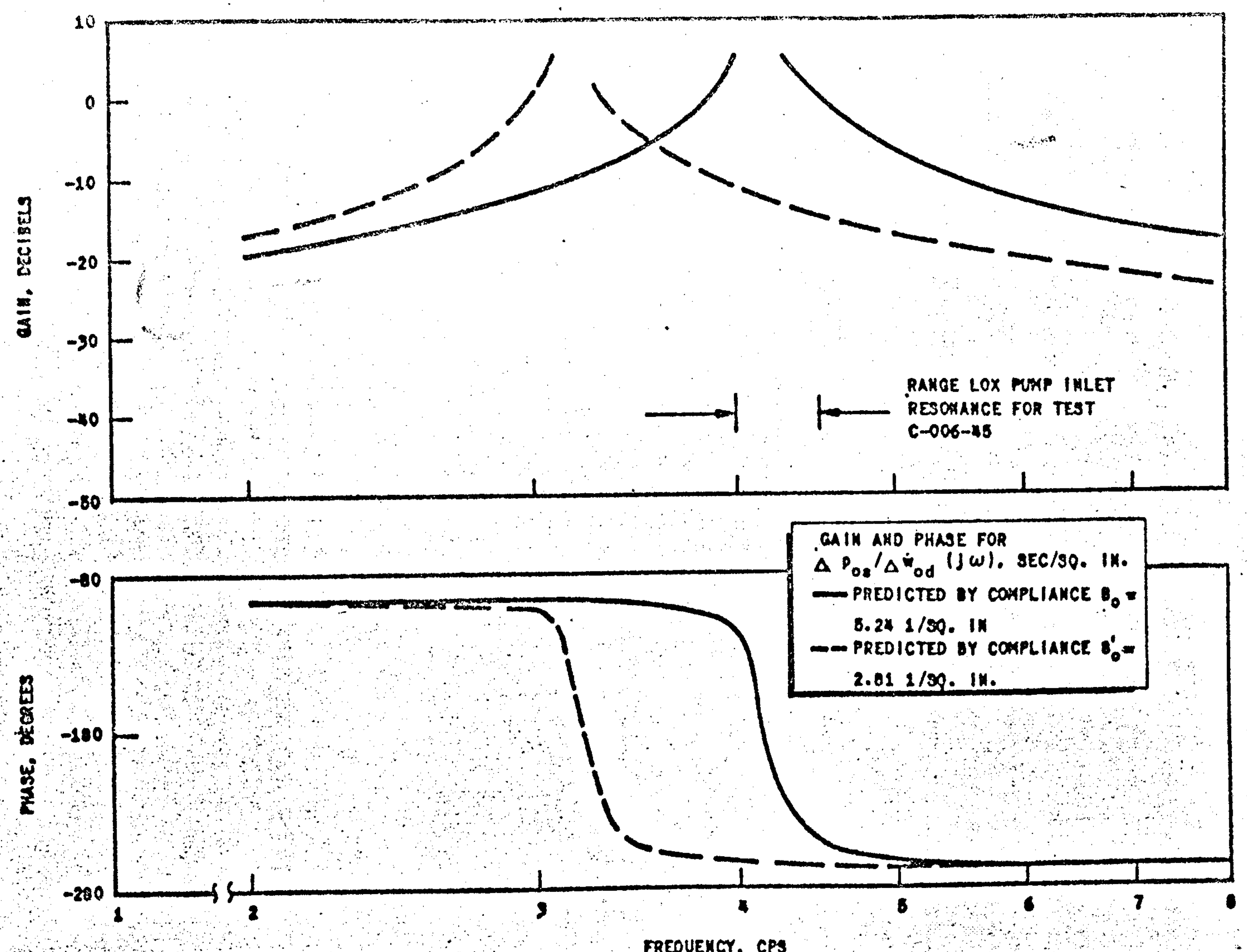

Figure 11. Change in LOX Pump Suction Pressure With Respect to a Change in Discharge Flowrate

A nominal value of A_o was obtained by averaging the values found for tests C-006-48, -49, -50. Nominal J_o was computed using Eq. 22 for a $NPSH_o$ of 98.2 feet. The nominal LOX pump parameters thus obtained are

$$B_o = 5.24 \text{ 1/sq in.}$$
$$A_o = 0.022 \text{ sec/sq in.}$$
$$J_o = 0.261$$

CONCLUSIONS

A large number of problems had to be solved and circumvented to prepare dynamic descriptions of the F-1 LOX and fuel turbopumps. The results obtained inevitably contain a significant degree of uncertainty. However, it is believed that the pump descriptions prepared are the best which are available under the circumstances, and, in fact, are in good agreement with the useable data. The recommended descriptions can be best summarized by the equations which describe the LOX and fuel pump dynamics at nominal NPSH conditions.

LOX Pump

$$\Delta P_{os} = \left(0.022 + \frac{5.24}{s}\right)\left(\Delta \dot{w}_{os} - \Delta \dot{w}_{od}\right) \tag{24}$$
$$\Delta P_{od} = (1 + 0.261)\,\Delta P_{os} - 0.216\,\Delta \dot{w}_{od} \tag{25}$$

Fuel Pump

$$\Delta P_{fs} = \left(0.022 + \frac{3.37}{s}\right)\left(\Delta \dot{w}_{fs} - \Delta \dot{w}_{fd}\right) \tag{26}$$
$$\Delta P_{fd} = (1 + 0.128)\,\Delta P_{fs} - 0.405\,\Delta \dot{w}_{fd} \tag{27}$$

SYSTEM TRANSFER FUNCTIONS

Linearized equations from the section entitled "Analytical Model Development" and the pump models developed in the section entitled "Lox and Fuel Pump Testing and Evaluation" were used to calculate engine system transfer functions. This section presents the following sets of transfer functions:

1. Linear engine model excluding pump cavitation dynamics (interface at pump inlet flanges)
2. Linear engine model including pump cavitation dynamics (interface at pump inlet flanges)
3. Engine system structural transfer functions

The frequency response data obtained in the above fluid system transfer functions were digitally curve fitted to obtain pole-zero form transfer functions. The curve fit technique used the least-square error criterion. The pole-zero transfer functions (in unnormalized form), the model Bode plots, and the data points showing their fitted approximations are included in this section.

LINEAR ENGINE MODEL

The interface for this model is at the pump inlet flange. The engine transfer function relates thrust and pump discharge flowrates to ΔP_{os} and ΔP_{fs} (Fig. 12). The curve fitted approximations of these functions are itemized in Table 6. Figures 13 through 18 show the system Bode plots and their fitted approximations.

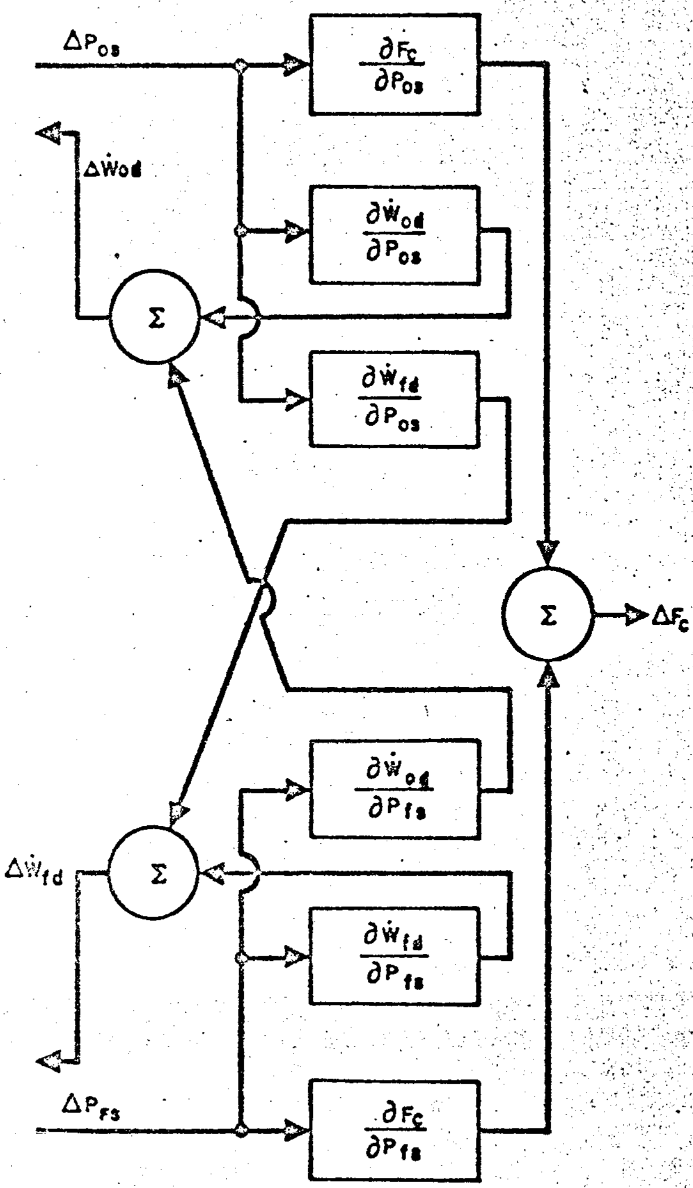

NOTE: Cavitation dynamics not included therefore, $\dot{W}_{od} \equiv \dot{W}_{os}$ and $\dot{W}_{fd} \equiv \dot{W}_{fs}$ in the above diagram

Figure 12. Linear Engine Model Block Diagram

TABLE 6

LINEAR ENGINE MODEL TRANSFER FUNCTIONS
EXCLUDING PUMP CAVITATION DYNAMICS*

$$\frac{\partial F_c}{\partial P_{os}} = \frac{1128.83 \left(1 + \frac{s}{18.51}\right)}{\left(1 + \frac{s}{6.193}\right)\left(1 + \frac{2(0.826)s}{390.4} + \frac{s^2}{(390.4)^2}\right)} \quad \frac{\text{lb}}{\text{lb/in.}^2}$$

$$\frac{\partial \dot{W}_{os}}{\partial P_{os}} = \frac{3.1472 \left(1 + \frac{s}{13.27}\right)}{\left(1 + \frac{s}{6.214}\right)\left(1 + \frac{s}{362.4}\right)} \quad \frac{\text{lb/sec}}{\text{lb/in.}^2}$$

$$\frac{\partial \dot{W}_{fs}}{\partial P_{os}} = \frac{0.5381 \left(1 - \frac{s}{16.32}\right)}{\left(1 + \frac{s}{6.138}\right)\left(1 + \frac{s}{153.9}\right)\left(1 + \frac{2(0.702)s}{457.5} + \frac{s^2}{(457.5)^2}\right)} \quad \frac{\text{lb/sec}}{\text{lb/in.}^2}$$

$$\frac{\partial F_c}{P_{fs}} = \frac{-216.46 \left(1 - \frac{s}{12.21}\right)\left(1 + \frac{s}{240.4}\right)}{\left(1 + \frac{s}{5.608}\right)\left(1 + \frac{s}{174.6}\right)\left(1 + \frac{2(0.567)s}{546.5} + \frac{s^2}{(546.5)^2}\right)} \quad \frac{\text{lb}}{\text{lb/in.}^2}$$

$$\frac{\partial \dot{W}_{os}}{\partial P_{fs}} = \frac{-1.2558 \left(1 + \frac{s}{32.49}\right)}{\left(1 + \frac{s}{6.168}\right)\left(1 + \frac{s}{100.4}\right)\left(1 + \frac{2(0.440)s}{552.7} + \frac{s^2}{(552.7)^2}\right)} \quad \frac{\text{lb/sec}}{\text{lb/in.}^2}$$

$$\frac{\partial \dot{W}_{fs}}{\partial P_{fs}} = \frac{0.36231 \left(1 + \frac{s}{1.644}\right)\left(1 + \frac{s}{149.7}\right)}{\left(1 + \frac{s}{6.204}\right)\left(1 + \frac{s}{97.3}\right)\left(1 + \frac{s}{721.6}\right)} \quad \frac{\text{lb/sec}}{\text{lb/in.}^2}$$

*All capitalized symbols in this table represent variables in the Laplace domain.
$\dot{W}_{od} \equiv \dot{W}_{os}$ and $\dot{W}_{sd} \equiv \dot{W}_{fs}$

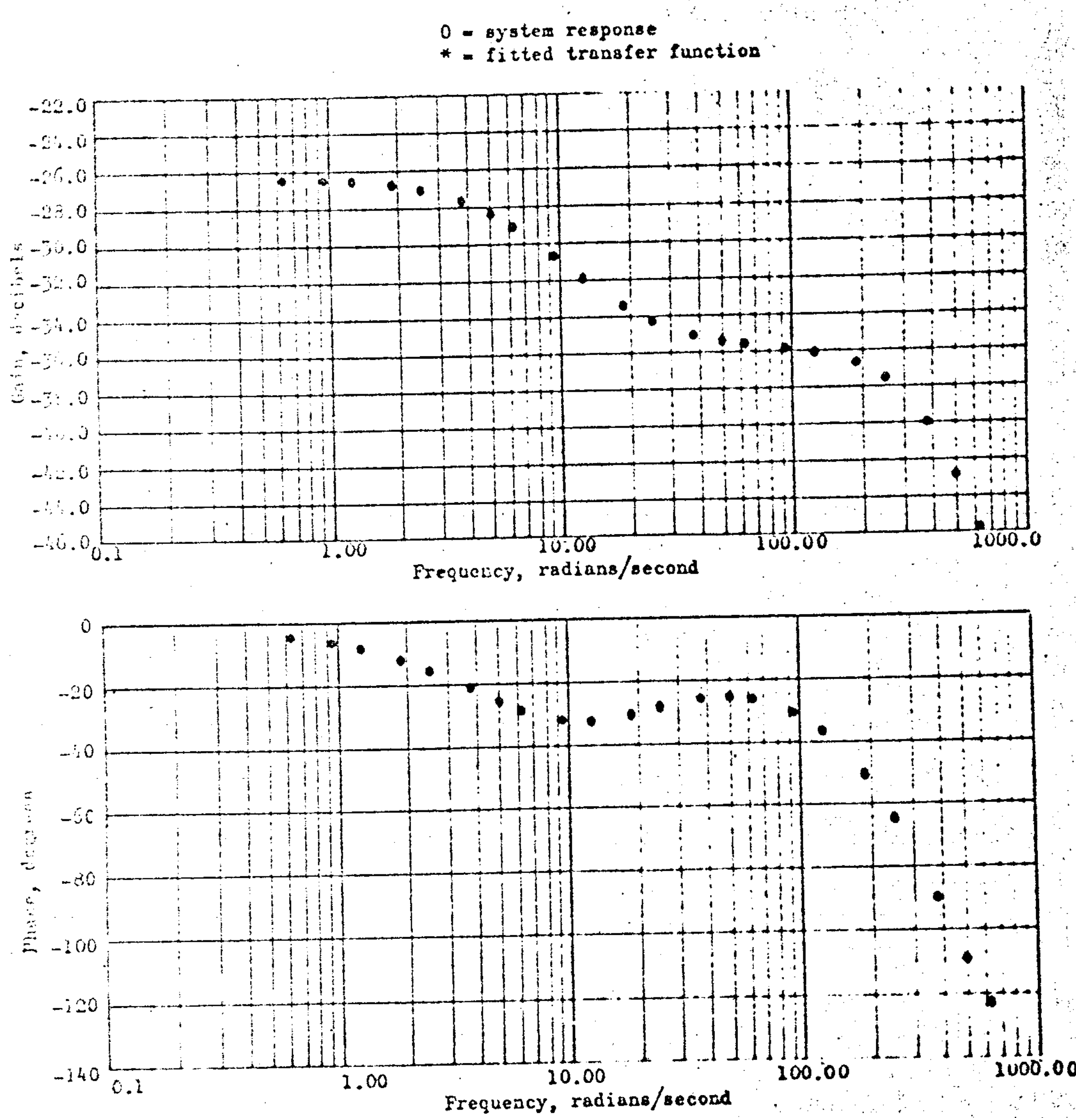

$$\frac{\widetilde{F}_c}{\widetilde{P}_{os}} = \frac{0.04821\left(1 + \frac{s}{18.51}\right)}{\left(1 + \frac{s}{6.193}\right)\left(1 + \frac{2(0.826)s}{390.4} + \frac{s^2}{(390.4)^2}\right)}, \text{ (Dimensionless)}$$

$$\overline{F}_c/\overline{P}_{os} = 2.3415 \times 10^4 \text{ lb/lb/in.}^2$$

Figure 13. Change in Thrust With Respect to a Change in LOX Pump Inlet Pressure

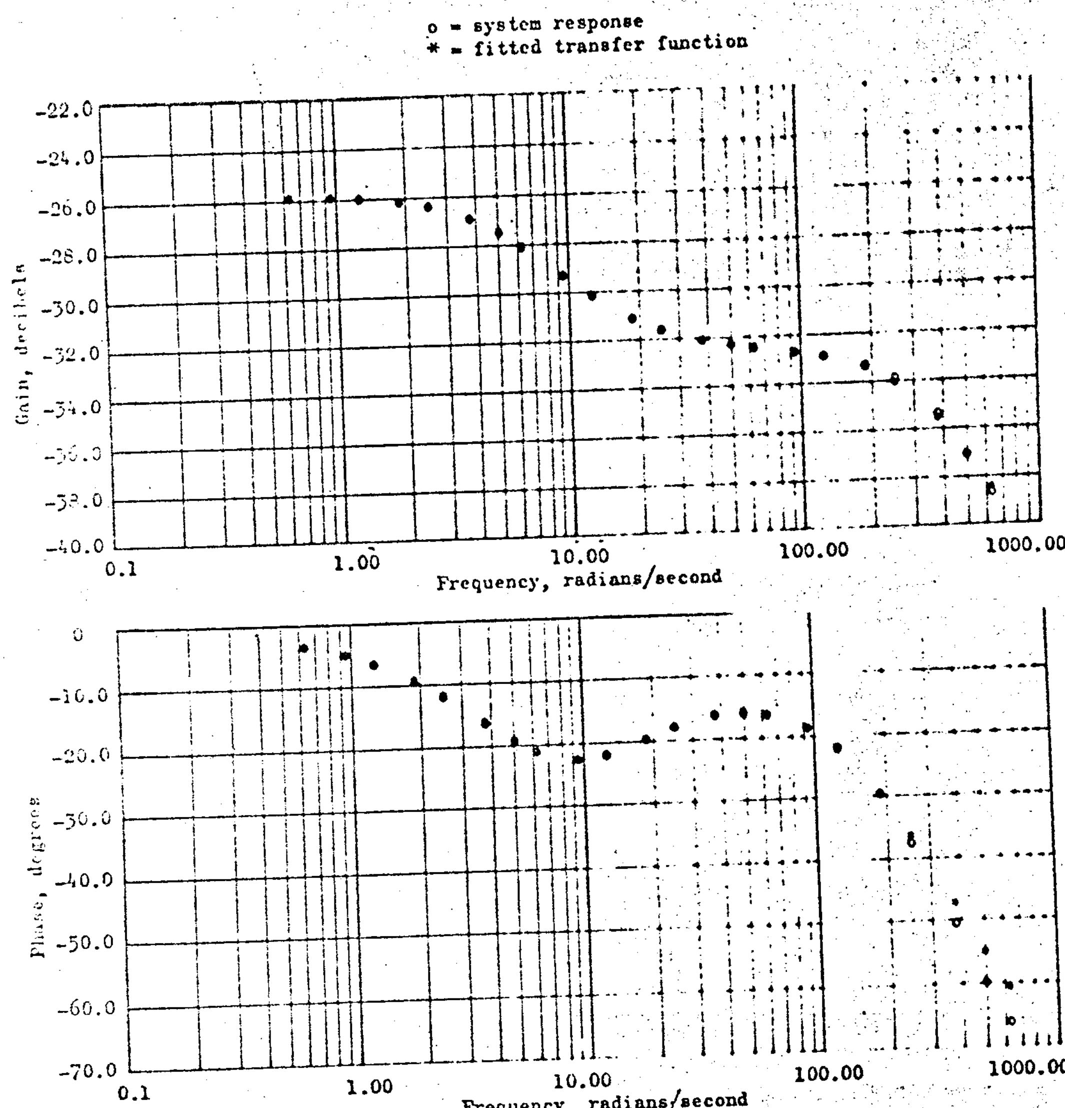

$$\frac{\tilde{\dot{W}}_{od}}{\tilde{P}_{os}} = \frac{0.05140\left(1 + \frac{s}{13.27}\right)}{\left(1 + \frac{s}{6.214}\right)\left(1 + \frac{s}{362.4}\right)}, \text{ (Dimensionless)}$$

$$\frac{\overline{W}_{od}}{\overline{P}_{os}} = 6.1230 \times 10^{1} \text{ lb/sec/lb/in.}^2$$

Figure 14. Change in LOX Pump Discharge Flowrate With Respect to a Change in LOX Pump Inlet Pressure

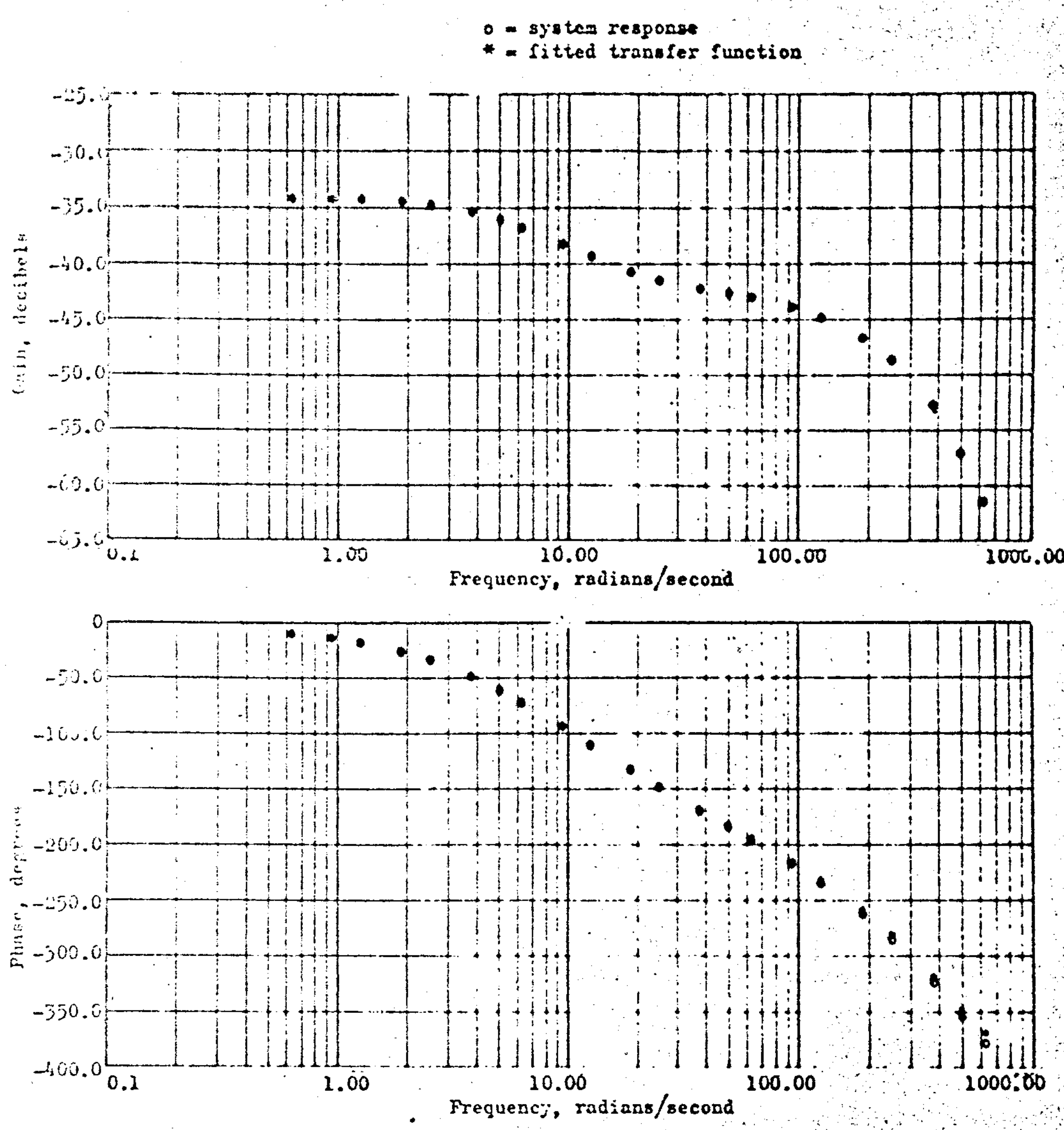

$$\frac{\tilde{\dot{W}}_{fd}}{\tilde{P}_{os}} = \frac{0.01993\left(1 - \frac{s}{16.32}\right)}{\left(1 + \frac{s}{6.158}\right)\left(1 + \frac{s}{153.9}\right)\left(1 + \frac{2(0.702)s}{457.5} + \frac{s^2}{(457.5)^2}\right)}, \text{ (Dimensionless)}$$

$$\frac{\bar{\dot{W}}_{fd}}{\bar{P}_{os}} = 2.700 \times 10^1 \text{ lb/sec/lb/in.}^2$$

Figure 15. Change in Fuel Pump Discharge Flowrate With Respect to a Change in LOX Pump Inlet Pressure

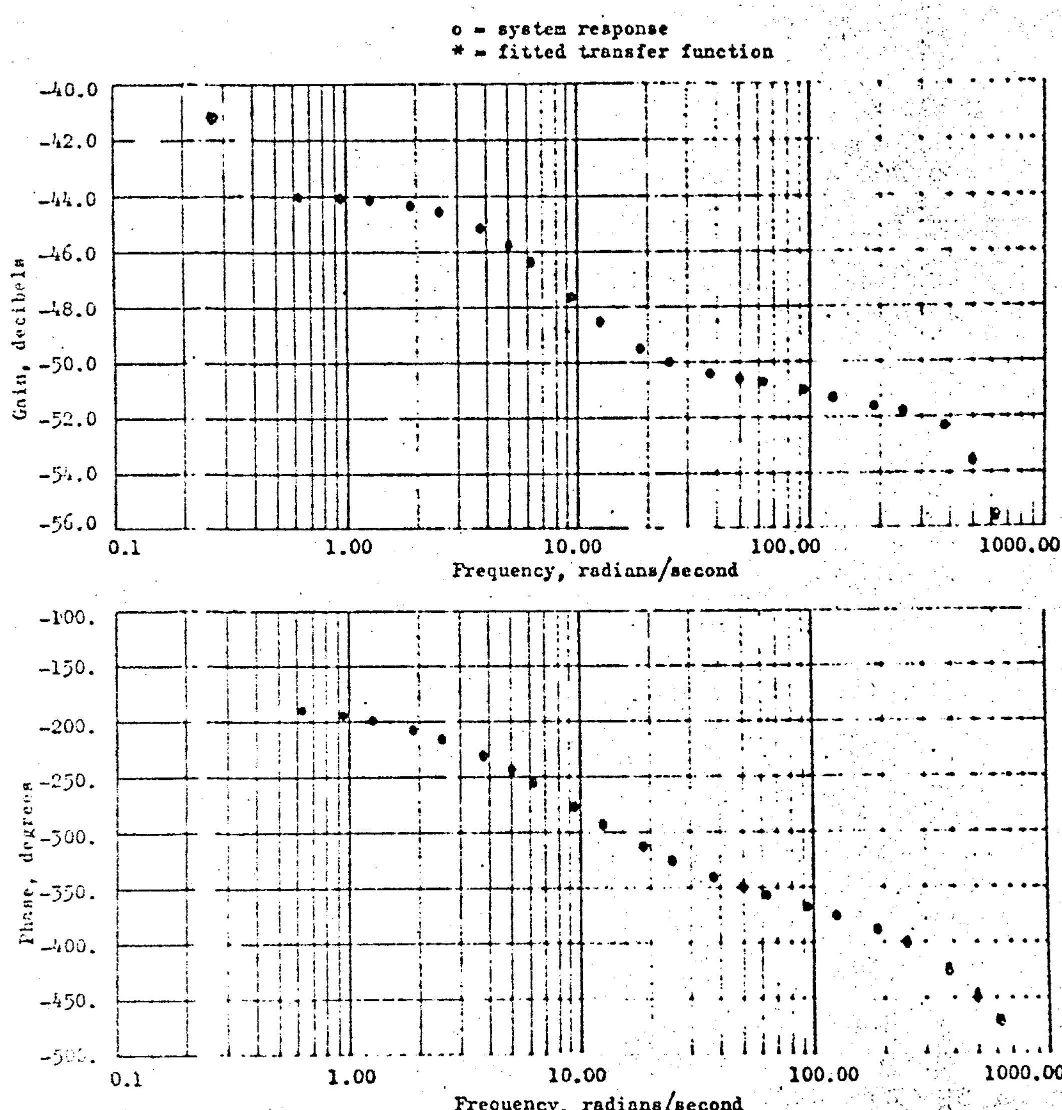

$$\frac{\tilde{F}_c}{\tilde{P}_{fs}} = \frac{-0.00640\left(1 - \frac{s}{12.21}\right)\left(1 + \frac{s}{240.4}\right)}{\left(1 + \frac{s}{5.608}\right)\left(1 + \frac{s}{174.6}\right)\left(1 + \frac{2(0.567)s}{546.5} + \frac{s^2}{(546.5)^2}\right)}, \text{ (Dimensionless)}$$

$$\frac{\overline{F}_c}{\overline{P}_{fs}} = 3.3822 \times 10^4 \text{ lb/lb/in.}^2$$

Figure 16. Change in Thrust With Respect to a Change in Fuel Pump Inlet Pressure

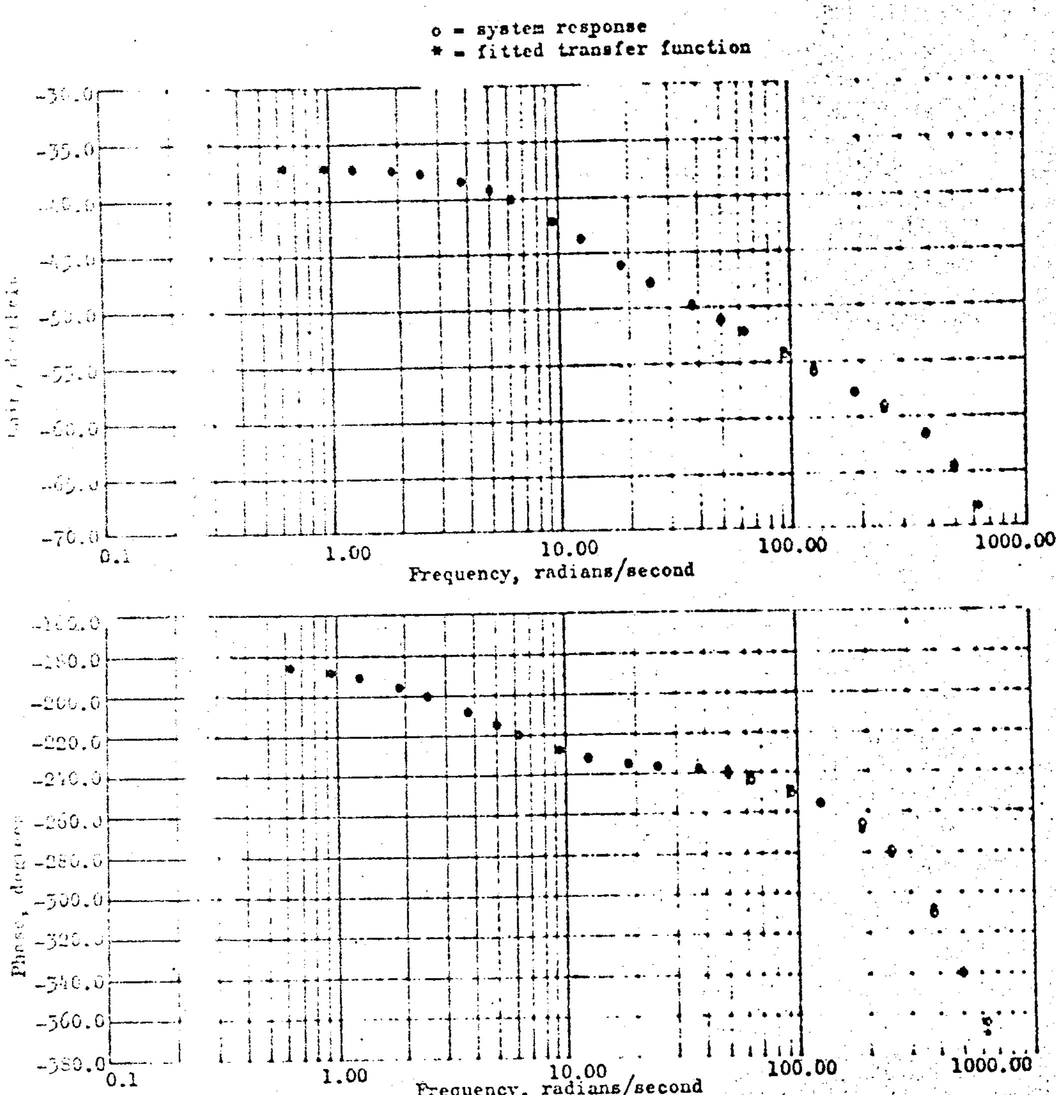

$$\frac{\tilde{W}_{od}}{\tilde{P}_{fs}} = \frac{-0.01420\left(1 + \frac{s}{32.49}\right)}{\left(1 + \frac{s}{0.168}\right)\left(1 + \frac{s}{100.4}\right)\left(1 + \frac{2(0.440)s}{552.7} + \frac{s^2}{(552.7)^2}\right)}, \text{ (Dimensionless)}$$

$$\frac{\overline{W}_{od}}{\overline{P}_{fs}} = 8.844 \times 10^1 \text{ lb/sec/lb/in.}^2$$

Figure 17. Change in LOX Pump Discharge Flowrate With Respect to a Change in Fuel Pump Inlet Pressure

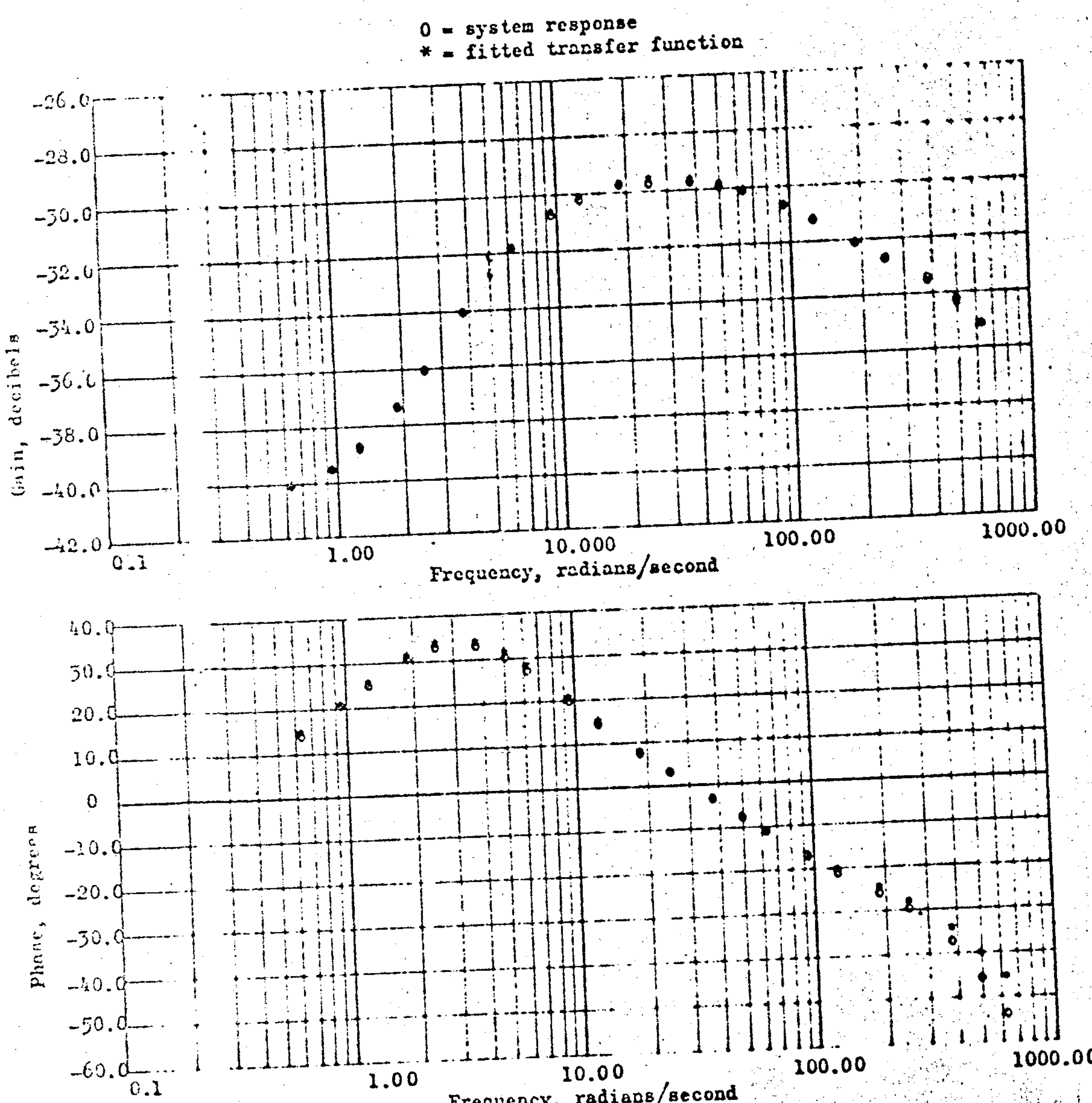

$$\frac{\tilde{W}_{fd}}{\tilde{P}_{fs}} = \frac{0.00929\left(1 + \frac{s}{1.644}\right)\left(1 + \frac{s}{149.7}\right)}{\left(1 + \frac{s}{6.204}\right)\left(1 + \frac{s}{97.3}\right)\left(1 + \frac{s}{721.6}\right)}, \text{ (Dimensionless)}$$

$$\frac{\bar{\dot{W}}_{fd}}{\bar{P}_{fs}} = 3.900 \times 10^{1} \text{ lb/sec/lb/in.}^2$$

Figure 18. Change in Fuel Pump Discharge Flowrate With Respect to a Change in Fuel Pump Inlet Pressure

The transfer functions presented are questionable above 220 radians per second. This limitation is due to the lumped parameter description of the high-pressure piping. Acoustic modes were not considered.

The values of J_f and J_o used in the model are respectively 0.261 and 0.126. These are the values calculated at mainstage NPSH. ("LOX and Fuel Pump Testing and Evaluation" section: Eq. 20 and 22.) Small linear corrections were applied to the Bode gains (fuel side driven) to establish closer agreement with the steady-state influence coefficients.

LINEAR ENGINE MODEL INCLUDING PUMP CAVITATION DYNAMICS

Identification of LOX and fuel pump dynamics was performed empirically. (LOX and Fuel Pump Testing and Evaluation section.) A block diagram of a typical pump is shown below.

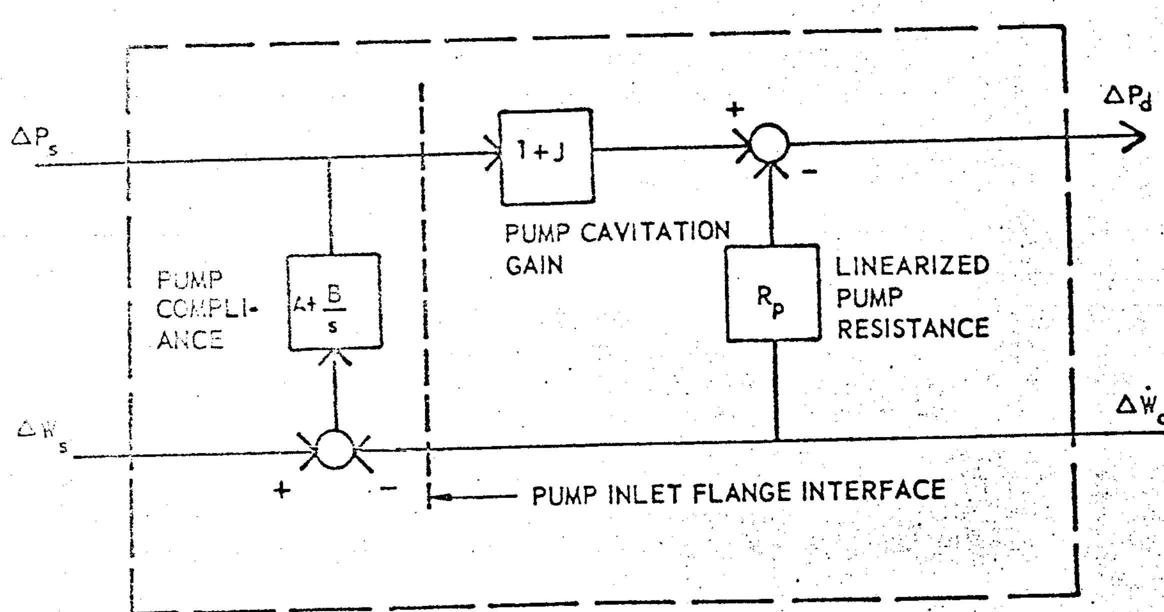

The equations which describe the pump at constant speed were developed and discussed in the prior section and are repeated below.

LOX Pump

$$\Delta p_{os} = \left(0.022 + \frac{5.24}{s}\right)\left(\Delta \dot{w}_{os} - \Delta \dot{w}_{od}\right) \tag{24}$$

$$\Delta p_{od} = (1 + 0.261)\Delta p_{os} - 0.216\Delta \dot{w}_{od} \tag{25}$$

Fuel Pump

$$\Delta p_{fs} = \left(0.022 + \frac{3.37}{s}\right)\left(\Delta \dot{w}_{fs} - \Delta \dot{w}_{fd}\right) \tag{26}$$

$$\Delta p_{fd} = (1 + 0.128)\Delta p_{fs} - 0.405\Delta \dot{w}_{fd} \tag{27}$$

The above equations apply at mainstage NPSH conditions. Equations 25 and 27 along with a description of speed variations were incorporated into the preceding engine system transfer functions entitled "Linear Engine Model".

Equations 24 and 26 represent the effect of cavitation compliance dynamics. The variables in these four equations were first normalized with respect to their mainstage value. Then they were combined with the linear engine model in order to prepare a description of engine system dynamics. including pump cavitation effects for mainstage conditions. The resultant system of transfer functions (shown unnormalized) relate thrust and pump inlet pressures to $\Delta \dot{W}_{os}$ and $\Delta \dot{W}_{fs}$ (Fig. 19). The curve fitted approximations of these functions are itemized in Table 7. Figures 20 through 25 show the system Bode plots and their fitted approximations. LOX and fuel pump inlet resonances were found to be in the range of 25.1 to 50.2 rps (4 to 8 cps). This frequency range corresponds to the highest signal-to-noise ratios observed in the Bobtail test data and is therefore

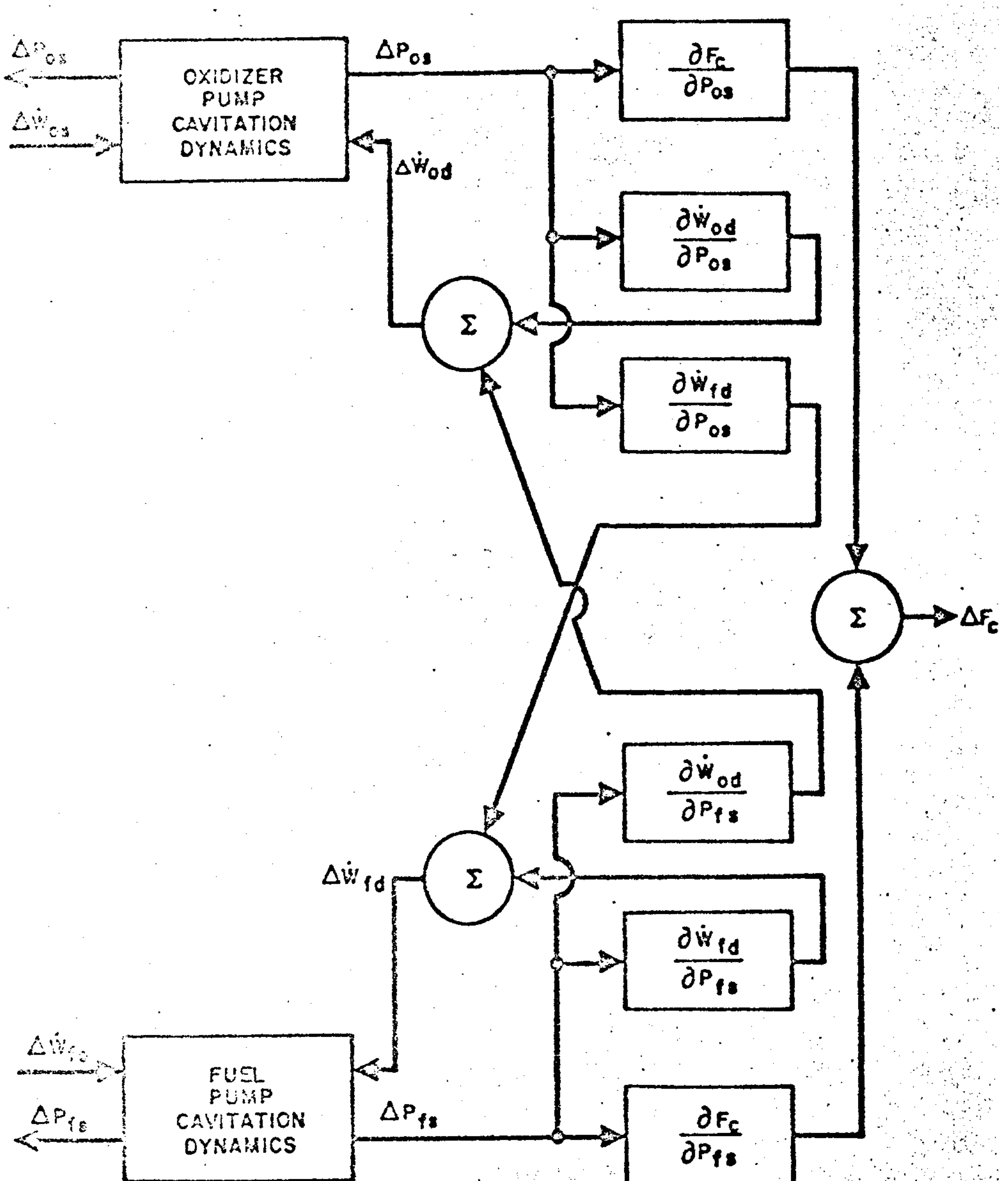

Figure 19. Linear Engine Model Including Pump Dynamics

TABLE 7

LINEAR ENGINE MODEL TRANSFER FUNCTIONS
INCLUDING PUMP CAVITATION DYNAMICS*

$$\frac{\partial F_c}{\partial \dot{W}_{os}} = \frac{293.57\left(1+\frac{s}{1034.0}\right)\left(1+\frac{s}{173.2}\right)}{\left(1+\frac{s}{383.4}\right)\left(1+\frac{s}{382.0}\right)\left(1+\frac{s}{696.1}\right)\left(1+\frac{s}{2.781}\right)} \quad \frac{\text{lb}}{\text{lb/sec}}$$

$$\frac{\partial P_{os}}{\partial \dot{W}_{os}} = \frac{1.298\left(1+\frac{s}{235.4}\right)}{\left(1+\frac{s}{3.972}\right)} \quad \frac{\text{lb/in.}^2}{\text{lb/sec}}$$

$$\frac{\partial P_{fs}}{\partial \dot{W}_{os}} = \frac{0.8309\left(1+\frac{s}{205.1}\right)}{\left(1+\frac{2\,(1.029)s}{3.345}+\frac{s^2}{(3.345)^2}\right)} \quad \frac{\text{lb/in.}^2}{\text{lb/sec}}$$

$$\frac{\partial F_c}{\partial \dot{W}_{fs}} = \frac{167.06\left(1+\frac{s}{230.9}\right)\left(1-\frac{s}{834.7}\right)}{\left(1+\frac{s}{2.231}\right)\left(1+\frac{s}{662.9}\right)} \quad \frac{\text{lb}}{\text{lb/sec}}$$

$$\frac{\partial P_{os}}{\partial \dot{W}_{fs}} = \frac{0.1537\left(1+\frac{s}{196.5}\right)\left(1-\frac{s}{874.3}\right)}{\left(1+\frac{s}{764.8}\right)\left(1+\frac{2(1.001)s}{3.273}+\frac{s^2}{(3.273)^2}\right)} \quad \frac{\text{lb/in.}^2}{\text{lb/sec}}$$

$$\frac{\partial P_{fs}}{\partial \dot{W}_{fs}} = \frac{1.251\left(1+\frac{s}{149.4}\right)}{\left(1+\frac{s}{2.636}\right)} \quad \frac{\text{lb/in.}^2}{\text{lb/sec}}$$

*All capitalized symbols in this table represent variables in the Laplace domain.

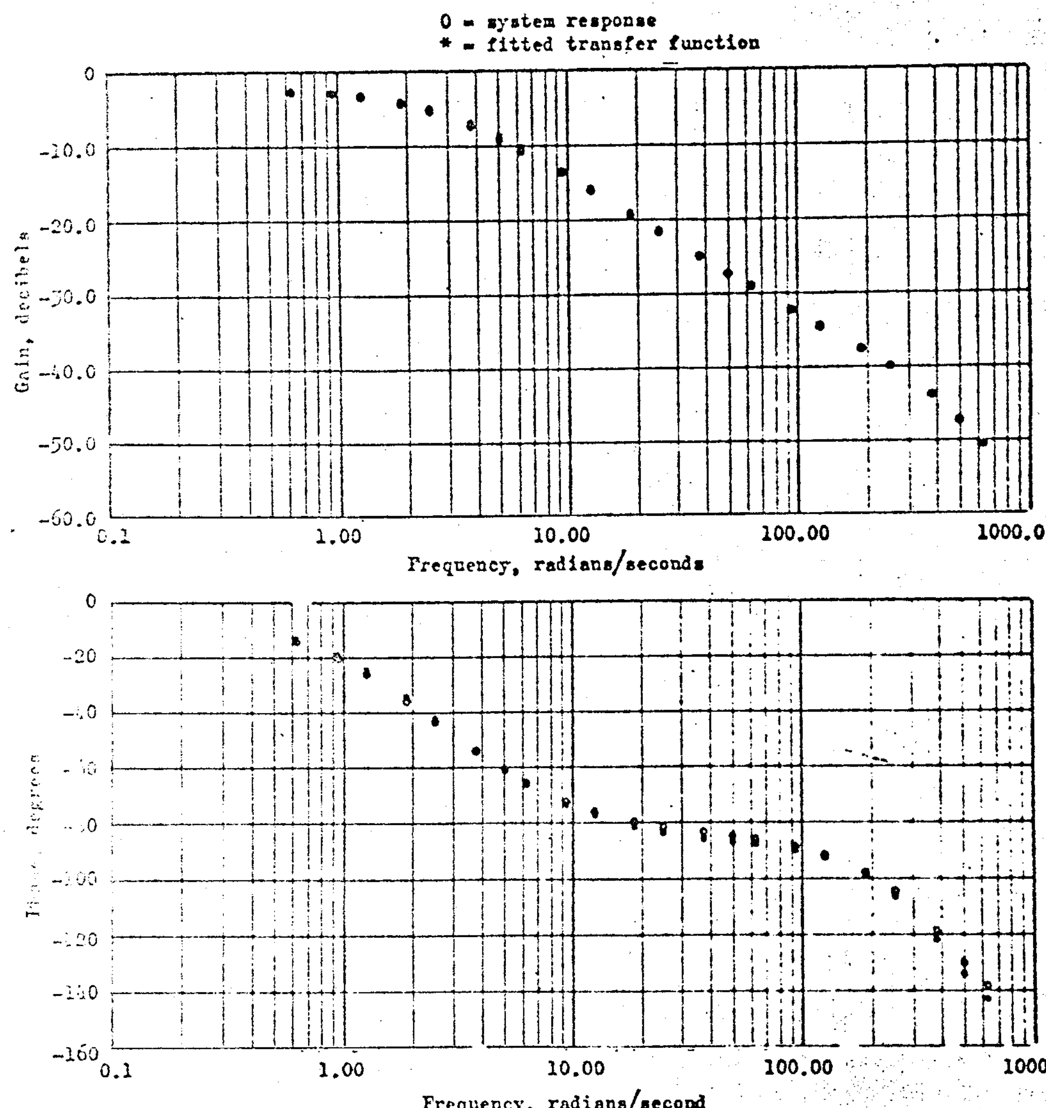

$$\frac{\tilde{F}_c}{\tilde{W}_{os}} = \frac{0.76750\left(1 + \frac{s}{1034.0}\right)\left(1 + \frac{s}{173.2}\right)}{\left(1 + \frac{s}{383.4}\right)\left(1 + \frac{s}{382.0}\right)\left(1 + \frac{s}{696.1}\right)\left(1 + \frac{s}{2.781}\right)}, \text{ (dimensionless)}$$

$$\frac{\overline{F}_c}{\overline{W}_{os}} = 3.825 \times 10^2 \ \frac{\text{lb}}{\text{lb/sec}}$$

Figure 20. Change in Thrust With Respect to a Change in LOX Pump Inlet Flowrate

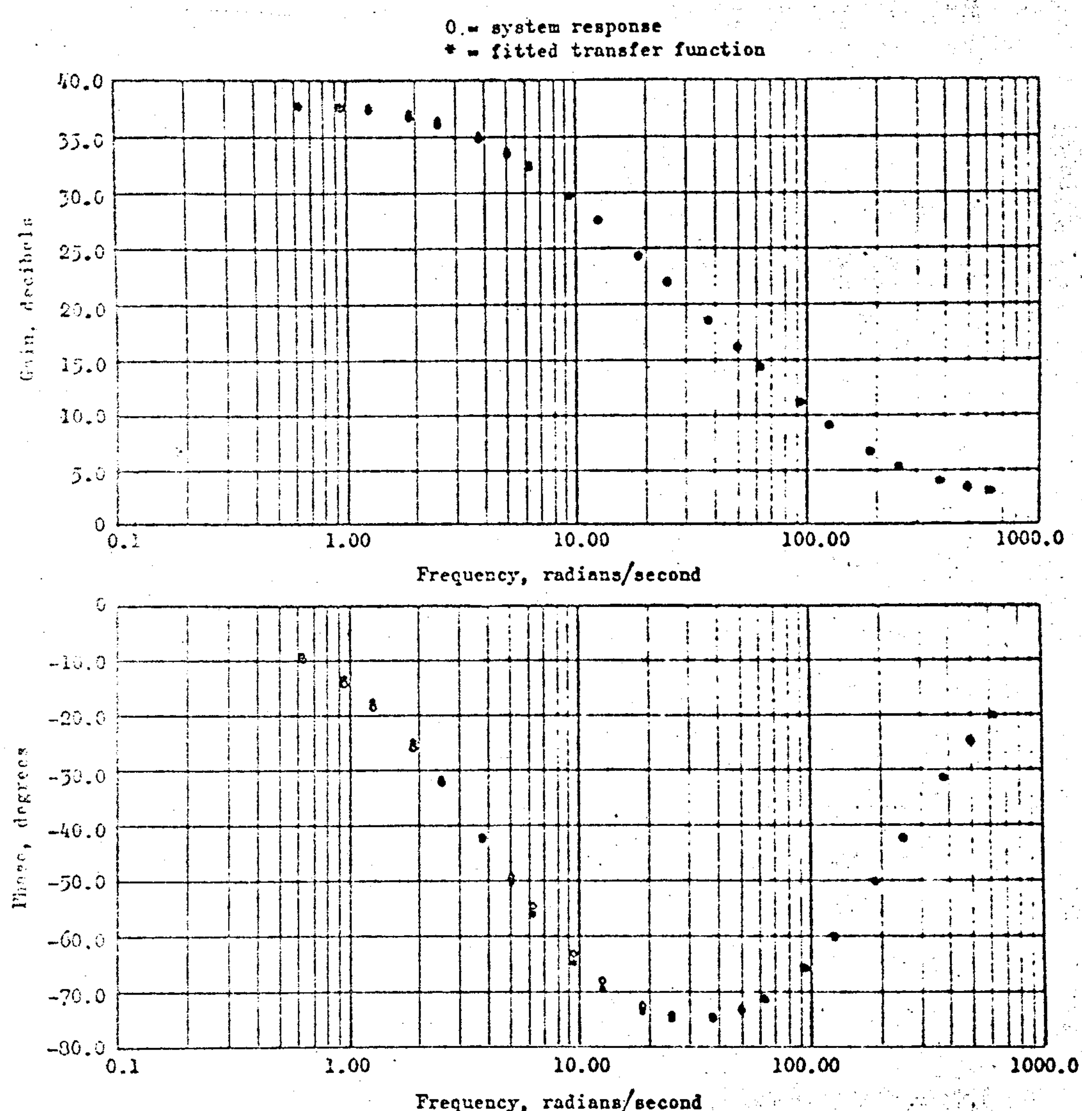

$$\frac{\tilde{P}_{os}}{\tilde{\dot{W}}_{os}} = \frac{79.62\left(1 + \frac{s}{235.4}\right)}{\left(1 + \frac{s}{3.972}\right)}, \text{ (dimensionless)}$$

$$\frac{\bar{P}_{os}}{\bar{\dot{W}}_{os}} = 1.633 \times 10^{-2} \frac{\text{lb/in.}^2}{\text{lb/sec}}$$

Figure 21. Change in LOX Pump Inlet Pressure With Respect to a Change in LOX Pump Inlet Flowrate

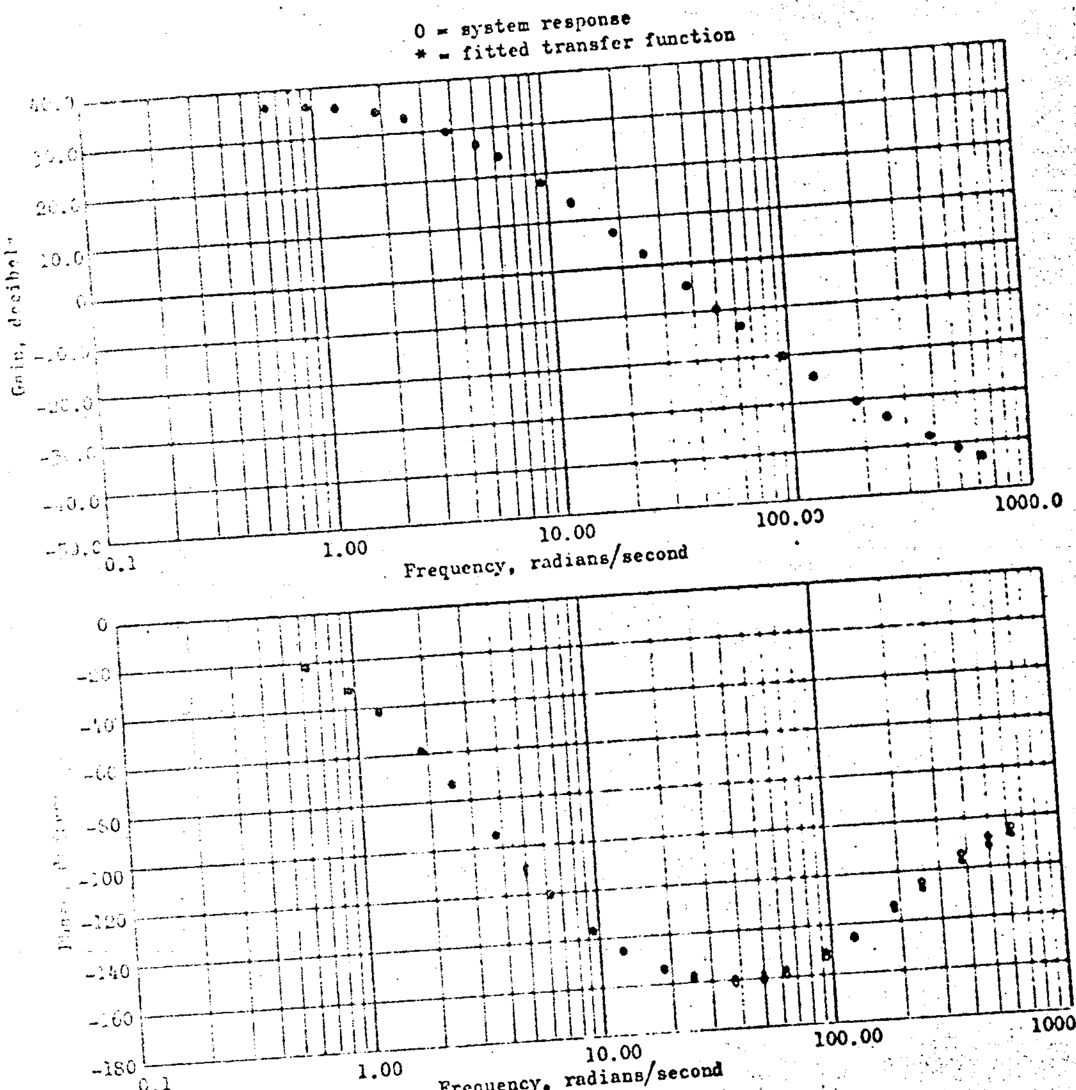

$$\frac{\tilde{P}_{fs}}{\tilde{W}_{os}} = \frac{73.53\left(1 + \frac{s}{205.1}\right)}{\left(1 + \frac{2(1.029)s}{3.345} + \frac{s^2}{(3.345)^2}\right)}, \text{ (dimensionless)}$$

$$\frac{\overline{P}_{fs}}{\overline{W}_{os}} = 1.130 \times 10^{-2} \frac{\text{lb/in.}^2}{\text{lb/sec}}$$

Figure 22. Change in Fuel Pump Inlet Pressure With Respect to a Change in LOX Pump Inlet Flowrate

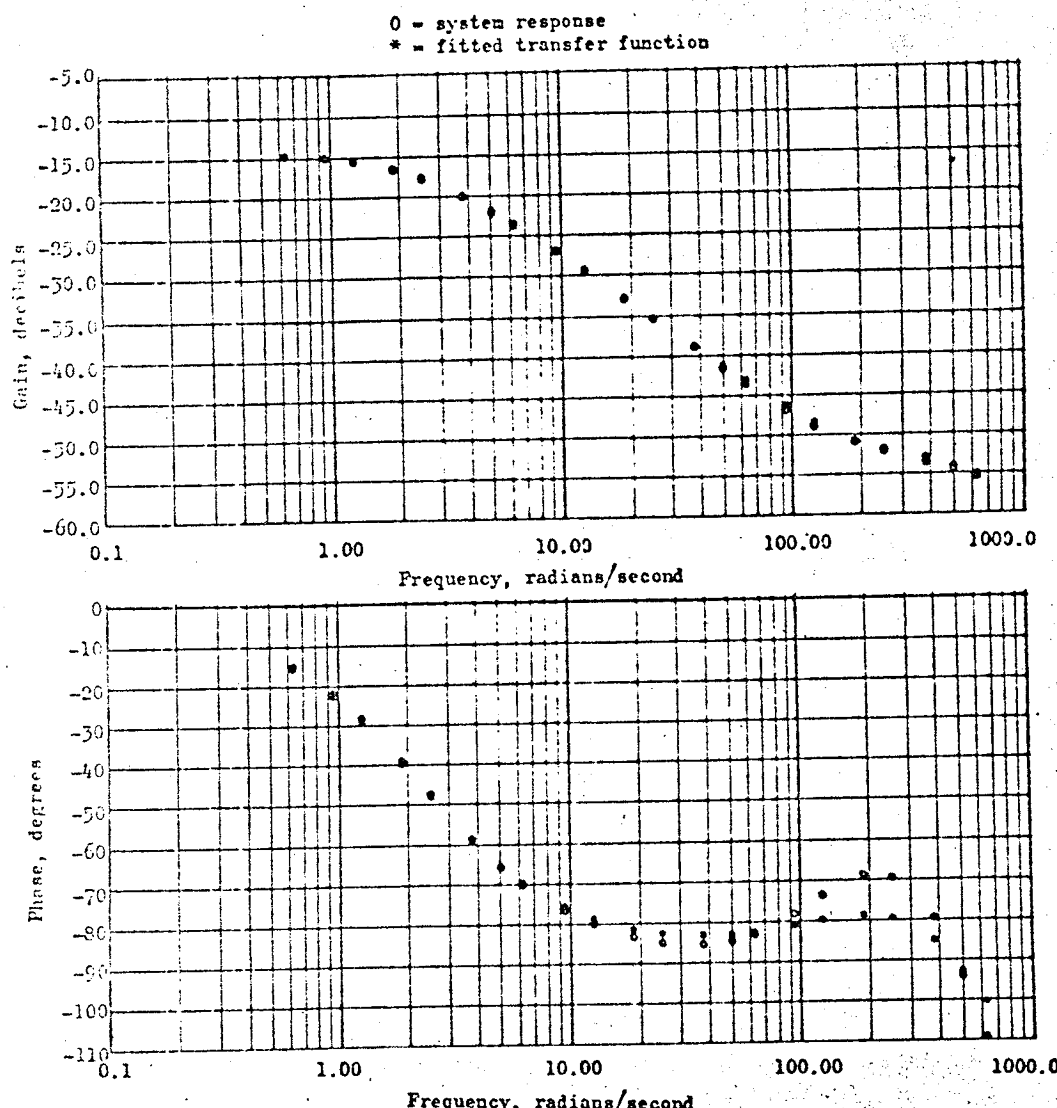

$$\frac{\tilde{F}_c}{\tilde{\dot{W}}_{fs}} = \frac{0.1924\left(1 + \frac{s}{230.9}\right)\left(1 - \frac{s}{834.7}\right)}{\left(1 + \frac{s}{2.231}\right)\left(1 + \frac{s}{662.9}\right)}, \text{ (dimensionless)}$$

$$\frac{\overline{F}_c}{\overline{\dot{W}}_{fs}} = 8.683 \times 10^2 \quad \frac{lb}{lb/sec}$$

Figure 23. Change in Thrust With Respect to a Change in Fuel Pump Inlet Flowrate

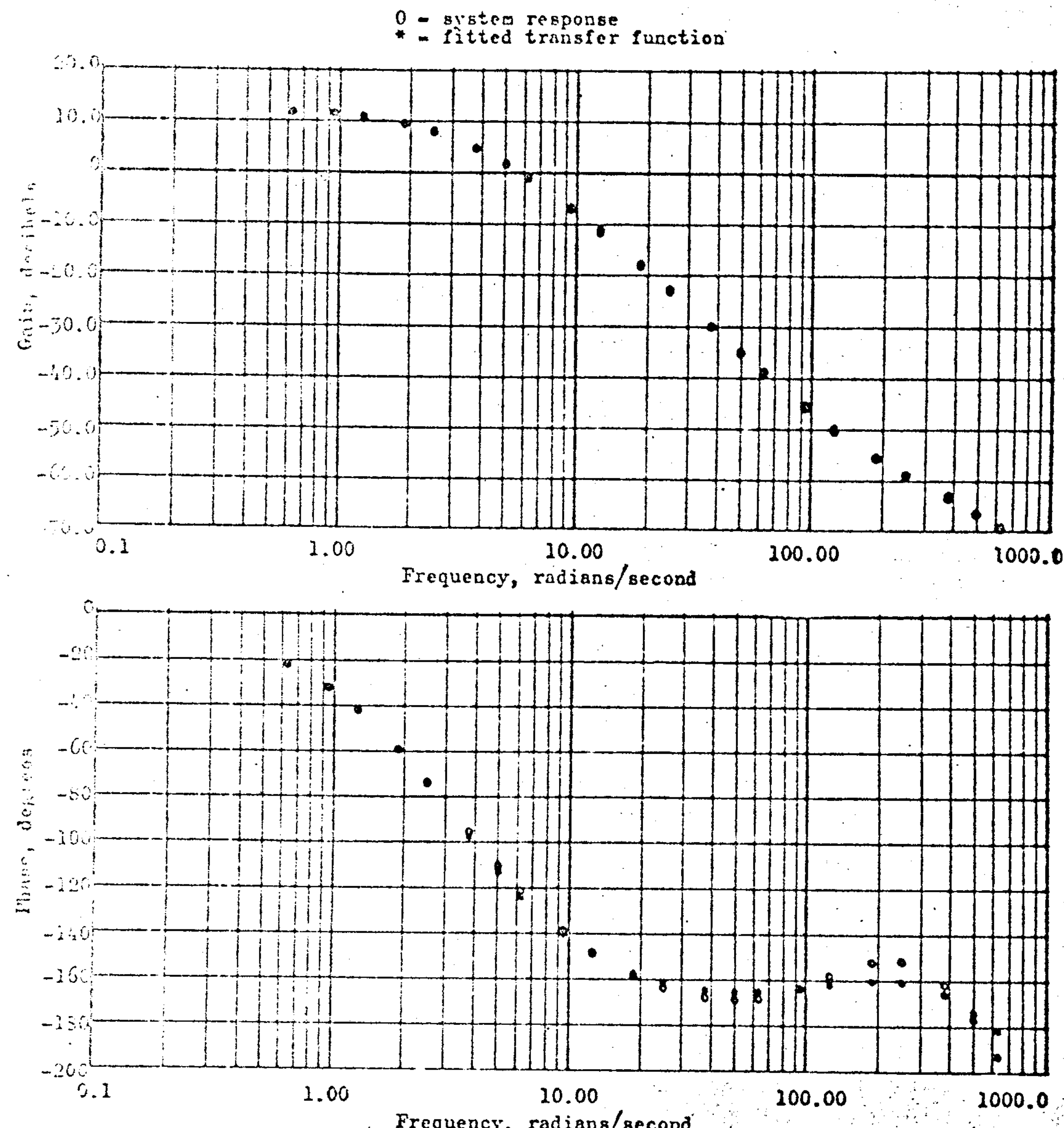

$$\frac{\tilde{P}_{os}}{\tilde{\dot{w}}_{fs}} = \frac{4.146\left(1 + \frac{s}{196.5}\right)\left(1 - \frac{s}{874.3}\right)}{\left(1 + \frac{s}{764.8}\right)\left(1 + \frac{2(1.001)s}{3.273} + \frac{s^2}{(3.273)^2}\right)}, \text{ (dimensionless)}$$

$$\frac{\overline{P}_{os}}{\overline{\dot{w}}_{fs}} = 3.708 \times 10^{-2} \ \frac{\text{lb/in.}^2}{\text{lb/sec}}$$

Figure 24. Change in LOX Pump Inlet Pressure With Respect to a Change in Fuel Pump Inlet Flowrate

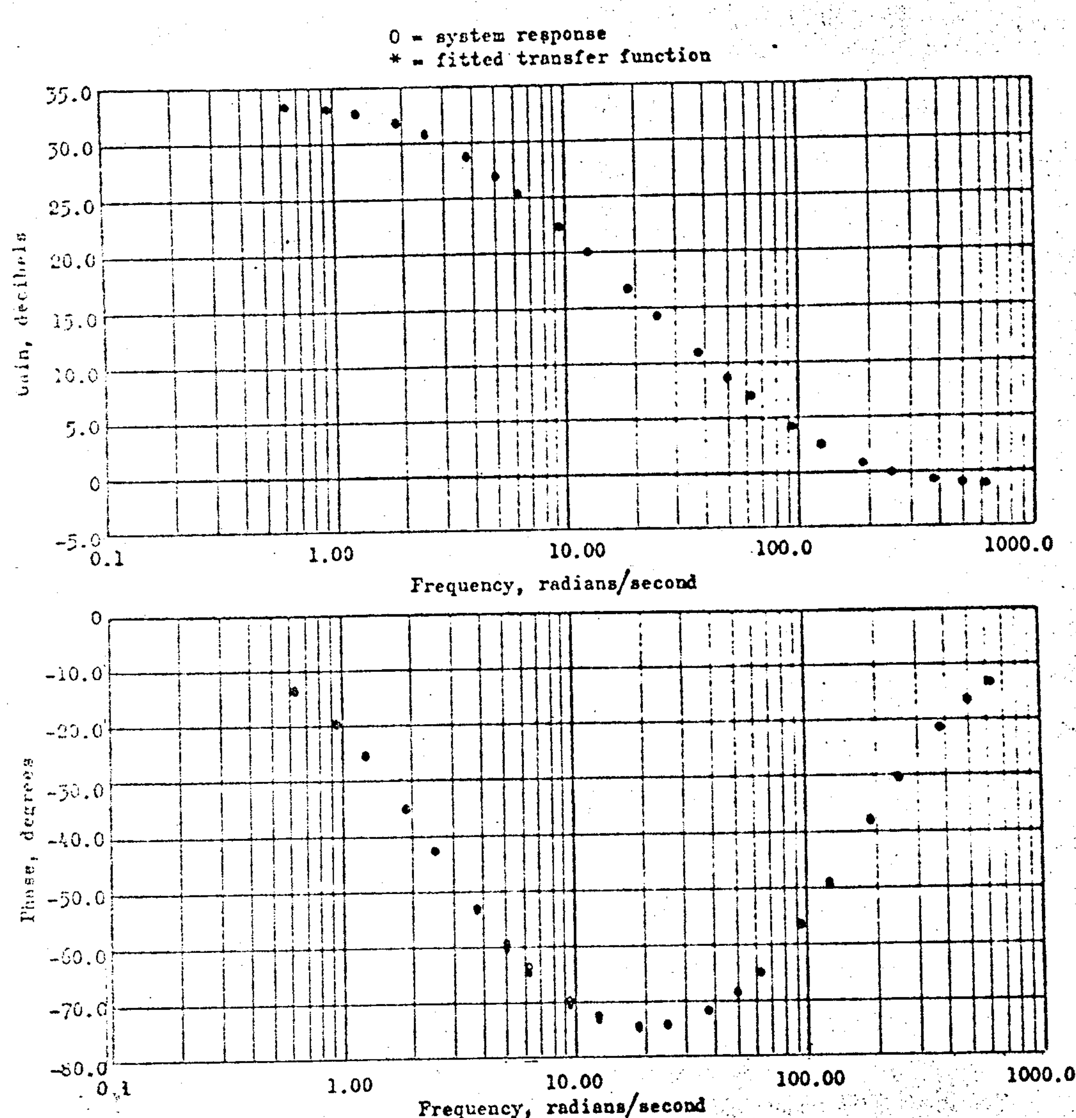

$$\frac{\tilde{P}_{fs}}{\tilde{\dot{W}}_{fs}} = \frac{48.68\left(1 + \frac{s}{149.4}\right)}{\left(1 + \frac{s}{2.636}\right)}, \text{ (dimensionless)}$$

$$\frac{\overline{P}_{fs}}{\overline{\dot{W}}_{fs}} = 2.567 \times 10^{-2} \frac{\text{lb/in.}^2}{\text{lb/sec}}$$

Figure 25. Change in Fuel Pump Inlet Pressure With Respect to a Change in Fuel Pump Inlet Flowrate

considered to be the region of highest confidence in these engine system transfer functions. It is also possible to investigate the effects of other than nominal NPSH conditions. Pump compliance functions are presented in Fig. 9 and 10. The cavitation gains are given as functions of NPSH in Eq. 20 and 22. The terms A_o and A_f can be assumed to be independent of NPSH.

The linear extrapolation in Fig. 10 is the recommended method of estimating B_o. B_f can be found directly from Fig. 9. However, in both cases a definite uncertainty exists in the compliance terms at lower $NPSH_o$ and $NPSH_f$ values. It would be prudent to consider a range of variation of compliance values around the values found from Fig. 9 and 10 at lower NPSH levels.

Values of compliance and cavitation gain obtained for other than nominal NPSH conditions can be then used to modify the turbopump descriptions, Eq. 24 through 27. These equations, when so modified, would be combined with the set of equations for the linear engine model to compute engine system transfer functions, including pump dynamics, at other than main-stage NPSH conditions.

Engine System Structural Transfer Functions

In support of the POGO studies, dynamic models were developed for the F-1 engine. Two models were necessary; (1) the engine with flexible high-pressure ducts (engines 2011-2016), and (2) the engine with rigid high-pressure ducts (engines 2017-2028). The basic models are similar, so the designation of stations as shown in Fig. 26 apply to both models.

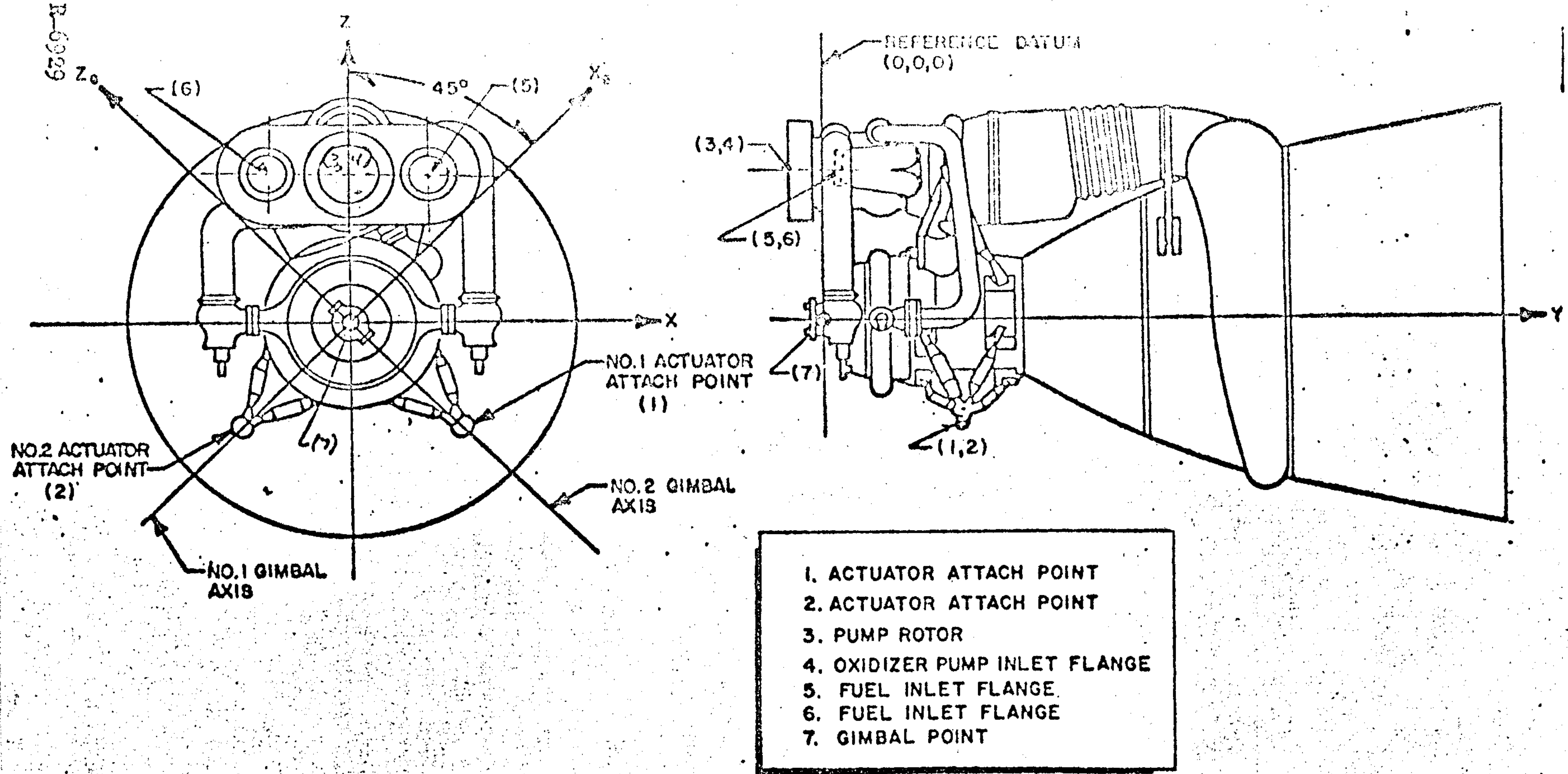

Figure 26. Schematic of F-1 Engine Transfer Function Stations

The transfer functions are presented in modal (partial fraction) form rather than as a ratio of factored polynomials and only the contribution of modes with natural frequencies below 100 cps are included.

Two types of inputs are considered: (1) acceleration at the gimbal point, and (2) force inputs at engine connect points (i.e. actuator attach points, the pump suction flanges, and the pump rotor). The outputs are (1) force on the gimbal point, and (2) acceleration at the engine connect points. Only axially directed forces and motion are considered.

The transfer functions are all of the following form

$$G_{ij} = \sum_{k=1}^{NM} \frac{C_{ijk} s^2}{s^2 + 2\,\zeta_k\,\omega_k s + \omega_k^2} \tag{28}$$

so that

$$\partial \ddot{X}_i / \partial F_j = \sum_{k=1}^{NM} \frac{C_{ijk} s^2}{s^2 + 2\,\zeta_k\,\omega_k s + \omega_k^2} = G_{ij} \tag{29}$$

$$\partial \ddot{X}_i / \partial \ddot{X}_7 = \sum_{k=1}^{NM} \frac{C_{i7k} s^2}{s^2 + 2\,\zeta_k\,\omega_k s + \omega_k^2} = G_{i7} \tag{30}$$

$$\partial F_7 / \partial F_j = \sum_{k=1}^{NM} \frac{C_{7jk} s^2}{s^2 + 2\,\zeta_k\,\omega_k s + \omega_k^2} = G_{7j} \tag{31}$$

$$\partial F_7 / \partial \ddot{X}_7 = \sum_{k=1}^{NM} \frac{C_{77k} s^2}{s^2 + 2\,\zeta_k\,\omega_k s + \omega_k^2} = G_{77} \tag{32}$$

The equations for gimbal point force and attach point accelerations are

$$\Delta F_7 = G_{77}\ddot{X}_7 + \sum_{j=1}^{6} G_{7j}\,\Delta F_j \qquad (33)$$

$$\ddot{X}_i = G_{i7}\ddot{X}_7 + \sum_{j=1}^{6} G_{ij}\,\Delta F_j \qquad (34)$$

where

C_{ijk} = coefficient representing the contribution of the "k" mode to the response at station "i" for an input at station "j" (consistent units in inches, pounds, seconds)

s = the Laplace transform operator

ω_k = natural frequency of the "kth" mode (radians/sec)

ζ_k = damping factor (2 percent of critical damping)

$\ddot{X}_i$ = acceleration (Laplace domain) at station "i" (inches/sec^2)

F_i = force (Laplace domain) at station "i" (pounds). Tension in gimbal block is taken as (+).

NM = number of modes

The transfer function coefficients and natural frequencies are presented in Tables 8 through 14. A block diagram showing the relationships between the various fluid and structural dynamic models is shown in Fig. 1.

TABLE 8

TRANSFER FUNCTION C_{i1k} FOR
AXIAL FORCE AT NO. 1 ACTUATOR ATTACH POINT
(NO. 1)

Mode No., k	Frequency, cps	10^2C_{11k}	10^2C_{21k}	10^2C_{31k}	10^2C_{41k}	10^2C_{51k}	10^2C_{61k}	10^2C_{71k}
				Engines 2011 – 2016				
1	0	1.038	−0.0967	−0.672	−0.672	−0.263	−1.081	157.4
2	26.1	0.0275	−0.0444	−0.0389	−0.0358	−0.2987	0.2270	0.48
3	29.4	0.0746	+0.1111	0.4998	0.4488	0.4139	0.4837	−9.82
4	42.2	0.1991	0.0326	0.5583	0.4408	0.2669	0.6148	−9.91
5	57.0	0.0240	0.0442	0.0818	0.0504	0.0860	0.0149	−0.44
6	80.1	0.0048	0.0054	0.0331	0.0080	0.0162	−0.0002	−0.63
7	93.7	0.0184	−0.0172	−0.0358	0.0013	0.0145	−0.0119	0.17
8	100.6	0.0185	0.0191	−0.7048	0.1367	0.1295	0.1438	−0.63
				Engines 2017 – 2028				
1	0	1.103	−0.093	−0.718	−0.717	−0.272	−1.163	157.4
2	11.2	0.0162	0.0116	−0.0346	−0.0341	−0.0430	−0.0253	1.195
3	27.7	0.0327	−0.0413	0.0014	0.0013	−0.2911	0.2937	0.098
4	32.3	0.1181	0.1843	0.6949	0.6094	0.6514	0.5673	− 11.868
5	45.1	0.1898	0.0056	0.5056	0.3840	0.1624	0.6056	− 8.264
6	77.6	0.0034	0.0079	0.0376	0.0109	0.0233	−0.0015	− 0.523
7	97.1	0.0214	−0.0184	−0.0586	0.0066	0.0205	−0.0072	+ 0.141
8	101.2	0.0208	0.0202	−0.7205	0.1500	0.1371	0.1629	− 0.540

TABLE 9

TRANSFER FUNCTION C_{i2k} FOR AXIAL FORCE
AT NO. 2 ACTUATOR ATTACH POINT (NO.2)

Mode No., k	Frequency, cps	$10^2 C_{12k}$	$10^2 C_{22k}$	$10^2 C_{32k}$	$10^2 C_{42k}$	$10^2 C_{52k}$	$10^2 C_{62k}$	$10^2 C_{72k}$
Engines 2011-2016								
1	0	-0.0967	1.032	-0.667	-0.6665	-1.073	-0.2596	157.2
2	26.1	-0.0444	0.0716	0.0628	0.0577	0.4816	-0.3661	- 0.61
3	29.4	0.1111	0.1656	0.7446	0.6687	0.6167	0.7207	-15.55
4	42.2	0.0326	0.0053	0.0915	0.0722	0.0437	0.1007	- 1.65
5	57.0	0.0442	0.0812	0.1503	0.0927	0.1581	0.0274	- 0.83
6	80.1	0.0054	0.0060	0.0368	0.0089	0.0180	-0.0002	- 0.69
7	93.7	-0.0172	0.0162	0.0336	-0.0012	-0.0136	0.0112	- 0.17
8	100.6	0.0191	0.0197	-0.7271	0.1410	0.1336	0.1484	- 0.64
Engines 2017-2028								
1	0	-0.093	1.094	-0.716	-0.715	-1.162	-0.269	157.2
2	11.2	0.0116	0.0083	-0.0249	-0.0245	-0.0308	-0.0182	0.858
3	27.7	-0.0413	0.0522	-0.0018	-0.0016	0.3674	-0.3706	- 0.123
4	32.3	0.1843	0.2876	1.0840	0.9509	1.0170	0.8853	-18.521
5	45.1	0.0056	0.0002	0.0149	0.0113	0.0048	0.0178	- 0.243
6	77.6	0.0079	0.0181	0.0863	0.0250	0.0534	-0.0035	- 1.200
7	97.1	-0.0184	0.0158	0.0503	-0.0057	-0.0176	0.0062	- 0.121
8	101.2	0.0202	0.0196	-0.7008	0.1459	0.1334	0.1585	- 0.525

TABLE 10

TRANSFER FUNCTION C_{i3k} FOR AXIAL FORCE ON PUMP ROTOR (NO. 3)

Mode No., k	Frequency, cps	$10^2 C_{13k}$	$10^2 C_{23k}$	$10^2 C_{33k}$	$10^2 C_{43k}$	$10^2 C_{53k}$	$10^2 C_{63k}$	$10^2 C_{73k}$
				Engines 2011-2016				
1	0	-0.672	-0.667	0.955	0.955	0.953	0.956	81.3
2	26.1	-0.0389	0.0628	0.0550	0.0506	0.4220	-0.3208	- 0.33
3	29.4	0.4998	0.7446	3.349	3.008	2.774	3.241	-65.75
4	42.2	0.5583	0.0915	1.566	1.236	0.7485	1.724	-27.92
5	57.0	0.0818	0.1503	0.2785	0.1718	0.2928	0.0508	- 1.50
6	80.1	0.0331	0.0368	0.2275	0.0551	0.1115	-0.0013	- 4.29
7	93.7	-0.0358	0.0336	0.0698	-0.0025	-0.0282	0.0233	- 0.35
8	100.6	-0.7048	-0.7271	26.86	-5.209	-4.937	-5.482	23.71
				Engines 2017-2028				
1	0	-0.718	-0.716	1.023	1.022	1.025	1.019	+81.3
2	11.2	-0.0346	-0.0249	0.0741	0.0730	0.0919	0.0541	- 2.558
3	27.7	0.0014	-0.0018	0.0001	0.0001	-0.0124	0.0126	0.004
4	32.3	0.6949	1.084	4.089	3.586	3.833	3.338	-69.83
5	45.1	0.5056	0.0149	1.347	1.023	0.4324	1.613	-22.009
6	77.6	0.3758	0.0862	0.4103	0.1188	0.2541	-0.0166	- 5.711
7	97.1	-0.0586	0.0503	0.1602	-0.0182	-0.0562	0.0198	- 0.386
8	101.2	-0.7205	-0.7008	25.00	-5.205	-4.758	-5.652	+18.721

TABLE 11

TRANSFER FUNCTION C_{i4k} FOR
AXIAL FORCE ON OXIDIZER PUMP INLET FLANGE
(NO. 4)

Mode No., k	Frequency, cps	10^2C_{14k}	10^2C_{24k}	10^2C_{34k}	10^2C_{44k}	10^2C_{54k}	10^2C_{64k}	10^2C_{74k}
				Engines 2011 -2016				
1	0	-0.672	-0.666	0.955	0.954	0.952	0.956	85.3
2	26.1	-0.0358	0.0577	0.0506	0.0465	0.3881	-0.2950	- 0.31
3	29.4	+0.4488	0.6687	3.008	2.701	2.491	2.911	-63.44
4	42.2	0.4408	0.0722	1.236	0.9763	0.5910	1.362	-21.54
5	57.0	0.0505	0.0927	0.1718	0.1060	0.1806	0.0314	- 0.93
6	80.0	0.0080	0.0089	0.0551	0.0133	0.0270	-0.0003	- 1.04
7	93.1	0.0013	-0.0012	-0.0025	0.0001	0.0010	-0.0008	0.01
8	100.6	0.1367	0.1410	-5.209	1.010	0.9574	1.063	- 4.59
				Engines 2017 - 2028				
1	0	-0.7174	-0.7153	1.022	1.021	1.024	1.018	85.3
2	11.2	-0.0341	-0.0245	0.0730	0.0719	0.0906	0.0533	- 2.52
3	27.7	0.0013	-0.0016	0.0001	0.0000	-0.0114	0.0115	0.004
4	32.3	0.6094	0.9509	3.586	3.144	3.361	2.927	-61.234
5	45.1	0.3840	0.0113	1.023	0.7766	0.3284	1.225	- 7.068
6	77.6	0.0109	0.0250	0.1188	0.0344	0.0736	-0.0048	- 1.653
7	97.1	0.0066	-0.0057	-0.0182	0.0021	0.0064	-0.0022	+ 0.044
8	101.2	0.1500	0.1459	-5.205	1.084	0.9906	1.177	- 3.897

TABLE 12

TRANSFER FUNCTION C_{15k} FOR AXIAL FORCE ON NO. 1
FUEL INLET FLANGE (NO.5)

Mode No., k	Frequency, cps	$10^2 C_{15k}$	$10^2 C_{25k}$	$10^2 C_{35k}$	$10^2 C_{45k}$	$10^2 C_{55k}$	$10^2 C_{65k}$	$10^2 C_{75k}$
				Engines 2011-2016				
1	0	-0.263	-1.073	0.953	0.952	1.245	0.660	84.9
2	26.1	-0.2987	0.4816	0.4220	0.3881	3.236	-2.460	- 4.96
3	29.4	0.4139	0.6167	2.774	2.491	2.298	2.685	-62.70
4	42.2	0.2669	0.0437	0.7485	0.5910	0.3578	0.8242	-13.42
5	57.0	0.0860	0.1581	0.2928	0.1806	0.3078	0.0534	- 1.62
6	80.0	0.0162	0.0180	0.1115	0.0270	0.0546	-0.0007	- 2.11
7	93.1	0.0145	-0.0136	-0.0282	0.0010	0.0114	-0.0094	0.14
8	100.6	0.1295	0.1336	-4.937	0.9574	0.9074	1.008	- 4.36
				Engines 2017-2028				
1	0	-0.272	-1.162	1.025	1.024	1.361	0.687	84.9
2	11.2	-0.0430	-0.0308	0.0919	0.0906	0.1140	0.0671	-3.172
3	27.7	-0.2911	0.3674	-0.0124	-0.0114	2.588	-2.611	- 0.870
4	32.3	0.6514	1.017	3.833	3.361	3.593	3.129	-65.459
5	45.1	0.1624	0.0048	0.4324	0.3284	0.1389	0.5179	- 7.068
6	77.6	0.0233	0.0534	0.2541	0.0736	0.1574	-0.0103	- 3.537
7	97.1	0.0205	-0.0176	-0.0562	0.0064	0.0197	-0.0069	+ 0.135
8	101.2	0.1371	0.1334	-4.758	0.9906	0.9054	1.076	- 3.563

TABLE 13

TRANSFER FUNCTION C_{i6k} FOR AXIAL FORCE ON NO. 2
FUEL INLET FLANGE (NO. 6)

Mode No., k	Frequency, cps	10^2C_{16k}	10^2C_{26k}	10^2C_{36k}	10^2C_{46k}	10^2C_{56k}	10^2C_{66k}	10^2C_{76k}
Engines 2011-2016								
1	0	-1.081	-0.250	0.956	0.956	0.660	1.252	86.4
2	26.1	0.2270	-0.3661	-0.3208	-0.2950	-2.460	1.870	4.37
3	29.4	0.4837	0.7207	3.241	2.911	2.685	3.137	-64.18
4	42.2	0.6148	0.1007	1.724	1.362	0.8242	1.899	-30.67
5	57.0	0.0149	0.0274	0.0508	0.0314	0.0534	0.009	- 0.24
6	80.0	-0.0002	-0.0002	-0.0013	-0.0003	-0.0007	0.000	0.04
7	93.1	-0.0119	0.0112	0.0233	-0.0008	-0.0094	0.0078	- 0.12
8	100.6	0.1438	0.1484	-5.482	1.063	1.008	1.119	- 4.82
Engines 2017-2028								
1	0	-1.163	-0.269	1.019	1.018	0.686	1.350	86.4
2	11.2	-0.0253	-0.0182	0.0541	0.0533	0.0671	0.0396	- 1.869
3	27.7	0.2937	-0.3706	0.0126	0.0115	-2.611	2.634	+ 0.878
4	32.3	0.5673	0.8853	3.338	2.927	3.129	2.725	-57.009
5	45.1	0.6056	0.0178	1.613	1.225	0.5179	1.932	-26.35
6	77.6	-0.0015	-0.0035	-0.0166	-0.0048	-0.0103	0.0007	+ 0.232
7	97.1	-0.0072	0.0062	0.0198	-0.0022	-0.0068	0.0024	- 0.048
8	101.2	0.1629	0.1585	-5.652	1.177	1.076	1.278	- 4.232

TABLE 14

TRANSFER FUNCTION C_{i7k} FOR

AXIAL ACCELERATION AT GIMBAL POINT

(NO. 7)

Mode No., k	Frequency, cps	10^2C_{17k}	10^2C_{27k}	10^2C_{37k}	10^2C_{47k}	10^2C_{57k}	10^2C_{67k}	10^2C_{77k}
				Engines 2011 - 2016				
1	0	157.4	157.2	81.3	85.3	84.9	86.4	-53.40
2	26.1	0.48	- 0.67	- 0.33	- 0.31	- 4.96	+ 4.37	0.08
3	29.4	- 9.82	-15.55	-65.75	-63.44	-62.70	-64.18	14.57
4	42.2	- 9.91	- 1.65	-27.92	-21.54	-13.42	-30.67	5.47
5	57.0	- 0.44	- 0.83	- 1.50	- 0.93	- 1.62	- 0.24	0.09
6	80.1	- 0.63	- 0.69	- 4.30	- 1.04	- 2.11	+ 0.04	0.82
7	93.7	+ 0.17	- 0.17	- 0.35	+ 0.01	+ 0.14	- 0.12	0.02
8	100.6	- 0.63	- 0.64	+23.71	- 4.59	- 4.36	- 4.82	0.21
				Engines 2017 - 2028				
1	0	157.4	157.2	81.3	85.3	84.9	86.4	-53.40
2	11.2	1.195	0.858	- 2.558	- 2.520	- 3.172	- 1.869	0.8828
3	27.7	0.098	- 0.123	+ 0.004	0.004	- 0.870	+ 0.878	0.0029
4	32.3	-11.868	-18.521	-69.83	-61.234	-65.459	-57.009	11.925
5	45.1	- 8.264	- 0.243	-22.009	-16.714	- 7.068	-26.351	3.597
6	77.6	- 0.523	- 1.200	- 5.711	- 1.653	- 3.537	+ 0.232	0.995
7	97.1	+ 0.141	- 0.121	- 0.386	+ 0.044	+ 0.135	- 0.048	0.009
8	101.2	- 0.540	- 0.525	+18.72	- 3.897	- 3.563	- 4.232	0.140

Example Illustrating the Use of the Transfer Function Tables

The acceleration of the number 1 actuator attach point for an engine in the 2017-2028 series is taken as an illustration. The form, as shown in Eq. 35, will be

$$\ddot{X}_1 = G_{17}\ddot{X}_7 + G_{11}\,\Delta F_1 + G_{12}\,\Delta F_2 + G_{13}\,\Delta F_3 + G_{14}\,\Delta F_4 + G_{15}\,\Delta F_5 + G_{16}\,\Delta F_6 \qquad (35)$$

Since all G_{ij} have the same form, we will expand only G_{14}, the effect of a force at the oxidizer inlet flange. Coefficients of G_{14} are found in coefficient column 1 of Table 11. Noting also that $\omega_k = 2\pi f_k$ the expression can be expanded as

$$G_{14} = -7.174\cdot 10^{-3} - \frac{3.412\cdot 10^{-4}\, s^2}{s^2 + 2\cdot 0.02s\,(70.37) + (70.37)^2} + \frac{1.279\cdot 10^{-5}\, s^2}{s^2 + 2\cdot 0.02s\,(174.04) + (174.04)^2} + \cdots + \frac{1.5\cdot 10^{-3}\, s^2}{s^2 + 2\cdot 0.02s\,(635.86) + (635.86)^2}$$

REFERENCES

1. Bekey, G. A. and H. F. Meissinger: "An Analysis of Continuous Parameter Identification Methods," Simulation, February 1966.

2. Bekey, G. A., H. F. Meissinger, and R. E. Rose: NASA Contractor Report CR-143, A Study of Model Matching Techniques for the Determination of Parameters in Human Pilot Models, January 1965.

3. R-6813, Engine System Transfer Functions for Support of S-IB Vehicle Longitudinal Stability (POGO) Analysis Program, Rocketdyne, a Division of North American Aviation, Inc., Canoga Park, California, 22 December 1966.

4. R-6283, J-2 Vehicle Longitudinal Stability (POGO) Analysis Program, Rocketdyne, a Division of North American Aviation, Inc., Canoga Park, California, 31 August 1965.

5. Rubin, S., "Longitudinal Instability of Liquid RocketsDue to Propulsion Feedback (POGO)," Journal of Spacecraft and Rockets, Vol. 3, No. 8, August 1966.

6. Bernhart, W. D., "Determination of Parameters and Operations in Dynamic Systems," Oklahoma State University, PhD Thesis, August 1964.

APPENDIX A

NOMENCLATURE

Symbol	Description	Units
A	cross sectional area	in.^{2}
A	cavitation resistance	sec/in.^{2}
B	cavitation compliance	1/in.^{2}
c^*	characteristic velocity	in./sec
C_p	specific heat at constant pressure	Btu/lb-R
D	differentiation (d/dt)	1/sec
f	frequency	cps
F_c	thrust	lb
ΔH	enthalpy	Btu/lb
I	moment of inertia	slug-in.^{2}
j	$\sqrt{-1}$	
J	pump cavitation gain	
K	general proportionality constant	
ℓ	length	in.
L	duct inertance	sec^2/in.^{2}
LF	LOX fraction	
M	torque	in.-lb
MW	molecular weight	$\frac{\text{lb}}{\text{lb-mole}}$
N	turbopump speed	radians/sec

Symbol	Description	Units
NPSH	net positive suction head	ft
p	pressure	psia
Δp	pressure perturbation (time domain)	psi
ΔP	pressure perturbation (Laplace domain)	psi
P_r	turbine pressure ratio	
R	square law duct resistance	$sec^2/lb\text{-}in.^2$
R_p	linearized pump resistance	$sec/in.^2$
R_u	universal gas constant	in.-lb/R lb-mole
s	Laplace operator	1/sec
T	temperature	R
V	volume	$in.^3$
w	stored weight	lb
$\dot{w}$	weight flowrate	lb/sec
$\Delta \dot{w}$	weight flowrate perturbation (time domain)	lb/sec
$\Delta \dot{W}$	weight flowrate perturbation (Laplace domain)	lb/sec
Δx_p	pulser position perturbation (time domain)	in.
ΔX_p	pulser position perturbation (Laplace domain)	in.
$\ddot{X}$	pump flange acceleration axial to thrust chamber (Laplace domain)	$in./sec^2$
Y	fluid dynamic admittance (inverse of impedance)	$in.^2/sec$

Symbol	Description	Units
Δ	signifies perturbation in a variable	
ζ	percent critical damping	
η	efficiency	
χ	nondimensional pump torque coefficient	
φ	nondimensional pump flow coefficient	
ψ	nondimensional pump head coefficient	
ω	frequency	radians/sec

Superscripts

$\cdot$	d/dt	
$\cdot\cdot$	d^2/dt^2	
(vinculum)	steady value of a variable	
~	perturbed variable normalized to mainstage (i.e., $\tilde{N} = \Delta N/\overline{N}$)	
$\longrightarrow$	vector quantity or signal flow	

Subscripts

c	thrust chamber	
d	discharge	
ex	exhaust	
f	fuel system	
g or gg	gas generator	
I	thrust chamber injector	

m	manifold
n	nozzle
o	LOX system
p	pump
s	suction
t	throat
tn	turbine
x	exit

NOTES:

1. Flowrate perturbations are defined as positive in the direction of steady flow.
2. Other nomenclature is defined in the text as required.

APPENDIX B

F-1 ENGINE WORK STATEMENT TO SUPPORT SATURN V VEHICLE POGO STUDY

Using F-1 Bobtail pump test data and other information supplied by the George C. Marshall Space Flight Center as well as data from the current F-1 Engine development and production test programs, Rocketdyne will supply the following dynamic models:

1. An engine model with pump cavitation compliance included over the range of operating conditions (flowrate, pump speed, NPSH, and suction pressure) for which data are supplied to Rocketdyne. The interface will be at the pump inlet flanges.
2. An engine model which does not include the pump cavitation compliance, at the nominal engine operating condition. The interface will be at the pump inlet flanges.

These engine models will be linear transfer functions in polynomial form to allow changes in the engine's operating point to be characterized. The dynamic models will relate thrust, flowrates, gimbal point and pump motion, and suction pressure through the effects on the engine system.

At least the following transfer functions should be furnished:

$$\frac{\partial F}{\partial P_{LS}}; \quad \frac{\partial F}{\partial P_{FS}}; \quad \frac{\partial Q_L}{\partial P_{LS}}; \quad \frac{\partial Q_L}{\partial P_{FS}}; \quad \frac{\partial Q_F}{\partial P_{LS}}; \quad \frac{\partial Q_F}{\partial P_{FS}}$$

where

∂F is thrust oscillations

∂Q_L is LOX pump inlet flowrate oscillation

∂Q_F is fuel pump inlet flowrate oscillation

∂P_{LS} is LOX pump inlet pressure oscillation

∂P_{FS} is fuel pump inlet pressure oscillation

APPENDIX C

DATA ANALYSIS TECHNIQUES

TECHNIQUES INVESTIGATED

At the outset of the H-1 POGO analysis, emphasis was placed on time domain methods of turbopump model parameter identification. It was desired to develop a procedure whereby dynamic model parameters could be computed on line during the playback of bobtail facility test data. Such a procedure, by minimizing intermediate data processing, promised to reduce significantly the time required to complete the analysis by providing the desired model parameters as direct output. Past experience at Rocketdyne indicated that the costs of executing such a time domain analysis would be appreciably lower than those of comparable frequency domain techniques.

The merits of data reduction in the time domain were enhanced by several practical considerations. If a method of optimal parameter identification were performed in the frequency domain, POGO pump test data would first have to be converted into a form useful in that domain. Available equipment dictated that the necessary frequency domain computations be performed by digital computers; therefore, an additional step of digitizing the FM magnetic tape data would be required. In contrast, the time domain technique contemplated required only a general-purpose analog computer and an FM tape playback capability. It is not intended to demean the value of frequency domain analysis; although it was not used for data reduction purposes, previously developed methods of frequency domain analysis were used for analytical purposes during the program.

TECHNIQUES DEVELOPED

The time domain method of model parameter optimization developed for the H-1 POGO analysis is similar in philosophy to one of the methods employed successfully in the J-2 POGO analysis program. It is necessary to hypothesize the form of a mathematical model which describes the physical system under study. From prior Rocketdyne experience, a basic idea of the form of the turbopump dynamics models existed at the start of the program. Coefficients or parameters in the models which are unknown are then determined empirically by employing some method of adjusting these parameters until the model agrees satisfactorily with test data taken from the physical system. Parameter optimization is achieved in automatic techniques by minimization of a selected criterion function based on the error between the model and the physical system.

In the J-2 analysis (Ref. 4, page 25) an integrated square error criterion function was used and parameter identification was obtained by algebraic solution of a set of equations evolving from the minimization condition. For the H-1 program, however, a method presented in Ref. 1 was adopted. The criterion function was real time model-system error squared, the integration with respect to time being omitted. Minimization of this criterion function,, which allows computation of optimized model parameters, was accomplished by the strategy of steepest descent. As indicated below, this method has the capability of continuous tracking of model parameters in the event the physical system is not stationary. Analog mechanization of the continuous parameter identification method is relatively simple and straightforward.

Continuous Parameter Identification Method

A linear physical system of order n, and having a single input, may be described by an nth order differential equation,

$$\frac{d^n y}{dt^n} + a_{n-1} \frac{d^{n-1} y}{dt^{n-1}} + \cdots + a_{oy} = f_1 \, r_1 \, (t) \qquad (C\text{-}1)$$

where r_1 (t) is the system forcing function. Initial conditions can be specified by

$$\left. \frac{d^i y}{dt^i} \right|_{t=0} = Y_i ; \; i = 1,2, \cdot \cdot \cdot, n \qquad (C\text{-}2)$$

The above equation may be rewritten by defining the state variable, h_i, in the following manner:

$$h_1 = y, \; h_2 \equiv \frac{dy}{dt}, \; \cdots, \; h_i \equiv \frac{d^{i-1} y}{dt^{i-1}} \; ; \; i = 1,2,\cdots, n \qquad (C\text{-}3)$$

thus

$$\dot{h}_1 = h_2$$

$$\dot{h}_2 = h_3$$

$$\vdots$$

$$\dot{h}_n = f_1 \, r_1 \, (t) - a_{n-1} \, h_n - \cdots, - a_o \, h_1 \qquad (C\text{-}4)$$

In matrix form the above set of equations is written,

$$\begin{bmatrix} \dot{h}_1 \\ \dot{h}_2 \\ \cdot \\ \cdot \\ \cdot \\ \dot{h}_n \end{bmatrix} = \begin{bmatrix} 0 & 1 & 0\,0\,0 & \cdots & 0 \\ 0 & 0 & 1\,0\,0 & \cdots & 0 \\ \cdot & \cdot & \cdots & & \cdot \\ \cdot & \cdot & \cdots & & \cdot \\ \cdot & \cdot & \cdots & & \cdot \\ -a_o & -a_i & \cdots & \cdots & -a_{n-1} \end{bmatrix} \begin{bmatrix} h_1 \\ h_2 \\ \cdot \\ \cdot \\ \cdot \\ h_n \end{bmatrix} + \begin{bmatrix} f_1 & 0\,0 & \cdots & 0 \\ 0 & \cdots & \cdots & \cdot \\ \cdot & & & \cdot \\ \cdot & & & \cdot \\ \cdot & & & \cdot \\ 0 & 0\,0 & \cdots & 0 \end{bmatrix} \begin{bmatrix} r_1\ (t) \\ 0 \\ \cdot \\ \cdot \\ \cdot \\ 0 \end{bmatrix} \qquad \text{(C-5)}$$

In simple vector form,

$$\dot{\bar{h}} = A\,\bar{h} + F\,\bar{r}\,(t) \qquad \text{(C-6)}$$

where initial conditions are now given by

$$\bar{h}\,(o) = \bar{h}_o \qquad \text{(C-7)}$$

For the general case of n equations and m inputs,

$$\dot{\bar{h}}\,(t) = \begin{bmatrix} \dot{h}_i \\ \dot{h}_2 \\ \cdot \\ \cdot \\ \cdot \\ \dot{h}_n \end{bmatrix}, \quad \bar{h}\,(t) = \begin{bmatrix} h_1 \\ h_2 \\ \cdot \\ \cdot \\ \cdot \\ h_n \end{bmatrix}, \quad \bar{r}(t) = \begin{bmatrix} r_1(t) \\ r_2(t) \\ \cdot \\ \cdot \\ \cdot \\ r_m(t) \end{bmatrix}, \qquad \text{(C-8)}$$

$$A = \begin{bmatrix} a_{11} & a_{12} & \cdots & a_{1n} \\ a_{21} & a_{22} & \cdots & \cdot \\ \cdot & \cdot & & \cdot \\ \cdot & \cdot & & \cdot \\ a_{n1} & a_{n2} & \cdots & a_{nn} \end{bmatrix}, \quad F = \begin{bmatrix} f_{11} & f_{12} & \cdots & f_{1m} \\ f_{21} & f_{22} & \cdots & \cdot \\ \cdot & \cdot & & \cdot \\ \cdot & \cdot & & \cdot \\ f_{n1} & f_{n2} & \cdots & f_{nm} \end{bmatrix} \qquad \text{(C-9)}$$

Here A is a general coefficient matrix and F is known as the distribution matrix, which shows the effect the input vector $\bar{r}(t)$ has on the rate of change of the system state variable vector $\bar{h}(t)$.

A mathematical model of the system (having adjustable parameters) is

$$\frac{d^n\xi}{dt^n} + \alpha_{n-1} \frac{d^{n-1}\xi}{dt^{n-1}} + \ldots + \alpha_o \xi = f_1 r_1(t) \tag{C-10}$$

Note that the system and the model have the same input. Defining the model state variable as

$$Z_i \equiv \frac{d^{i-1}\xi}{dt^{i-1}} ; \ i = 1, 2, \ldots, n \tag{C-11}$$

the resulting vector equation is

$$\dot{\bar{Z}} = \alpha \bar{Z} + F \bar{r} (t) \tag{C-12}$$

where

$$\alpha = \begin{bmatrix} 0 & 1 & 0 & 0 & \ldots & 0 \\ 0 & 0 & 1 & 0 & \ldots & 0 \\ \cdot & \cdot & \cdot & \cdot & \cdot & \cdot \\ \cdot & \cdot & \cdot & & \cdot & \\ \cdot & \cdot & \cdot & \cdot & & \cdot \\ -\alpha_o & -\alpha_1 & \cdot & \cdot & \cdot & -\alpha_{n-1} \end{bmatrix} \tag{C-13}$$

is the adjustable parameter matrix.

In the interest of clarity, the derivation presented here implies that the physical system can be described by linear differential equations. However, the methods employed may be extended to nonlinear systems, in which case Eq. C-6 would be replaced by

$$\dot{\bar{h}} = \bar{f}\,(\bar{h}, \bar{a}, t) \tag{C-14}$$

and Eq. C-12 becomes

$$\dot{\bar{Z}} = \bar{g}\,(\bar{Z}, \bar{\alpha}, t) \tag{C-15}$$

Such state vector equations, in fact, can be regarded as the starting point for a discussion of parameter optimization methods (Ref. 1).

Criterion Function. The parameter optimization problem consists of adjusting some initially selected value of the parameter matrix such that a performance criterion function, H, based on an error term, is minimized.

Two types of errors have been successfully used:

$$\text{output error} = \text{system output} - \text{model output} = h_1 - Z_1 \tag{C-16}$$

$$\text{equation error} = \dot{Z}_n + \alpha_{n-1} Z_n + \ldots + \alpha_o Z_1 - f_1 r_1 (t) \tag{C-17}$$

Throughout the H-1 analysis the output error definition was used. Two important criterion functions are

$$H_1 = 1/2\, e^2 \tag{C-18}$$

and

$$H_2 = 1/2 \int_o^T e^2 dt \tag{C-19}$$

The second criterion function is suitable for either iterative or algebraic optimization. A digital program which employs this function is discussed in subsequent paragraphs. The first criterion function, H_1, is more suitable for on-line parameter identification because it facilitates continuous solution for optimal parameter values.

Adjustment Strategy. A suitable adjustment scheme, either continuous or iterative, is based on the steepest descent optimization strategy. The gradient vector, $\overrightarrow{\Delta H}$, of the criterion function in parameter space is found and the parameter matrix is adjusted at a rate proportional to the negative of $\overrightarrow{\Delta H}$. Thus the "valley" of the criterion function is sought; the gradient as well as the rate of change of the gradient approaches zero, and the solution becomes stationary.

When criterion function H_1 is used, the gradient components are

$$\frac{\partial H}{\partial \alpha_i} = e \frac{\partial e}{\partial \alpha_i} \equiv e\, u_i \qquad \text{(C-20)}$$

Applying the steepest descent strategy the rate of parameter adjustment is

$$\dot{\overline{\alpha}} = -K\, eu_i \qquad \text{(C-21)}$$

Integration of $\dot{\overline{\alpha}}$ with respect to time results in the mechanization of a continuous optimal parameter matrix tracking capability. In some cases definition of gradient components presents some difficulties. In evaluating the influence coefficients, u_i, it is assumed that the model parameters, α_i, are not functions of time; the time history of parameter adjustment is therefore neglected.

Examination of the time-varying criterion surface and linear extrapolation of the output error term in the vicinity of fixed initial parameter values shows that the method of accomplishing the adjustment strategy outlined above will usually be successful. Amplification of these considerations is presented in Ref. 1 and 2. For purposes of the H-1 POGO analysis, the continuous parameter identification method developed above was checked by analysis of known dummy physical systems similar to those employed in the turbopump dynamic descriptions.

Filtering Requirement. Successful analysis of POGO pump test data was found to be dependent on the introduction of a carefully designed and balanced system of filtering into the analog mechanization. The equation which represents the computation of output error was operated on with a derivative-lag (a-c couple) transfer function before analog mechanization. In effect, a new output error, e', is defined. Although e' is basically the same function over the bandwidth of interest, d-c errors in the mathematical model are eliminated. Such errors result because initial conditions on the simple integrators in the model are not well known. The a-c couple operation results in the incorporation of feedback loops around the integrators and the effect of initial conditions decays exponentially.

It was found that d-c errors in the influence coefficients or in the output error signal resulted in oscillatory parameter computation. It is especially important, therefore, to adopt some systematic method of handling initial conditions in the continuous parameter identification technique.

To block the d-c content in the data, a-c couples were also incorporated in the tape data scaling circuits. Mechanization of the differentiation process in the pulser flowrate reconstructions required the incorporation of a first-order lag. The phase shift of this lag was compensated for by mechanizing similar lags in the pressure data scaling circuits. A final stage of fourth-order Butterworth bandpass filters was used to process the data inputs to the optimization circuitry. These Butterworth filters, while not entirely necessary, simplified parameter identification by their strong rolloff of noise components outside of the pulsing bandwidth. The balance of all the combined filtering operations was checked by the analysis of a known dummy physical system. Successful computation of the known parameters indicated a satisfactory condition of filter balancing.

The aggregate effect of the various filters incorporated into the analog data reduction method was to perform a linear operation on the output error equation. The bandwidths of the filters passed the POGO pulsing frequency range, and their center frequencies were centered on the center frequency of the pulsing range. Influence coefficients were derived from the new effective output error defined by the total filtering operation. Because the filtering operation was a linear dynamic operation, the linear interrelation between the data inputs was preserved. It is important that the raw data acquired at the test facility is not filtered so that dynamic relationships between the data are not distorted. Proper filtration, when incorporated into the data analysis system, facilitates the identification of optimal parameter values over the bandwidth of interest. In some cases, it appears that filters are essential to successful parameter optimization in linear dynamic systems.

<u>Forcing Function.</u> A successful empirical identification of linear system dynamics requires that the physical system be driven by a forcing function which exposes the poles and zeros of interest. Therefore, in some circumstances a broadband forcing function, such as that produced by a

random-period pulses, is of considerable value. As a corollary to the tracking ability of the continuous parameter identification method, a capability exists for optimization on a broad band of frequencies in a relatively short time increment. Thus, if a nonstationary physical system is subjected to broadband excitation, the variations in optimal parameter values can be found with respect to time. This capability has the potential of producing considerable savings in testing. By programming a slow change in a known operating variable (e.g., pump NPSH), it would be possible in one test to discover the functional relationship between optimized model parameters and this operating variable.

There are cases where sinusoidal excitation has certain advantages over a broadband forcing function. A variable frequency sinusoidal input signal can clearly reveal system resonances and provides considerable insight into system dynamics. With such a forcing function, optimized parameters are determined at a given time increment for a relatively narrow bandwidth of frequencies. Assuming the hypothesized linear model to be correct, its parameters should be independent of frequency. If, however, a significant parameter frequency dependence is found when test data are analyzed, then the model chosen is not correct and must be changed.

A problem of parameter indeterminacy can arise with sinusoidal forcing. Essentially, a set of complex algebraic equations is being solved by the optimization procedure, and a single equation can be associated with each two terminal network. At one frequency only two unknowns in a single complex equation can be found. Determination of a greater number of parameters requires at least a forcing function composed of a sum of nonharmonic sinusoids.

It should be apparent that the success of a program of empirical parameter determination is dependent on the form of dynamic excitation chosen. Selection of an appropriate forcing function (or set of forcing functions) requires some prior knowledge of the type of dynamic models which will be used to describe the physical system being tested. In the case of the H-1 POGO analysis, the ramped frequency sinusoidal excitation has proved to be adequate for identification of pump cavitation dynamics.

Digital Parameter Identification Method

A method of parameter optimization was developed for the J-2 analysis using an integrated square error criterion and direct algebraic solution. A complete discussion is given in Ref. 6. For backup purposes, a digital program was written employing the methods developed above. The program (DIFFY) has the capability of determining optimal values for the unknown parameters in a physical system which can be described by an ordinary linear differential equation. The equation can be of an order less than or equal to 6, and the number of input-output observation sets which can be accommodated is equal to 6. Application of the program would have required the digitizing of selected slices of data from the FM magnetic tapes transmitted to Rocketdyne by MSFC. The program has been essentially checked out; however, it is not yet ready for production application.

TECHNIQUES UTILIZED

Analysis of the H-1 turbopump dynamic test data was accomplished by utilizing the continuous parameter identification method which was mechanized on a high-capacity, general-purpose analog computer. Scaling, flowrate reconstruction, and optimization were performed on line as data on magnetic tape was played back. Figure C-1 is a typical record of the analysis output.

The time record of model-system error was found to be particularly valuable in interpreting the results and in determining when optimization had been achieved. The single parameter optimization shown in Fig. C-1 is the result of a pump inlet cavitation compliance computation. A supplementary function, σ, was computed. This quantity is defined as the time-averaged ratio of model-system error squared to system output squared. This ratio amounts to power in the error signal divided by power in the system signal. Low values of σ (approximately 10 percent) correspond to a high confidence level in the optimal parameter value. It can be seen from Fig. C-1 that confidence levels are low when the dynamic power or signal-to-noise ratio in the system output is low. (This situation occurs in the H-1 pump test data on the low frequency side of the inlet resonance, and in the event pump driven oscillations occur.)

Figure C-2 is a section of Fig. C-1 recorded with a 10 times greater paper speed. Examination of the error trace shows that frequency components in this signal are basically not associated with the pulsing frequency. It is a feature of linear systems optimization that frequency components not related to the input signal are treated as noise and appear in the model-system error.

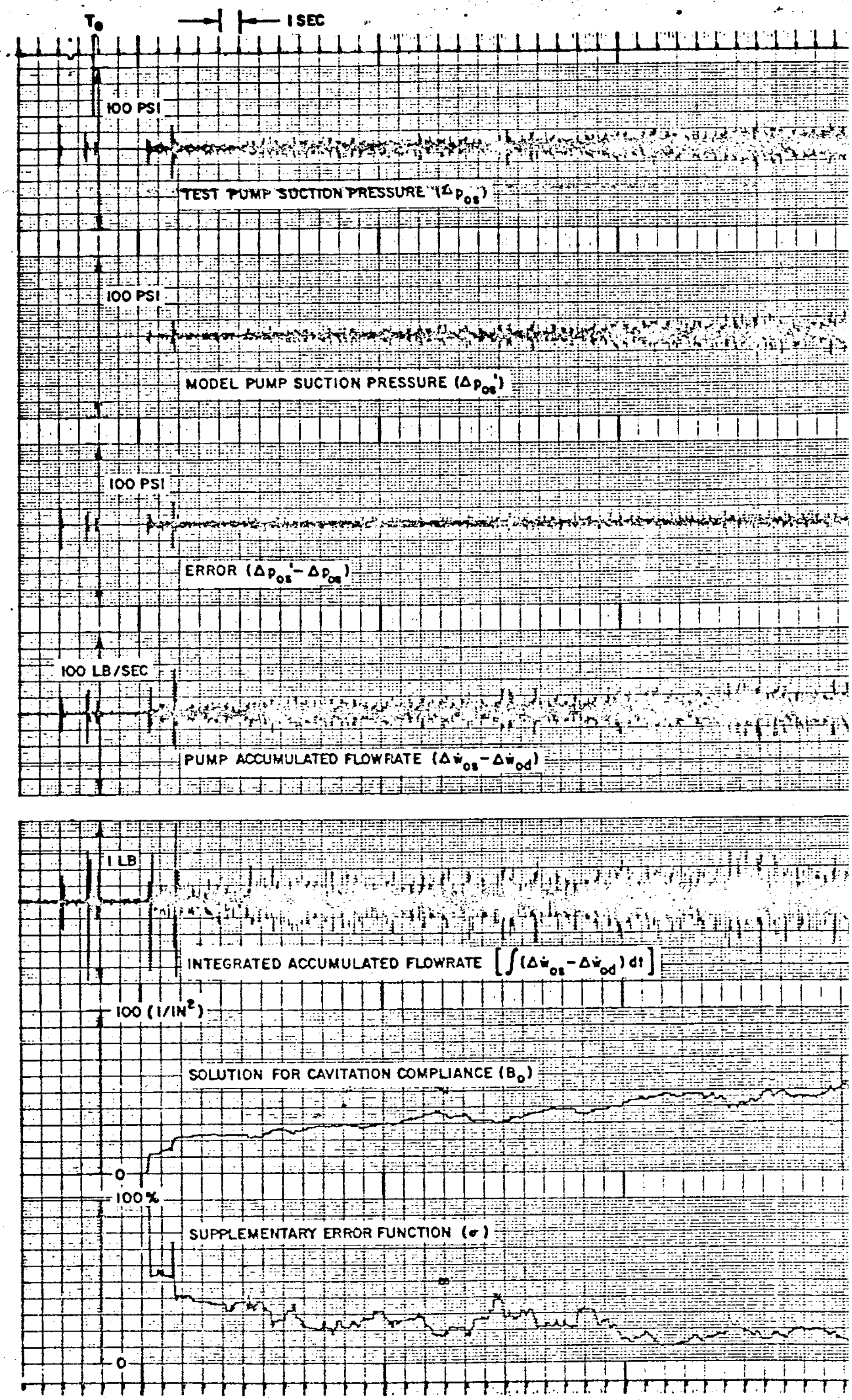

T_0
1 SEC
100 PSI
TEST PUMP SUCTION PRESSURE (Δp_{os})
100 PSI
MODEL PUMP SUCTION PRESSURE ($\Delta p_{os}'$)
100 PSI
ERROR ($\Delta p_{os}' - \Delta p_{os}$)
100 LB/SEC
PUMP ACCUMULATED FLOWRATE ($\Delta \dot{w}_{os} - \Delta \dot{w}_{od}$)
1 LB
INTEGRATED ACCUMULATED FLOWRATE $\left[\int (\Delta \dot{w}_{os} - \Delta \dot{w}_{od})\,dt\right]$
100 ($1/IN^2$)
SOLUTION FOR CAVITATION COMPLIANCE (B_o)
0
100%
SUPPLEMENTARY ERROR FUNCTION (σ)
0

C-13 (A)

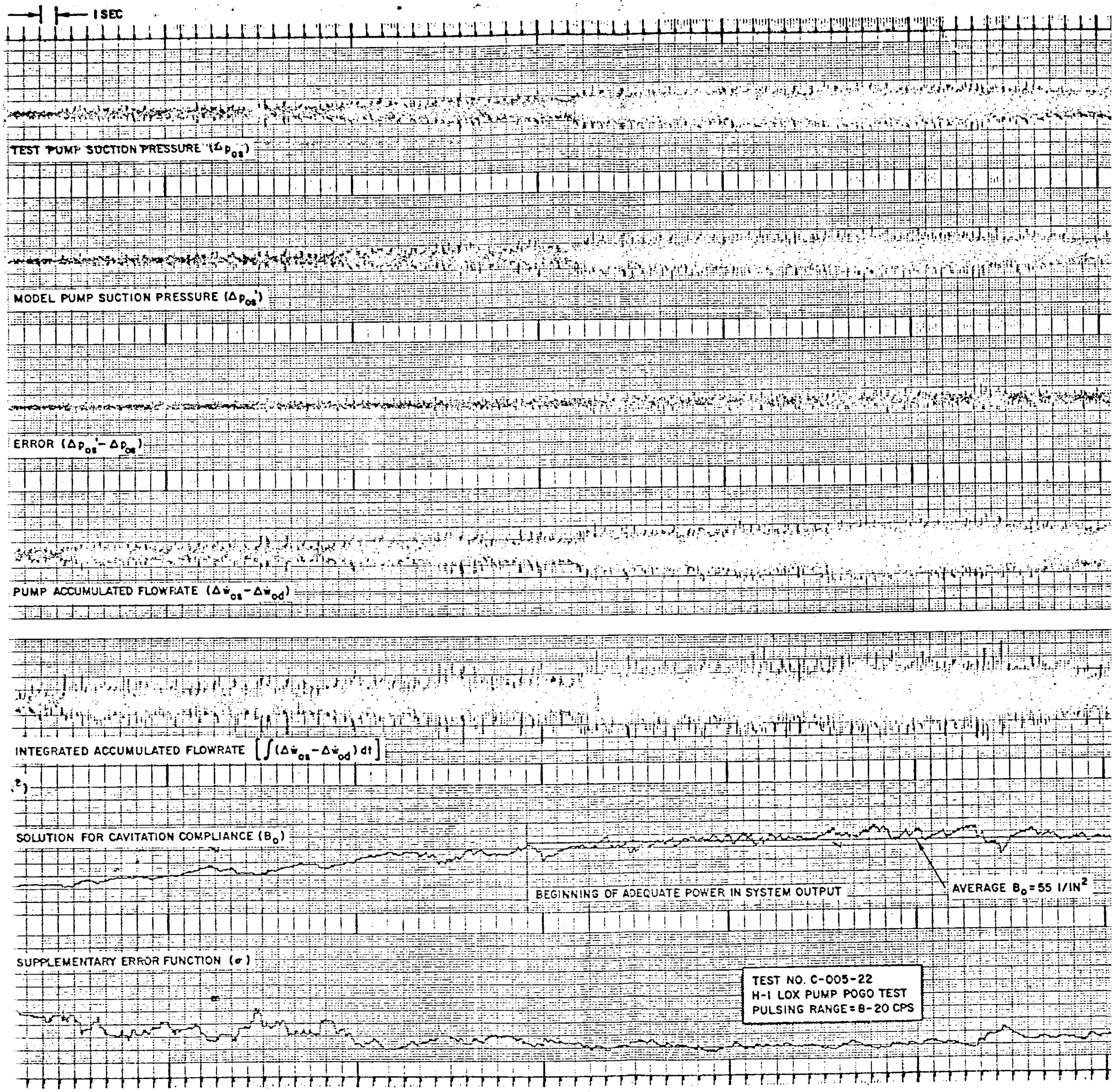
1 SEC
TEST PUMP SUCTION PRESSURE (Δp_{os})
MODEL PUMP SUCTION PRESSURE ($\Delta p_{os}'$)
ERROR ($\Delta p_{os}' - \Delta p_{os}$)
PUMP ACCUMULATED FLOWRATE ($\Delta \dot{w}_{os} - \Delta \dot{w}_{od}$)
INTEGRATED ACCUMULATED FLOWRATE $\left[\int (\Delta \dot{w}_{os} - \Delta \dot{w}_{od})\, dt\right]$
SOLUTION FOR CAVITATION COMPLIANCE (B_o)
BEGINNING OF ADEQUATE POWER IN SYSTEM OUTPUT
AVERAGE $B_o = 55$ $1/IN^2$
SUPPLEMENTARY ERROR FUNCTION (σ)
TEST NO. C-005-22
H-1 LOX PUMP POGO TEST
PULSING RANGE = 8-20 CPS

C-13 (A)

(B

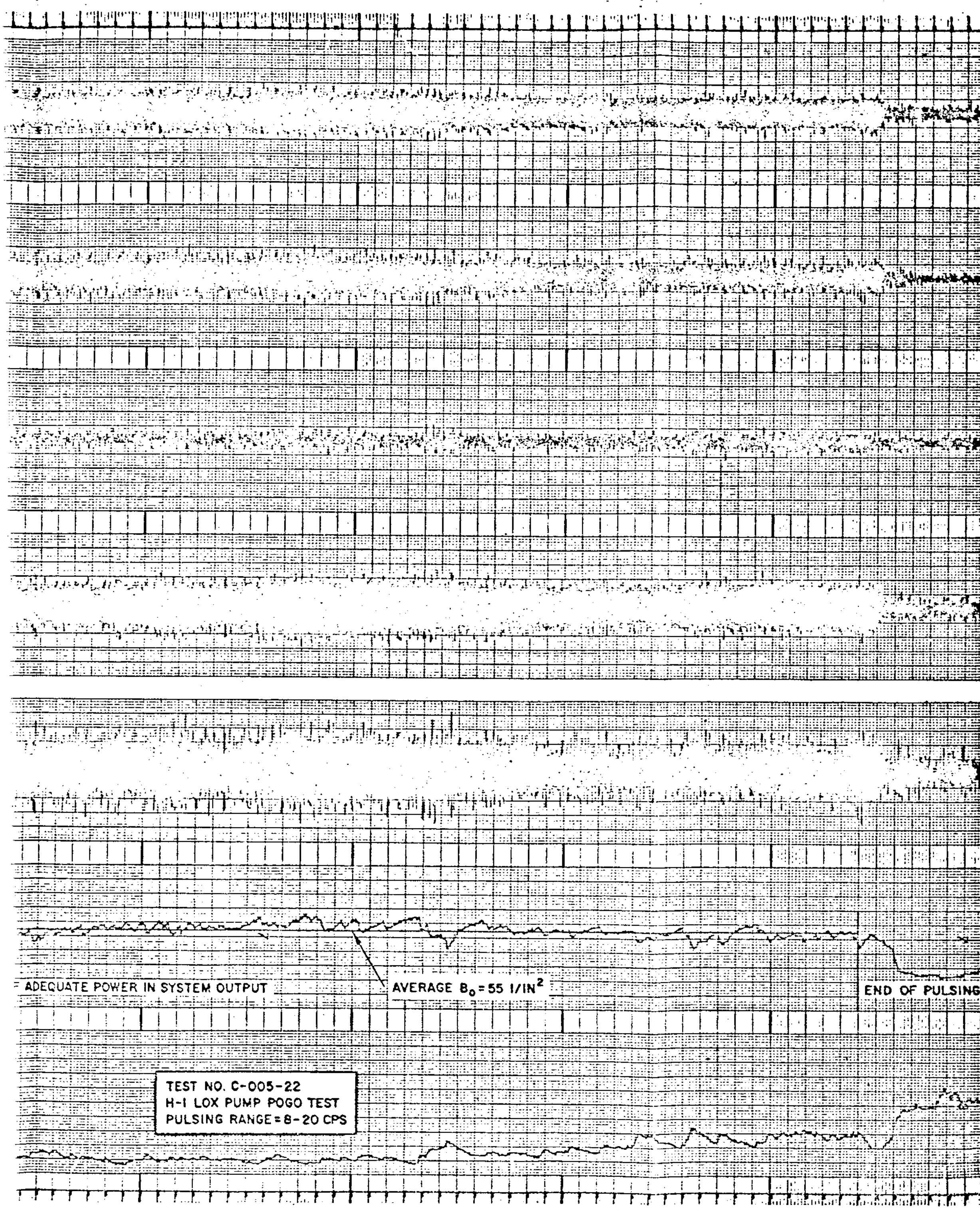

Figure C-1. Example of Continuous Parameter Identification as Used in Computation of Cavitation Compliance

(B)

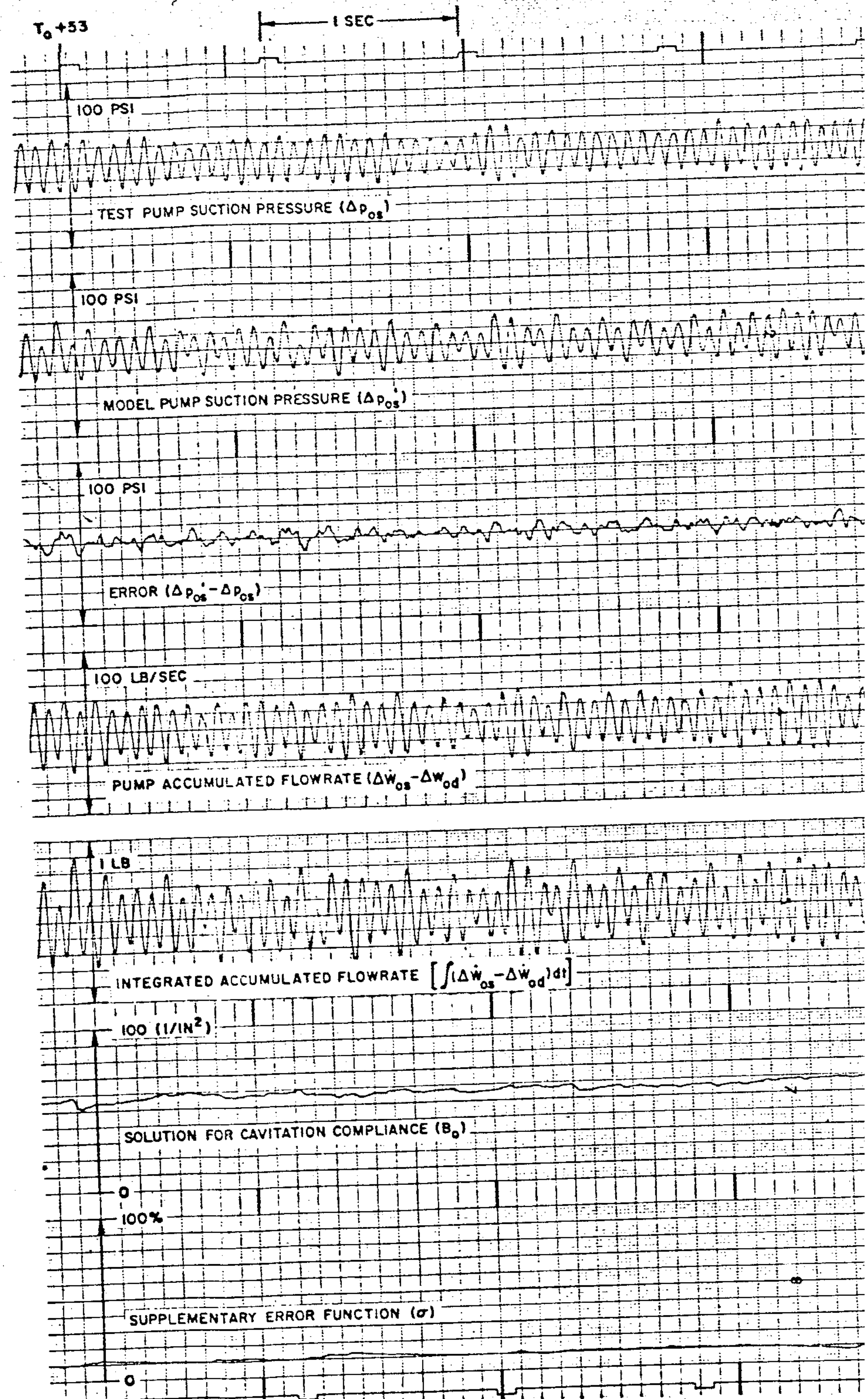
$T_o + 53$
1 SEC
100 PSI
TEST PUMP SUCTION PRESSURE (Δp_{os})
100 PSI
MODEL PUMP SUCTION PRESSURE ($\Delta p_{os}'$)
100 PSI
ERROR ($\Delta p_{os}' - \Delta p_{os}$)
100 LB/SEC
PUMP ACCUMULATED FLOWRATE ($\Delta \dot{w}_{os} - \Delta \dot{w}_{od}$)
1 LB
INTEGRATED ACCUMULATED FLOWRATE $\left[\int(\Delta \dot{w}_{os} - \Delta \dot{w}_{od})dt\right]$
100 ($1/IN^2$)
SOLUTION FOR CAVITATION COMPLIANCE (B_o)
0
100%
SUPPLEMENTARY ERROR FUNCTION (σ)
0

CH-(A)

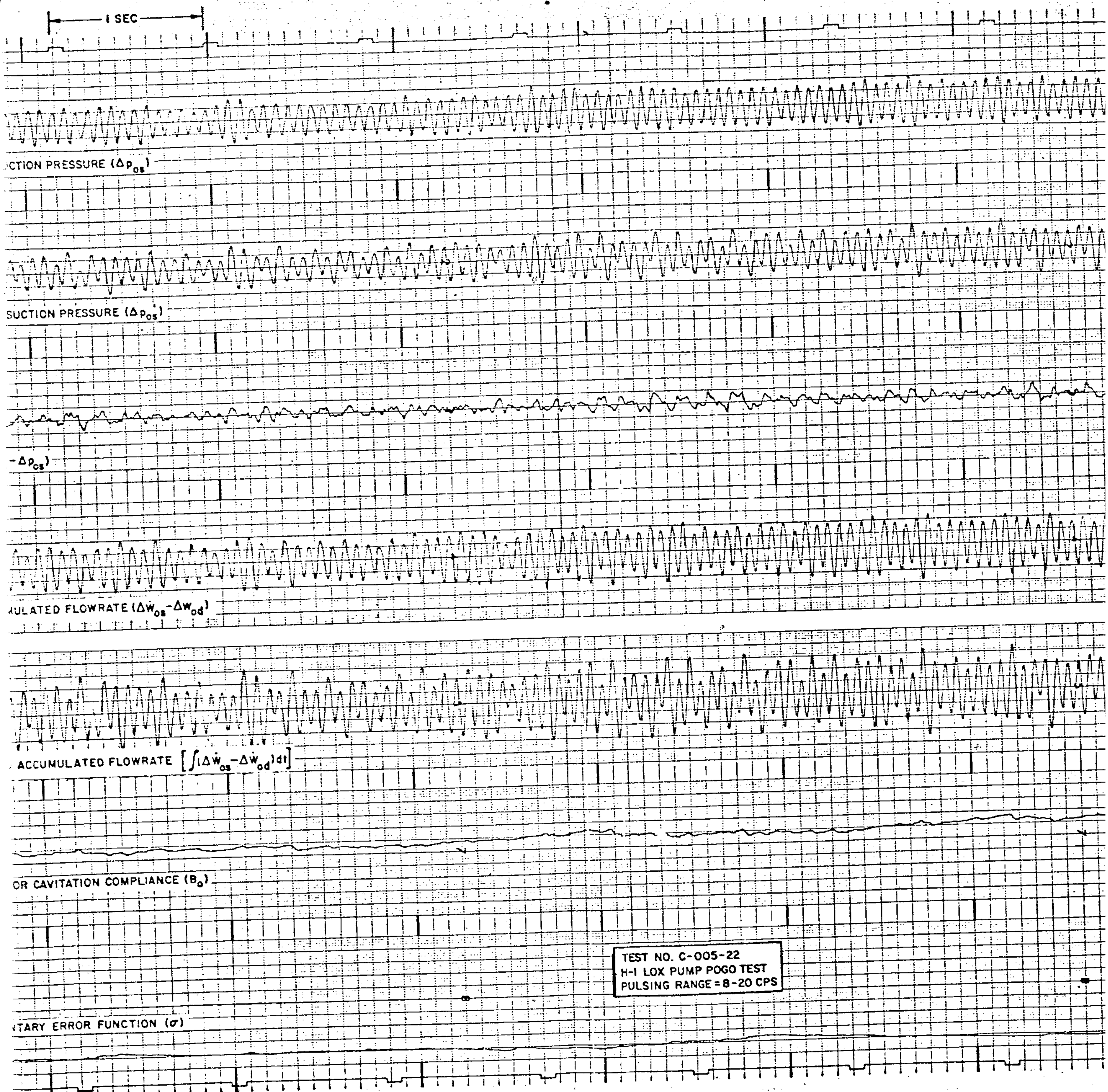

1 SEC
CTION PRESSURE (Δp_{os})
SUCTION PRESSURE ($\Delta p_{os}'$)
- Δp_{os})
ULATED FLOWRATE ($\Delta \dot{w}_{os} - \Delta \dot{w}_{od}$)
ACCUMULATED FLOWRATE $\left[\int (\Delta \dot{w}_{os} - \Delta \dot{w}_{od}) dt\right]$
OR CAVITATION COMPLIANCE (B_o)
TEST NO. C-005-22
H-1 LOX PUMP POGO TEST
PULSING RANGE = 8-20 CPS
TARY ERROR FUNCTION (σ)

H-(A)

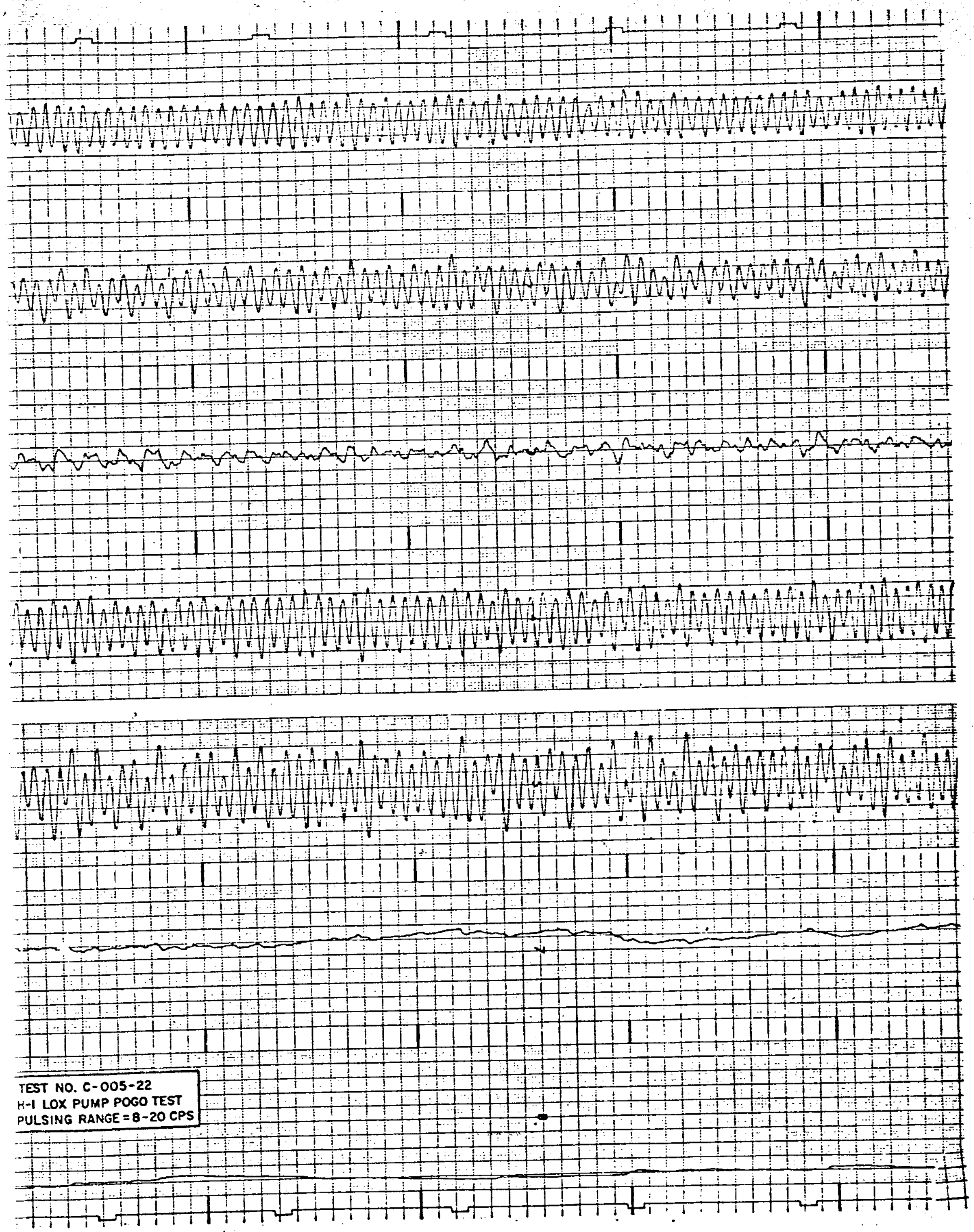

Figure C-2. Example of Continuous Parameter Identification as Used in Computation of Cavitation Compliance (Time Base Expanded) reconstruction, and optimization were performed on line as data on magnetic tape was played back. Figure C-1 is a typical record of the analysis output.

The time record of model-system error was found to be particularly valuable in interpreting the results and in determining when optimization had been [illegible] the single parameter optimization shown in Fig. C-1 is the result [illegible] excitation compliance computation. A supplementary function [illegible] defined as the time-averaged ratio of [illegible]